1-1-2019

Physical and chemical trace evidence from 3d-printed firearms, and use of a quadcopter for targeted sampling of gaseous mercury in the atmosphere

Oscar Beauchamp Black

PHYSICAL AND CHEMICAL TRACE EVIDENCE FROM 3D-PRINTED FIREARMS, AND USE OF A QUADCOPTER FOR TARGETED SAMPLING OF GASEOUS MERCURY IN THE ATMOSPHERE

A Dissertation
presented in partial fulfillment of requirements
for the degree of Doctor of Philosophy
in the Department of Chemistry and Biochemistry
The University of Mississippi

by

OSCAR B BLACK V

August 2019

ABSTRACT

Several novel analytical methods were developed in the course of this dissertation work, including forensic analysis of trace chemical evidence from 3D-printed firearms using direct analysis in real time-mass spectrometry (DART-MS), and targeted aerial sampling for quantitation of gaseous mercury. The mercury project utilized a quadcopter unmanned aerial vehicle (UAV) and gold-coated quartz sorbent tubes to target and capture gaseous mercury, which was then quantified both in the laboratory and in the field using cold vapor atomic fluorescence spectrometry (CVAFS). This method was verified to effectively capture and quantify mercury in the atmosphere near point sources, and was applied near a coal-fired power plants, petroleum refinery, and municipal landfill. Average concentrations (± standard deviation) immediately downwind of the landfill were higher at ground level and 30 m compared to 60 m and 120 m (5.3 ± 0.5 ng m^{-3}, 5.4 ± 0.7 ng m^{-3},4.2 ± 0.7 ng m^{-3}, and 2.5 ± 0.3 ng m^{-3}, respectively). Concentrations were also higher at an urban/industrial area (Memphis) (3.3 ± 0.9 ng m^{-3}) compared with a rural/background area (1.5 ± 0.2 ng m^{-3}). Overall we showed the method is useful to probe Hg concentrations aloft and quantify emissions from potential point sources in the field, using an inexpensive quadcopter and sampling setup.

My forensic research resulted in the first peer-reviewed paper to address the forensic challenges presented by 3D-printed polymer firearms. The work involved a systematic approach to the analysis of evidence stemming from 3D-printed firearms, filling a critical void in current

forensic knowledge. We used DART-MS to characterize the polymer evidence left behind by 3D-printed firearms, as well as an evaluation of pre-existing firearm and toolmark techniques and fingerprint analysis. We demonstrated that 3D-printed firearms leave behind characteristic polymer residue on cartridge cases, bullets, and the receiving surface, which can be identified using DART-MS. The culmination of the work includes a database / reference library that can give forensic practitioners the ability to identify and source unknown polymer evidence using chemometric analysis including principle component analysis (PCA) and ongoing work with supervised statistical classification methods.

The forensic research was funded by NIJ Graduate Research Fellowship (Award # 2017-IJ-CX-0001). The opinions, findings, and conclusions or recommendations expressed here are those of the authors and do not necessarily reflect those of the U.S. Department of Justice.

LIST OF ABBREVIATIONS, SYMBOLS, AND INSTRUMENTS

ADFS	Alabama Department of Forensic Sciences
amu	atomic mass units
CFPP	Coal-fired Power Plants
CVAFS	Cold Vapor Atomic Fluorescence Spectroscopy
DART	Direct Analysis in Real Time
FDM	Fused Deposition Modeling
GEM	Gaseous Elemental Mercury
GOM	Gaseous Oxidized Mercury
GSR	Gunshot Residue
Hg	Elemental Mercury
ICP-MS	Inductively Coupled Plasma Mass Spectrometry
MCL	Mississippi Forensic Crime Laboratory
MS	Mass Spectrometry/Mass Spectrometer
m/z	mass to charge ratio
NIJ	National Institute of Justice
OGSR	Organic Gunshot Residue
PBM	Particulate Bound Mercury
PC	Principal Component

PCA	Principal Component Analysis
TD	Thermal Desorption
TDM-II	Brooks Rand brand CVAFS Hg Analyzer
Tekran 2505	Tekran brand Hg Vapor Calibration Unit
Tekran 2600	Tekran brand CVAFS Hg Analyzer
TOFMS	Time-of-Flight Mass Spectrometer
UAV	Unmanned Aerial Vehicle
UV	Ultraviolet Radiation

ACKNOWLEDGEMENTS

I would like to thank my graduate advisor, Dr. James V. Cizdziel, for all his help and guidance throughout my undergraduate and graduate career at the University of Mississippi. He was always available to discuss new directions, troubleshooting, and refinement of the work. His contacts and instrumental knowledge were critical in this analytical method development research. I would also like to thank my committee members, Dr. Murrell Godfrey, Dr. Steven Davis, and Dr. John Brewer, for their helpful critiques of my research. Dr. Davis' generous loaning of his personal land outside Oxford, MS provided an ideal environment to conduct proof of concept field studies for both the firearm and UAV work. I especially wish to think Dr. Godfrey, whose contacts in the forensic arena enabled many portions of this dissertation work. I also wish to express my appreciation to the National Institute of Justice for funding the bulk of my research.

LIST OF TABLES

LIST OF FIGURES

CHAPTER ONE

INTRODUCTION AND BACKGROUND INFORMATION

INTRODUCTION TO THE DISSERTATION

My dissertation research focused on analytical method development in two distinct fields: environmental and forensic chemistry. More specifically, my research has centered on atmospheric monitoring using an unmanned aerial vehicle (UAV) and the chemical and physical analysis of 3D-printed firearms. The latter was funded by the Department of Justice through a three-year Graduate Research Fellowship. Included within this dissertation are my first-authored papers that were recently published on these topics, as well as unpublished work that is being adapted for future publication. Chapter Two covers the atmospheric mercury project, while Chapters Three through Five covers various aspects of the 3D-printed firearms project. This current chapter will provide an introduction and background information into the underlying chemistry and other facets involved in my dissertation work, including atmospheric mercury, analytical instrumentation principles, firearm and toolmark analysis, and 3D-printing.

MERCURY IN THE ATMOSPHERE

Mercury (Hg) is a persistent pollutant that stems from natural sources, but also has major anthropogenic sources. Coal-fired power plants (CFPPs), refineries, and combustion engines are just a few of the contributors to gaseous mercury in our atmosphere.

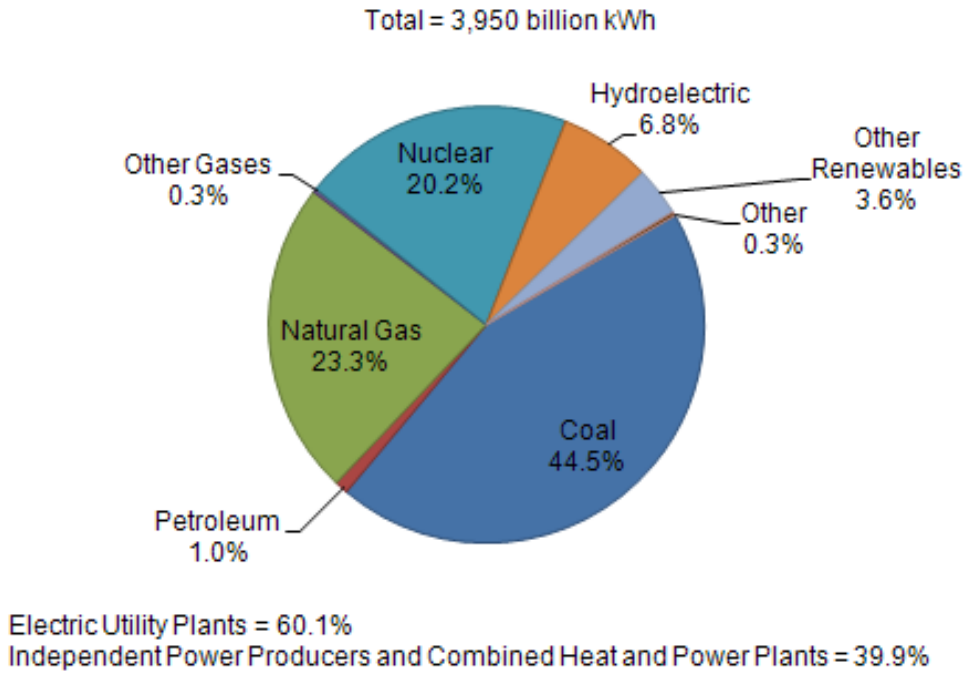

Figure 1. U.S. Electric Power Industry Net Generation, 2009 (U.S. Energy Information Administration. 2009)

Mercury is of environmental concern due to its ability to persist and transport across the globe, due in part to its high volatility. Gaseous Hg commonly exists as either gaseous elemental mercury (GEM), gaseous oxidized mercury (GOM), or particulate bound mercury (PBM). GEM, due to its inert nature, is estimated to remain in the atmosphere for up to a year, while slowly undergoing photocatalyzed oxidation to GOM, which more readily deposits during precipitation events. Atmospheric movement of Hg is a key facet of the complex biogeochemical cycling of Hg, providing the means for the mobilization and transfer of mercury between terrestrial and

aquatic systems. Of particular concern is the production of methyl-Hg, which is a potent neurotoxin that can bio-accumulate up food chains (Mason et al. 1995; Selin 2009), and has been shown to create developmental abnormalities when humans are exposed in-utero. By monitoring potential point sources of Hg, environmental scientists seek to better understand the sources, sinks, and ultimate fates of various chemical species of Hg, as outlined in the Minamata Convention of 2013.

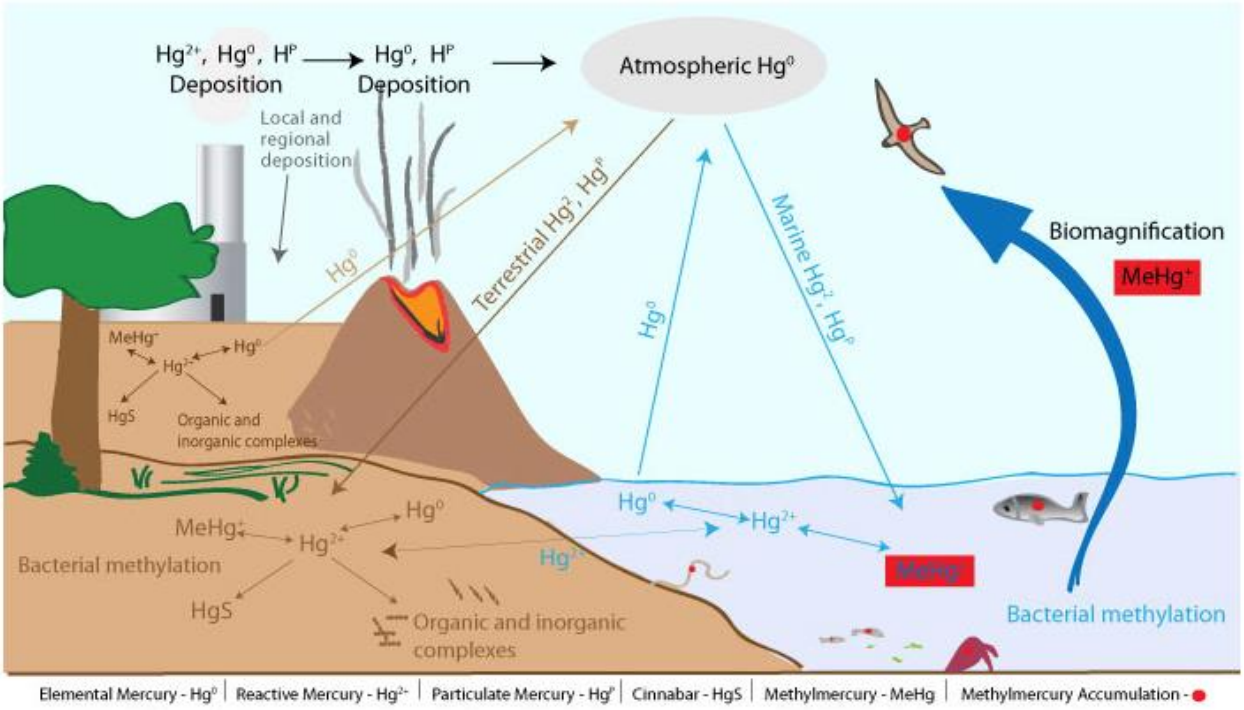

Figure 2. Biogeochemical cycling of mercury (photo credit: *https://www.learner.org/courses/envsci/visual/visual.php?shortname=mercury_cycle*)

As shown in Figure 2, elemental Hg and Hg^{2+} can be transported through wet and dry deposition mechanisms, and converted to methyl-Hg through the activity of microorganisms. The formation of methyl-Hg in aquatic systems leads to bioaccumulation in fish, which provides the primary exposure route for humans. Figures 3 and 4 highlight the concentration of CFPPs in the southeastern region of the United States, as well as the significant annual wet deposition of

Hg, lending further credence to the need for atmospheric monitoring studies conducted in the region.

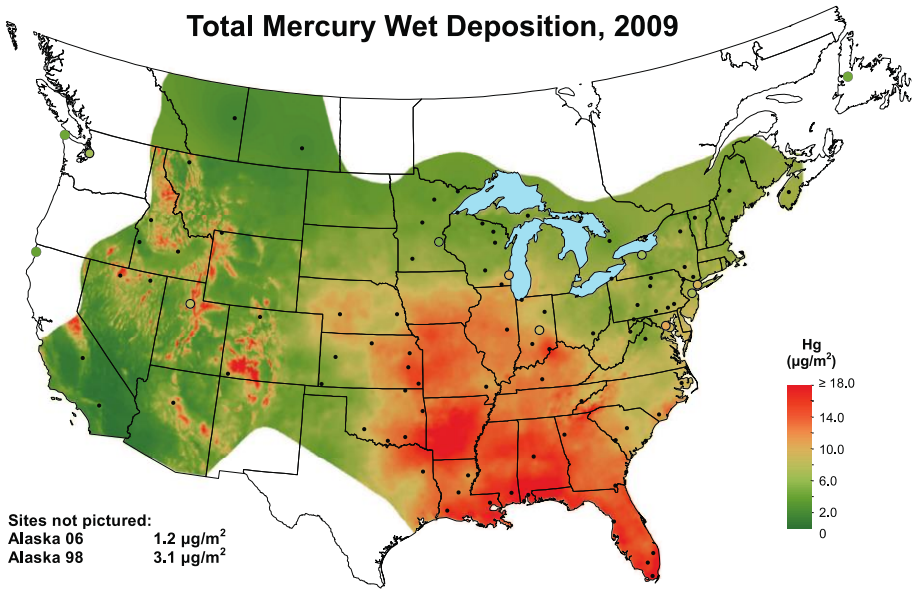

Figure 3. Mercury wet deposition map for USA, 2009 (NADP)

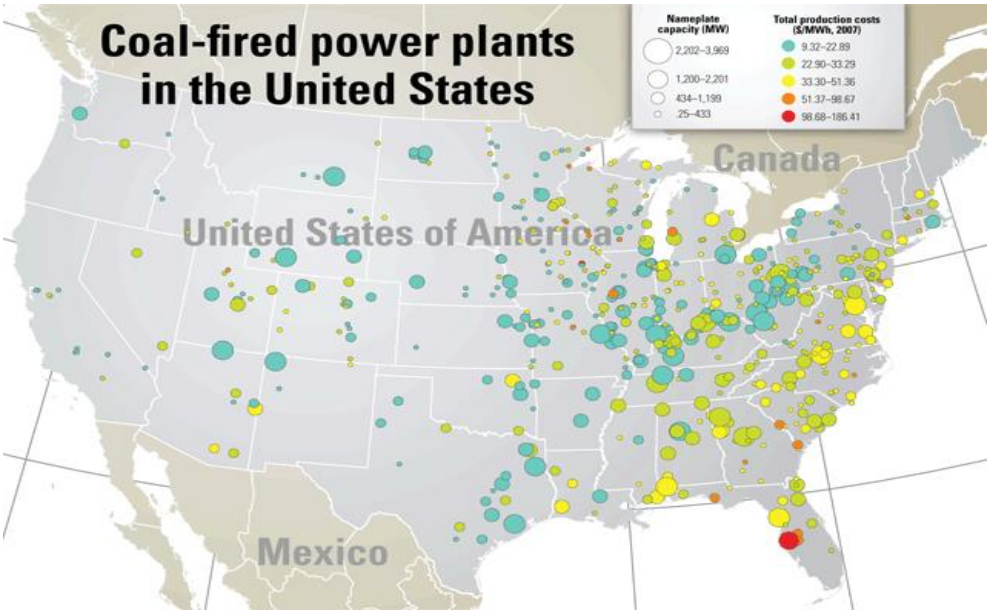

Figure 4. Distribution of CFPPs in USA (US Environmental Protection Agency, 2007)

COLD-VAPOR ATOMIC FLUORESCENCE SPECTROMETRY

Cold-vapor atomic fluorescence spectrometry (CVAFS) is a highly sensitive technique for elemental Hg quantitation. The technique derives its name from the unique properties of Hg that allow it to be analyzed in vapor form at room temperature. CVAFS owes its innate high sensitivity for Hg to its low background, in part because the UV excitation source (253.7nm), emits at a wavelength that is specific for the excitation of elemental Hg. The resultant fluorescence of the Hg atoms is detected by a photodiode array or photomultiplier tube placed orthogonal to the excitation pathway. Detector signal is correlated to Hg concentration through a calibration curve.

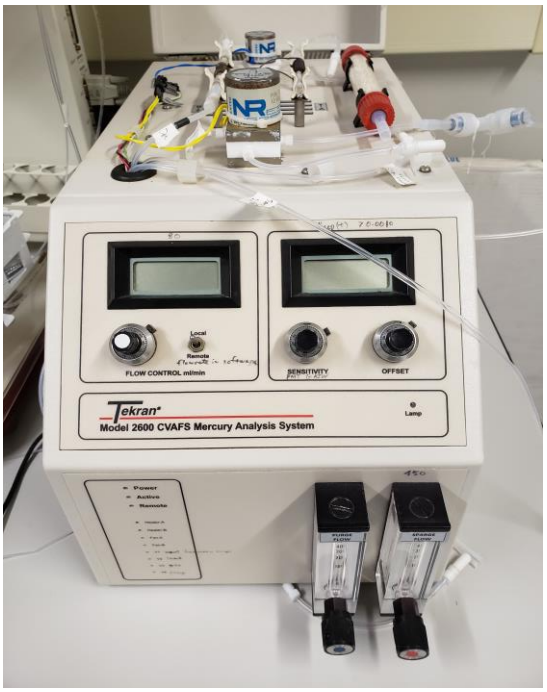

Figure 5. Tekran 2600 CVAFS laboratory setup

Figure 6. Brooks-Rand TDM-II CVAFS field setup

For this work, our lab utilized a Tekran 2600 unit (Figure 5) in the laboratory and a Brooks Rand TDM-II unit (Figure 6) in the field. Both units utilize dual-trap desorption pathways for sample analysis. Atmospheric Hg is collected by drawing air through gold-coated quartz sorption tubes. The gold trap used for sampling is then placed within the first heating coil of the instrument and heated in a stream of Hg-free argon. The desorbed Hg is concentrated onto

a second gold trap in series, which is then subsequently heated, releasing the Hg directly into the atomic fluorescence detector system. These instruments can be calibrated using a temperature-controlled Hg-vapor calibration source, such as the Tekran 2505 (Figure 8), a digital gas-tight syringe, and a loading rig to transfer known quantities of Hg to a gold-coated trap. Known quantities of Hg are then analyzed by the CVAFS to build a calibration curve of concentration vs instrument detector response.

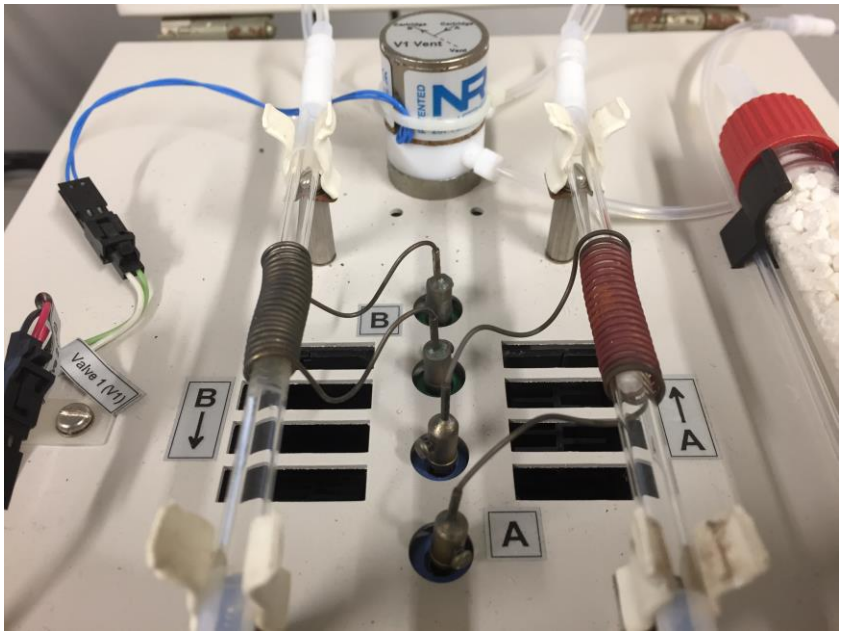

Figure 7. Close-up of the Tekran 2600 CVAFS showing the dual gold coated quartz Hg traps (surrounded by heating elements)

Figure 8. Gaseous Hg calibration unit (Tekran 2505) with digital syringe

3D-Printing and Firearms

Recent years have witnessed an increased sophistication in 3D-printing technology, enabling a variety of possibilities that need to be investigated by modern science. One such concern is the ability to produce a class of firearms that we know almost nothing about, forensically speaking, due to their polymer-based nature. Due to ease of access and relatively inexpensive cost compared to traditional firearms, the movement to self-manufacture firearms with 3D-printing technology is expected to increase significantly in the near future. As 3D-printed firearm designs increase in functionality and reliability, it is reasonable to assume that they will be used increasingly in crimes, especially by individuals who may have less access to

traditional firearms. Due to their polymer components, plastic firearms and bullets also raise the concern for their ability to potentially go undetected by metal detectors into high security areas. Combined with their lack of serial numbers, 3D-printed firearms present a series of new challenges to traditional forensic practices, demonstrating the need for new forensic methods to analyze and detect the use of this new class of firearms.

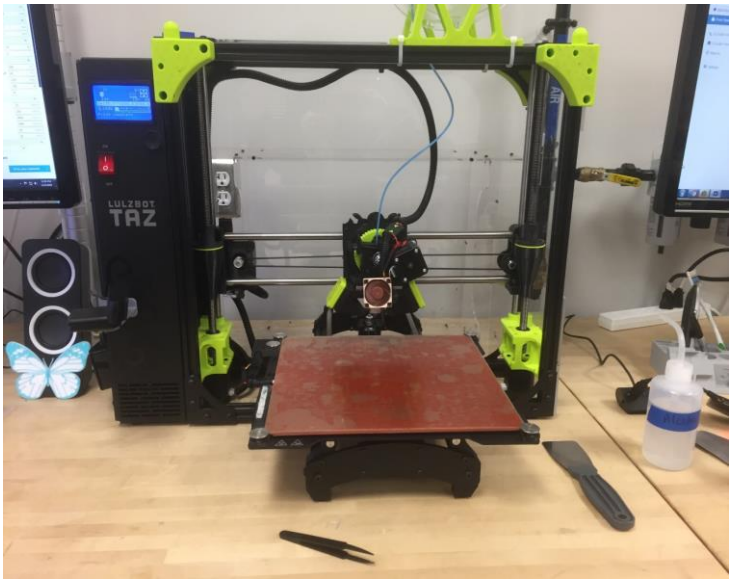

Figure 9. Lulzbot TAZ 6 FDM 3D-printer

Below is an excerpt from one of my chapters from the book I was the co-editor of: "Forensic Analysis of Gunshot Residue, 3D-Printed Firearms, and Gunshot Injuries: Current Research and Future Perspectives."

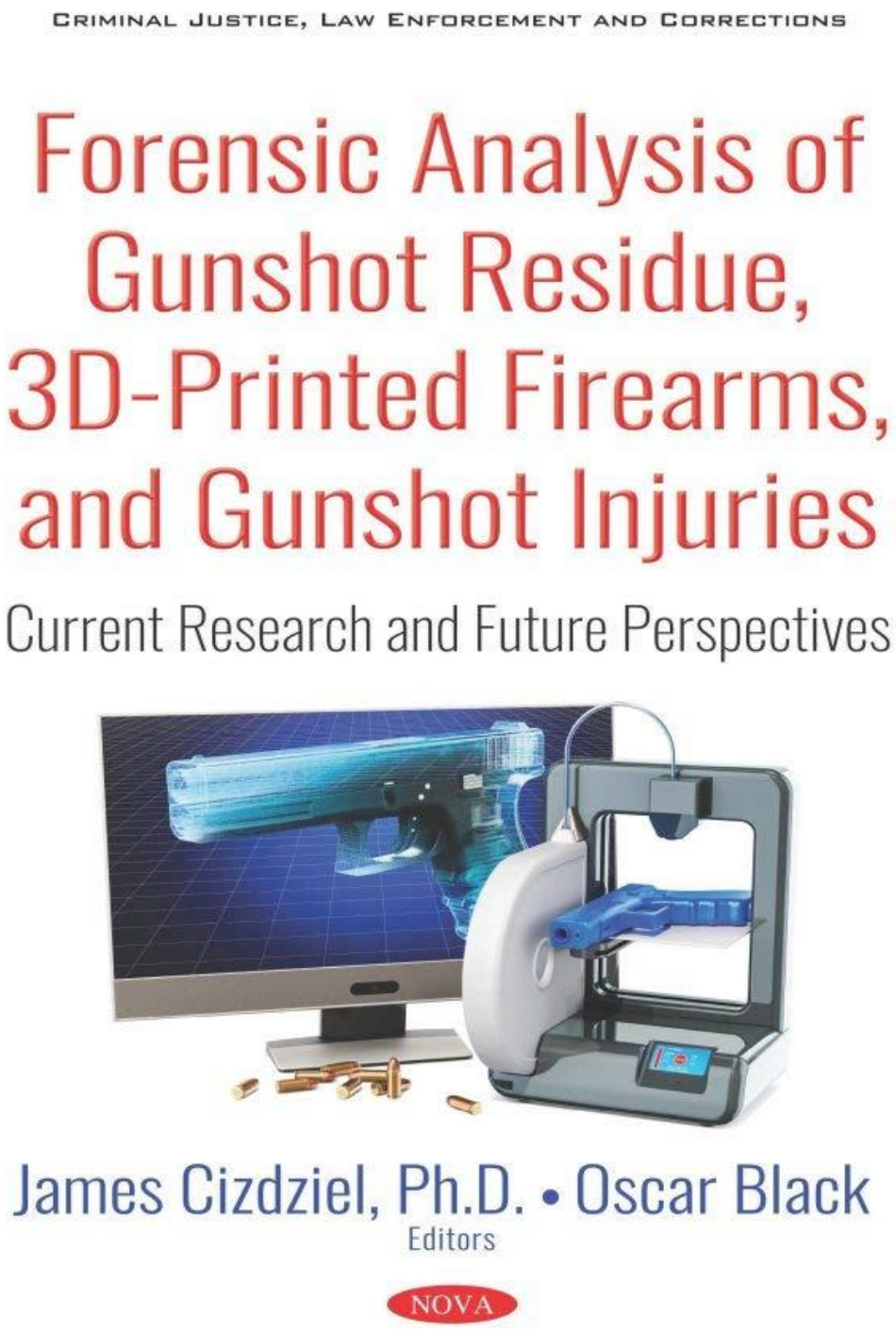

Figure 10. Cover of our firearm forensics research book

"The most common type of 3D-printer on the market today utilizes fused deposition modeling, an additive manufacturing technology that builds parts layer-by-layer from the bottom up by heating and extruding thermoplastic filaments. A variety of user-friendly slicing software is freely available to generate 3D-printer files that control the printer to produce objects. Most 3D-printer blueprints are presented as stereolithography files (.stl). Challenges to building 3D-printed guns include material performance and dimensional accuracy, as limited by individual printer models and filaments. Moreover, when a gun is fired, sudden and severe changes in temperatures and pressures can compromise its structural integrity, and early models were known to explode. However, improved technology (and experience) in the 3D-printing community has made functional 3D-printed guns a reality."

"While fully 3D-printed firearms have been a relatively recent innovation, computer-aided design (CAD) files for components of firearms have existed since at least the beginning of the 2000's (Snider 2003). These early years witnessed experimentation with 3D-printed components paired with low-caliber ammunition in a predominantly metal firearm frame. The technology involved in 3D-printing a firearm received national media attention in 2012 when the organization Defense Distributed announced its plan to create the world's first fully 3D-printed firearm, and again in 2013 with the release of the "Liberator" 3D-printable file (Greenberg 2013). The subsequent five years since the release of the Liberator have witnessed the creation of many more firearm designs and models, created by hobbyists and gun enthusiasts around the world. These firearms are subjected to revisions and adaptations that continually push them toward better functionality, making their widespread use a more imminent reality."

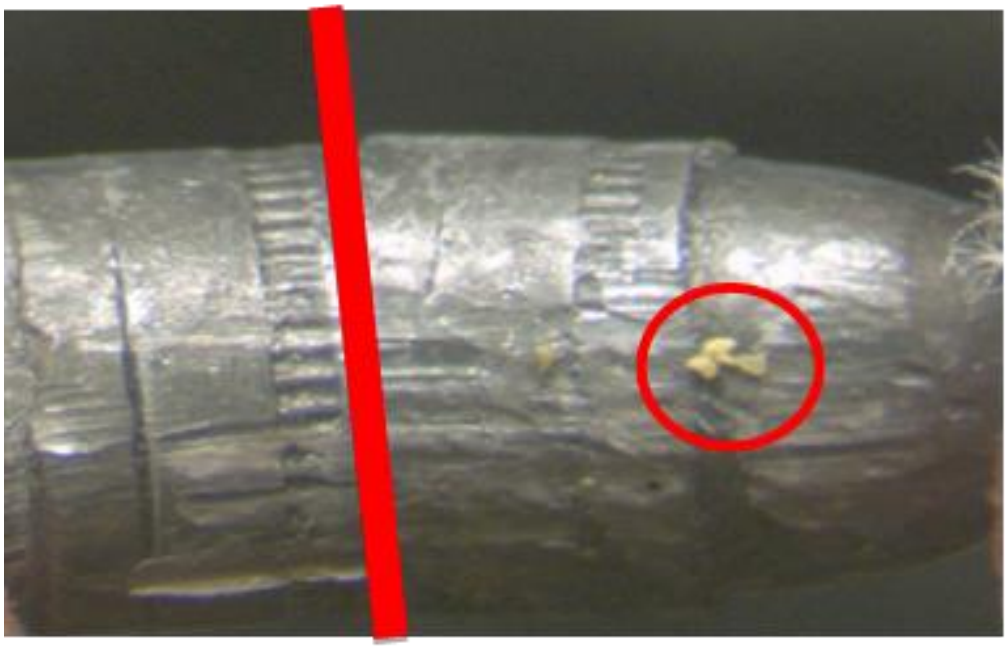

Figure 11. Comparison Microscope image of a bullet fired from a 3D-printed firearm, with transferred polymer flakes circled

PRE-EXISTING FORENSIC METHODS FOR FIREARM ANALYSIS

The two main forms of forensic analysis that are pertinent to this research are the analysis of gunshot residue (GSR) and toolmark analysis, which evaluates the striations, indentations, and impressions left behind by a firearm on the bullets and cartridge cases that pass through it. GSR is produced from the combustion of the primer and propellant, and is composed of combustion products, unburned and partially burned propellant, primer particles, as well as lubricants and metal from the cartridge and weapon (Laza et al 2007). Inorganic GSR often includes heavy metals such as lead (Pb), barium (Ba), and antimony (Sb) from the primer, trace metals from metallic parts, and nitrates and nitrites (Laza et al 2007). Organic gunshot residue (OGSR) may contain nitroglycerine, dinitrotoluene, phthalates, ethyl centralite, and diphenylamine, among other compounds (Bell 2013, Goudsmits et al 2015). Some crime laboratories are moving away from traditional (inorganic) GSR testing due to budget constraints, sample backlogs, and

concerns regarding interpretation, such as potential environmental sources of particles resembling inorganic primer [Dalby et al 2010, Burleson et al 2009). In addition, "lead-free" ammunition has introduced the potential for false negatives with some GSR tests, such as primer GSR analysis by conventional SEM/EDX protocols (Moran and Bell 2014). Recently, several new methods have focused attention on OGSR (Moran and Bell 2014). Advantages of targeting OGSR for analysis include condensates that stick to the skin and are not prone to secondary transfer, multiple target compounds with options for chemical analysis, and low background which improves limits of detection (Moran and Bell 2014). However, these techniques are often tedious and time-consuming. A relatively new technique that has the capability to detect and identify a wide-range of compounds in GSR is direct analysis in real time (DART) mass spectrometry.

Toolmark analysis primarily focuses on three main sources of characteristic markings: breech face/extractor/ejector scratches, firing pin impressions, and rifling land/groove striations. Toolmark analysis can be applied to firearm evidence to forensically match a specific firearm to the bullets/cartridge cases at a crime scene. This level of characteristic discrimination is possible due to the nature of the toolmarks themselves: unique imperfections during the manufacturing process and lifetime of each firearm are accrued and generate a unique profile for the firearm and any cartridges that are discharged within it (AFTE Committee 1992). A forensic professional can compare these markings left behind on evidence to confirm that a suspect's firearm was indeed used. The main tool for these analyses is confocal microscopy, where two bullets or cartridge cases can be compared concurrently.

DART-MASS SPECTROMETRY

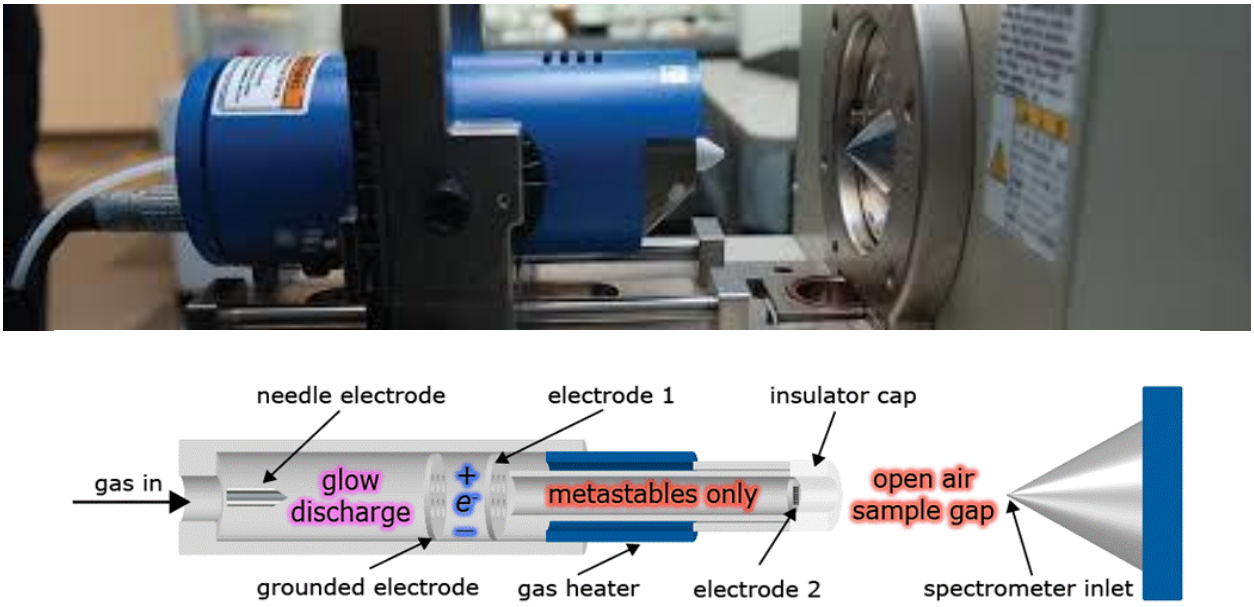

Figure 12. DART Source and diagram (diagram credit: Dr. Chip Cody)

DART is a versatile atmospheric pressure ion source allowing the analysis of materials in open air under ambient conditions (Laramée et al 2007). Desorbed ions are carried by the gas stream into the sampling orifice of a mass spectrometer. When coupled with a high-resolution mass spectrometer, the system has significant advantages because it can determine the chemical composition of a sample without the need for sample preparation, derivitization, or phase change. Since so little sample is needed, it can be considered a pseudo-non-destructive technique, a key feature for its forensic applications. DART-MS is a powerful analytical technique that is currently used in many federal, state and private laboratories for forensic applications, including the identification of drugs of abuse, trace evidence analysis, and sexual assault investigations (Lesiak and Shephard 2014, Laramée et al 2007, Musah et al 2012, Cody et al 2005, Chernetsova and Morlock 2011, Laramée et al 2009).

DART-MS has been used to identify trace particles of explosives in fingerprints (Clemons et al 2013). The technique can measure nitrated propellants and burn stabilizers such as nitroglycerin and dinitrotoluene, in negative-ion mode, and centralites and phthalates in positive-mode (Meyers 2009). In addition, DART-MS can provide “fingerprint” mass spectra for the identification of polymers, their additives, and other materials, and is used at NASA for the identification of spaceflight-related contaminants, including industrial polymers (Loftin 2009, Anderson 2014, Klampfl 2013). However, DART-MS has not been sufficiently applied to GSR and other trace evidence from firearms, in part, because fundamental studies are lacking.

CHAPTER TWO

ADAPTION AND USE OF A QUADCOPTER FOR TARGETED SAMPLING OF GASEOUS MERCURY IN THE ATMOSPHERE

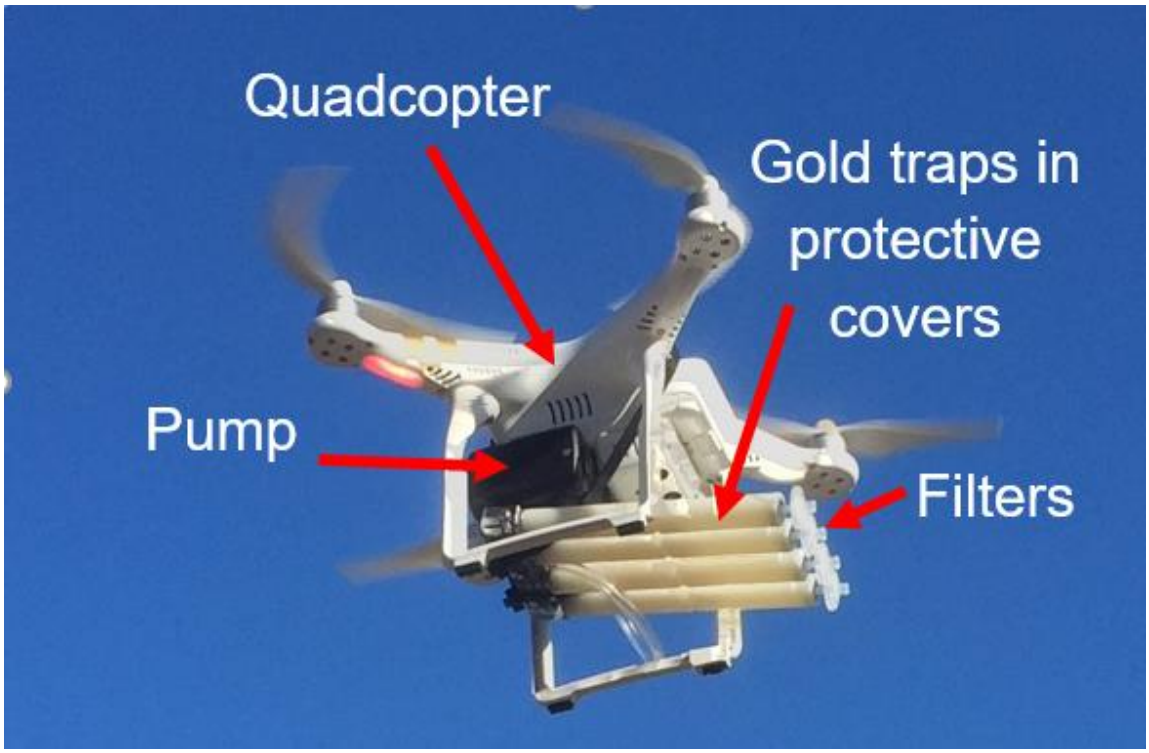

Black O., Chen J., Scircle A., Zhou Y., Cizdziel JV (2018) *Environ Sci Pollut Res Int*. **25**, 13195-13202.

ABSTRACT

We modified a popular and inexpensive quadcopter to collect gaseous mercury (Hg) on gold-coated quartz cartridges, and analyzed the traps using cold vapor atomic fluorescence spectrometry. Flight times averaged 16 minutes, limited by battery life, and yielded >5 pg of Hg, well above the limit of detection (<0.2 pg). We measured progressively higher concentrations upon both vertical and lateral approaches to a dish containing elemental Hg, demonstrating that the method can detect Hg emissions from a point source. Using the quadcopter, we measured atmospheric Hg near anthropogenic emission sources in the mid-south USA, including a municipal landfill, coal-fired power plant (CFPP), and a petroleum refinery. Average concentrations (± standard deviation) immediately downwind of the landfill were higher at ground level and 30 m compared to 60 m and 120 m (5.3 ± 0.5 ng m^{-3}, 5.4 ± 0.7 ng m^{-3},4.2 ± 0.7 ng m^{-3}, and 2.5 ± 0.3 ng m^{-3}, respectively). Concentrations were also higher at an urban/industrial area (Memphis) (3.3 ± 0.9 ng m^{-3}) compared with a rural/background area (1.5 ± 0.2 ng m^{-3}). Due to airspace flight restrictions near the CFPP and refinery, we were unable to access near field (stack) plumes and did not observe differences between upwind and downwind locations. Overall, this study demonstrates that highly maneuverable multicopters can be used to probe Hg concentrations aloft, which may be particularly useful for evaluating Hg emissions from remote landscapes and transient sources that are poorly characterized and leading to uncertainties in ecosystem budgets.

Keywords: Atmospheric mercury; Landfill; Unmanned aerial vehicle; Multicopter; Coal fired power plant; Petroleum refinery; Cold vapor atomic fluorescence spectrometry

INTRODUCTION

Mercury (Hg) is a persistent and toxic pollutant transported globally through the atmosphere (Schroeder and Munthe 1998; Gustin 2011). Airborne Hg stems from both natural and anthropogenic sources, and the latter, particularly the burning of fossil fuels, have led to an increase in Hg in the atmosphere (Pirrone et al. 2010; Krabbenhoft and Sunderland 2013). This increase is a worldwide environmental concern because airborne Hg deposits to terrestrial and aquatic systems where it can be transformed to methylmercury, a neurotoxin that accumulates in biological tissues and concentrates up food-chains to levels that can be toxic to wildlife and humans (Mason et al. 1995; Selin 2009). Thus, measuring Hg in the atmosphere is important to support models that help us understand Hg sources, deposition, cycling, and spatial and temporal trends in airborne Hg concentration. Furthermore, more comprehensive atmospheric monitoring is essential for evaluating the effectiveness of the recent Minamata Convention, a global regulatory mechanism to decrease environmental Hg loadings (Gustin et al. 2016).

Airborne Hg exists as gaseous elemental mercury (GEM = Hg^0), gaseous oxidized mercury (GOM; e.g., HgX_2, where X = Cl, Br, I), or particulate bound mercury (PBM), each with distinctive properties and environmental behavior (Seigneur et al. 2004). GEM is the predominant form and has a residence time estimated from months to years (Schroeder and Munthe, 1998; Weiss-Penzias et al. 2003). GEM is slowly converted to soluble GOM through photochemical reactions and direct interaction with oxidants in the atmosphere (Holmes et al. 2010). GOM and PBM have shorter residence times than GEM and are readily removed through wet and dry deposition mechanisms (Lyman et al. 2007). Transport of PBM depends on the particle size and the meteorological conditions (Keeler et al. 1995). Natural emissions are primarily in the form of GEM, whereas anthropogenic emissions often include GEM, GOM and

PBM (Schroeder and Munthe, 1998). In 2010, coal combustion accounted for the largest source (~70%) of Hg emissions in North America (UNEP 2013). A less-investigated source of Hg emissions are municipal landfills, which emit alkyl-Hg species and inorganic Hg during and after operation (Kim and Kim, 2002; Lindberg et al. 2005).

Studies of airborne Hg, particularly those that involve semi-continuous measurements, are typically performed at ground-level at fixed locations due to constraints of the instruments, such as electrical power and carrier gas tanks. Others have used portable instruments such as the Lumex, a Hg analyzer based on cold vapor atomic absorption spectrometry, although they tend to be used in areas with relatively high concentrations of Hg^0, such as near artisanal and small-scale gold mining operations and in some work place environments (Cordy et al. 2011). A few studies have used mobile laboratories for spatially resolved data (Lan et al. 2015) or aircraft and helium airships for semi-continuous measurements aloft (Slemr et al. 2009; Lyman and Jaffe, 2012; Deeds et al. 2013; Landis et al. 2014). Passive air samplers can also provide accurate measurements and improve the resolution and spatial range of data (McLagan et al. 2015). However, these samplers typically require extended deployment times (weeks to months) and are not suited for short-term targeted measurements aloft. Therefore, there remains an urgent need for simple and affordable methods that enable measurements of Hg in air at precise locations.

Probing chemical composition aloft is important for determining the sources, distribution, interactions, and fate of pollutants in the atmosphere. Unmanned aerial vehicles (UAVs) are increasingly being used for a variety of scientific studies, including investigations of pollutants in the lower troposphere (Chang et al. 2016). Whereas fixed wing UAVs have been used to sample the atmosphere over long distances (Corrigan et al. 2008), rotary-wing UAVs (multicopter drones) have several advantages that make them ideal for more localized studies, including

maneuverability (vertical movement and hovering, negotiating confined spaces and limited takeoff terrain), low cost (as low as a few hundred U.S. dollars), lack of engine exhaust for electrically-powered UAVs (no contamination), capability to land on small spaces (e.g. ships and flat rooftops), and placement of more than rotors at the periphery equidistant around a central core (allowing sensors and sampling devices in the center of the craft) (Chang et al. 2016). Indeed, the adaptation of multicopters for air sampling may facilitate precise vertical and spatial contaminant profiling to ferret out point sources and gas leaks (Rossi et al. 2014). In another example, albeit a single rotor UAV, McGonigle et al. 2008 used a gas-powered helicopter with ultraviolet and infrared spectrometers and electrochemical sensors to measure volcanic carbon dioxide fluxes.

Sampling atmospheric Hg with a multicopter allows rapid deployment and may provide a means to better assess poorly characterized and/or intermittent sources of Hg emissions, such as remote landscapes and biomass burning (Friedli et al. 2009). In this study, we modified a common and inexpensive quadcopter for sampling gaseous Hg and evaluated its effectiveness to measure airborne Hg at specific heights and locations aloft. The aim was to optimize and evaluate the approach and to demonstrate application with field measurements near known emission sources. Because this short communication is the first paper on the use of multicopters for atmospheric Hg research, we include commentary on considerations and limitations when sampling gaseous Hg with multicopters. While we report field results, fully characterizing the Hg sources and their emission fluxes, either spatially or temporally, is beyond the scope of this work.

MATERIALS AND METHODS

NOMENCLATURE

Because gold effectively captures all gaseous Hg species that are efficiently transported to its surface, including organic forms of Hg, measurements from gold traps that collect filtered air are referred to as "gaseous" or "vapor phase" Hg. A small percentage of Hg, usually as oxidized Hg species like $HgCl_2$, may adhere to the filter and tubing before the gold trap; however, this is the case for nearly all atmospheric Hg sampling equipment, and gaseous oxidized Hg is typically an order of magnitude lower than gaseous elemental Hg in ambient air (Schroeder and Munthe, 1998). Herein we refer to our measurements as gaseous Hg. Additionally, a drone is generally any unmanned aircraft that can be autonomous or remote controlled, while a multicopter is an unmanned helicopter with greater than two rotors.

SITE DESCRIPTIONS

Concentrations of airborne Hg were determined from near a municipal landfill, a CFPP, and a petroleum refinery. Offsite locations near these facilities were chosen to avoid interfering with federal aviation laws regarding minimum proximity to commercial property and considering predominant wind directions at each site. To avoid interference with aircraft, sampling was restricted >8 km from the nearest airport and to heights of <120 m.

Three Rivers Landfill, located in Pontotoc, Mississippi, is an active municipal solid waste landfill that began operation in 1994. We sampled <200 m downwind of the site on private land (34.299726 N; -89.056689W) on 10 January 2018. The landfill occupies about 0.1 km^2 of land, has a depth of about 33.5 m, and is about one-third full with an estimated capacity of ~13 million metric tons.

The Red Hills CFPP is a 440 MW facility located in Ackerman, MS; it reported a release of 186 kg of Hg in 2010 (USEPA, 2010). The Red Hills facility uses lignite coal mined adjacent to the site. Upwind samples were collected ~5 km northwest near Jeff Busby State Park (33.412487 N, -89.260724 W) and downwind samples ~1.5 km southwest off of Highway 9 (33.3725932 N, -89.1983115 W) on 6 December 2016.

The Valero refinery, located in Memphis, TN, has a capacity of ~195,000 barrels per day and is a major supplier of jet fuel to the FedEx Corporation hub in Memphis. Upwind samples were collected ~3 km southwest near T.O. Fuller State Park (35.068225 N, -90.118496 N) and downwind ~ 250 m north at Martin Luther King Park (35.089112 N, -90.085740 W) on 10 December 2016.

QUADCOPTER MODIFICATION FOR GASEOUS Hg SAMPLING

We modified a popular and inexpensive quadcopter (Phantom 3 Professional, DJI Inc.) for sampling ambient air for gaseous Hg. The camera was removed and the quadcopter was outfitted with an air pump (AirLite, SKC Inc.) and a multiple (quad) tube holder with protective covers (Fig. 1). The holes in the covers were widened to fit a syringe filter (0.2 µm, PTFE). The exact particle size cutoff of the filter is not known because they were designed for a liquid rather than air, which has different fluid dynamics, but it is expected to be close to 0.2 µm.

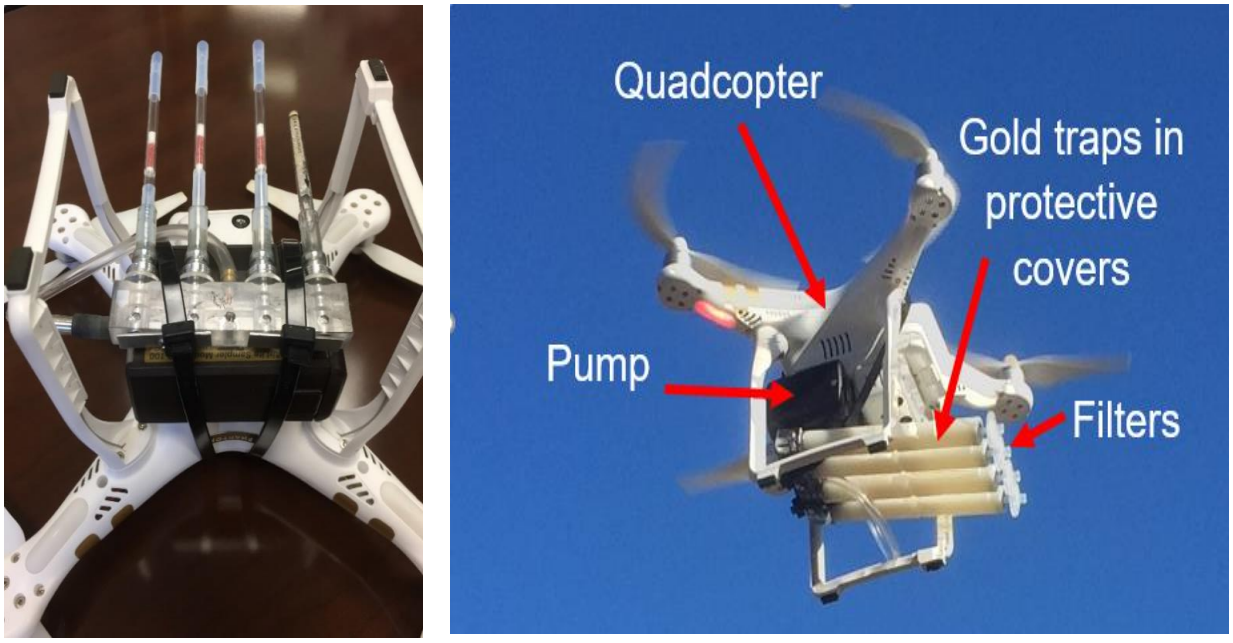

Figure 13. Quadcopter outfitted with sampling equipment. Underneath view showing pump, acrylic quad-tube holder, and three gold-coated cartridges (Hg traps) and a single SO_2 tube without protective tube covers (left), and aerial view showing the quadcopter, pump, tube covers, and syringe filters (right)

Prior to sampling, gold-coated quartz cartridges (Tekran Inc.) were heated in a stream of Hg-free argon (blanked) and sealed with Teflon plugs. Each gold trap has a serial number etched into its glass for identification and tracking, and has heat-shrunk Teflon sleeves on each end that enable easy connection with instrument gas lines. The gold traps were connected to the quad tube holder with a small (~1-2-cm) portion of tygon tubing; the Teflon sleeve being inserted into the tygon tubing to the acrylic holder. The sampling equipment was secured to the quadcopter using zip ties. The air pump was turned on immediately before takeoff and was shut off immediately after landing. No portion of the air sampling apparatus was heated during sampling. The average flight time was about 15 minutes, limited by the battery life. Because the pump was manually turned on and off at ground-level, airborne Hg was collected during UAV transit to the desired sampling height, however, this was <5% of the total sample collection time. Adding a pump that can be remotely turned on and off would allow sampling from only the desired height and

location. For some multicopters, this may be possible by using the remote channels or circuitry of the gimbal for switching on and off the pump. Also, more-costly multicopter drones could provide longer sampling times and have additional carrying capacity. The pump flow rate was set to 300 ml min^{-1}, resulting in about 4-5 L air passing through the gold cartridges. The flow rate was checked using a calibrated rotameter. The gold traps were sealed with Teflon inserts, stored in a fridge at ~4°C, and analyzed the next day by CVAFS, except for the landfill study where the traps were analyzed in the field (both analytical methods are described below).

For sampling near the CFPP and refinery, we used three gold traps and one sulfur dioxide (SO_2) colorimetric tube and collected samples at heights of ~50 m and ~75 m as indicated by the multicopter. With a total of thirteen gold traps available, we were limited to four sampling flights (two upwind and two downwind), with one gold trap as a field (trip) blank. For sampling near the landfill, we used four gold traps per flight.

PROOF-OF-CONCEPT AND FIELD SAMPLING

To verify that the sampling method using the modified quadcopter can detect a point source of Hg emissions, we placed a 100 g pool of liquid Hg in an evaporating dish on the top of a 2.5 m ladder in an open field. For a lateral profile, we hovered the quadcopter outfitted with four gold traps at a height of 3 to 4 m and sampled at approximately 2, 5, and 10 m downwind from the source. We also sampled the ambient (upwind) air for comparison. For the vertical profile, we hovered at heights of approximately 2, 5, and 10 m over the mercury dish.

DETERMINATION OF GASEOUS Hg BY CVAFS AND CALCULATION OF AIRBORNE Hg CONCENTRATIONS

Mercury collected on the gold traps was measured by CVAFS (cold vapor atomic fluorescence spectrometry) following U.S. Environmental Protection Agency Method IO-5 "Sampling and Analysis for Atmospheric Mercury" (USEPA, 1999). This EPA-approved method was established to provide for uniform monitoring of atmospheric mercury levels. Two different instruments were used: a Tekran 2600 Hg analyzer for in-laboratory measurements, and a Brooks Rand TDM-II for field measurements. Both units utilize dual trap desorption modules. Briefly, the gold trap used for sampling was placed within the first heating coil of the instrument and heated in a stream of Hg-free argon. The desorbed Hg was collected onto a second gold trap and it was subsequently heated, releasing the Hg directly into the atomic fluorescence detector system. The instrument was calibrated using a temperature-controlled Hg-vapor calibration source, a digital gas-tight syringe, and a loading rig to transfer a known amount of Hg to a gold-coated trap.

For our later work at the landfill site, we chose to bring the Hg analyzer into the field (Fig. 2). Field measurements are advantageous because analyzing traps in the laboratory limits the number of samples collected to the number of costly traps available and increases the likelihood of contamination during transport and storage. Moreover, it allows sampling and analysis using the same set of gold traps repetitively (in the same sampling configuration) to improve precision, generate more data (~40 min per sampling/analytical cycle), and provides an opportunity to adjust sampling (e.g., heights, locations) based on data obtained in the field. The instrument was setup on a portable table and supplied with high-purity argon via a lecture-bottle

and with power using a 3500 W portable, gas-powered generator. The generator was placed approximately 30 m downwind of the analyzer and did not increase background values.

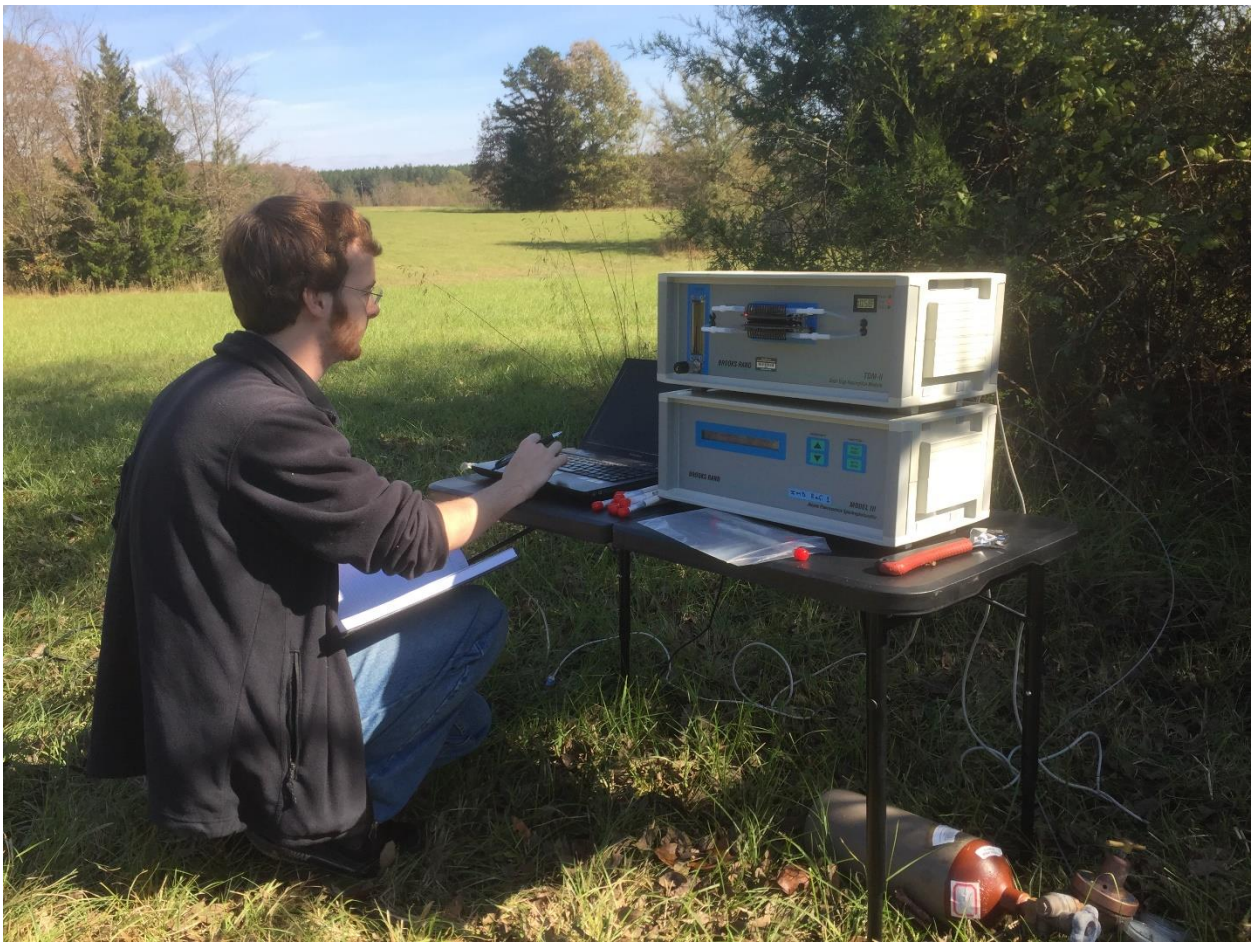

Figure 14. Field analysis of quadcopter-deployed gold-coated Hg traps by CVAFS

Gaseous Hg concentrations were calculated based on amounts of Hg determined using peak areas, the calibration equation, and the volume of air determined using the flow rate and sampling time. The limit of detection (3σ criteria) for both instruments was <0.2 pg of Hg, well below the >5 pg typically collected in the field. Recoveries for external calibration checks were within 15% of expected values. All trip blanks were confirmed to be below the detection limit of

the analyzers. Using two gold traps in series in the sampling apparatus, we found no evidence of breakthrough at the 0.3 L min^{-1} flow rate used in this study. We also compared quadcopter data with continuous monitoring data (Tekran airborne speciation system). Background (ambient) Hg concentrations measured with the quadcopter were 1.7 ± 0.3 ng m^3, similar to the 1.5 ± 0.2 ng m^3 measured previously at the same location under similar conditions and time of year (Jiang et al. 2013). Taken together, this suggests that the quadcopter-sampling scheme does not alter the results and that the method yields reliable gaseous Hg concentration data.

RELATIVE LEVELS OF SULFUR DIOXIDE

As a combustion plume tracer species, SO_2 was qualitatively compared between upwind and downwind sites using a Drager colorimetric tube. Because the flow rate used for the gold traps did not match that required by the SO_2 tube, concentrations read off the tubes are inaccurate and are not reported here. However, tubes showing more color change suggest higher levels of SO_2, which might be expected if sampling occurred in a CFPP plume. Thus, we report the relative distance of color change in millimeters.

RESULTS AND DISCUSSION

PROOF-OF-CONCEPT FOR A POINT SOURCE

To demonstrate capability for detecting a Hg point source, we measured airborne Hg concentrations when sampling progressively closer to a pool of elemental Hg, in both lateral and vertical directions. Mercury has a relatively high vapor pressure (2.613×10^{-7} MPa at 25°C) (Huber et al. 2006), and thus our source would continually emit a detectable quantity of atoms to the atmosphere. Despite the downdraft generated by the quadcopter blades, we observed higher concentrations when sampling closer to the Hg source from both directions (Table 1). This

capability is pertinent for measuring vertical profiles of gaseous Hg from contaminated soils or industrial sites, including municipal landfills. In a separate experiment to evaluate the effect of turbulence in the air column on sampling, we sampled air with and without the UAV rotors active near the point source dish of Hg. The former was obtained while hovering, the later by placing the quadcopter at the same hovering location using a long pole. We found no statistical difference ($p=0.96$) between the groups, indicating that the turbulence in the air column has no measurable effect on sampling. Further, air velocity modeling for the quadcopter suggests that the air parcel above the active rotors being drawn down and sampled extends upward about 1 m (Yoon et al. 2017; Diaz and Yoon, 2018). Thus, the bulk of the air parcel being sampled is relatively close to the true UAV position/height.

Table 1. Summary of proof-of-concept point-source study

Purpose	Source	Wind direction & speed (km hr^{-1})	Position	Gaseous Hg (ng m^{-3}) (n=4)
Vertical Profile	100 g pool of elemental Hg in an evaporating dish on the top of a 9 foot ladder	NE, calm to 4	Ambient	1.2 ± 0.3
			2 m vertical	40.4 ± 4.1
			5 m vertical	5.4 ± 0.3
			10 m vertical	4.5 ± 0.9
Lateral Profile		ESE, 6-8	Ambient / Upwind	1.7 ± 0.3
			2 m Downwind	40.7 ± 1.7
			5 m Downwind	15.8 ± 1.9
			10 m Downwind	5.9 ± 1.4

VERTICAL PROFILE AT A MUNICIPAL LANDFILL

Mercury is in a variety of products that end up in municipal landfills, including fluorescent lights, batteries, electrical components, and thermometers. Mercury emissions from landfills have been poorly investigated despite their high source potential (Kim and Kim 2002). Gaseous Hg concentrations in landfill gas have been measured at μg m^{-3} levels, while methylated species occur at ng m^{-3} levels (Lindberg et al. 2005). One of the most important advantages of sampling with multicopters is its capability to conduct vertical profiles. Here, we measured gaseous Hg concentrations immediately downwind of an active municipal landfill at ground-level, 30 m, 60 m, and 120 m. Average Hg concentrations (± standard deviation) were 5.3 ± 0.5 ng m^{-3}, 5.4 ± 0.7 ng m^{-3}, 4.2 ± 0.2 ng m^{-3}, 2.5 ± 0.2 ng m^{-3}, respectively. This demonstrates that the technique is indeed capable of measuring a vertical gradient above a source known for environmental Hg emissions to the atmosphere. Moreover, the downwind concentrations at ground-level and 30 m above the ground are about four to five times higher than both the rural Ackerman site (1.3 ± 0.2 ng m^{3}) and the background of the region (Jiang et al. 2013), which is consistent with levels reported elsewhere for downwind of the working face of municipal landfills (Lindberg et al. 2005). Others have reported even higher Hg concentrations (up to 420 ng m^{-3}) in municipal landfill gas (Kim and Kim 2002; Tao et al. 2017).

DIFFERENCES IN AMBIENT Hg CONCENTRATIONS BETWEEN AN URBAN (MEMPHIS, TN) AND RURAL (ACKERMANN, MS) AREAS

Whereas atmospheric Hg at both urban and rural areas vary considerably on different temporal scales and with wind patterns, urban concentrations tend to be higher and are often directly impacted by local anthropogenic sources (Liu et al. 2010). Here, we compare data

between the urban (Memphis) site when the wind was coming from a direction over the city, with a rural background (Ackermann) site. The rural (upwind) site is relatively free of anthropogenic sources compared to the urban site, which has chemical and manufacturing plants, as well as traffic emissions. The ambient urban/industrial concentrations are at least double that of rural concentrations (3.3 ± 0.9 ng m^3 versus 1.3 ± 0.2 ng m^3), consistent with other studies of urban-rural differences (e.g., Liu et al. 2010). The concentrations in Memphis are slightly higher than those measured in Detroit (2.5 ± 1.4 ng m^{-3}) (Liu et al. 2010), similar to those reported in Seoul, South Korea (3.7 ± 0.8 ng m^{-3}) (Kim et al. 2013), but lower than Nanjing, China (7.9 ± 7.0 ng m^{-3}) (Zhu et al. 2012). Mercury concentrations in Oxford, MS, nearly equidistant between Memphis and Ackerman, tend to be highest when air masses stem from the Memphis direction (Jiang et al. 2013). A more detailed examination of urban-rural differences is beyond the scope of this methodology study; instead, the reader is referred Jiang et al. (2013) for detailed information on patterns of atmospheric Hg in northern Mississippi or Liu et al. (2010) for urban-rural differences in Hg speciation.

AMBIENT Hg CONCENTRATIONS NEAR A CFPP AND REFINERY

Measurement precision for the sampling flights averaged 12% (range 4.3% to 28%). Because there was no significant difference between them, data from the 50 m and 75 m sampling heights were combined. Although the colorimetric tubes suggest (qualitatively) higher levels of SO_2 downwind of the CFPP, we found no significant difference for gaseous Hg between downwind and upwind locations (Table 2). Gaseous Hg concentrations near the refinery were also similar between downwind and upwind sites. However, given restrictions in airspace around power plants, we sampled over a kilometer from the stacks. Thus, it is likely that

emissions from the power plant were either missed or already greatly diluted. Indeed, the measured concentrations seem to reflect ambient background rather than plume enhanced concentrations, the latter has been shown to increase GEM by as much as 6 ng m^{-3} (Deeds et al. 2013).

Table 2. Summary of gaseous Hg concentrations measured in this study

Source / Location	Wind direction & speed (km hr^{-1})	Relative position or setting	Average Gaseous Hg (ng m^{-3})	SO_2 colorimetric change (mm)
Three Rivers Landfill / Pontotoc, MS	SSE, 4-10	Ground	5.3 ± 0.5 (n=4)	Not Used
		30 m	5.4 ± 0.7 (n=8)	
		60 m	4.3 ± 0.7 (n=4)	
		120 m	2.5 ± 0.3 (n=4)	
Red Hills CFPP / Ackerman, MS	NNW, 10-16	Upwind / background	1.3 ± 0.2 (n=6)	no change
		Downwind	1.5 ± 0.2 (n=6)	7
Valero Refinery / Memphis, TN	SE, 8-12	Upwind / background	3.3 ± 0.9 (n=6)	24
		Downwind	3.2 ± 0.6 (n=6)	23

SAMPLING CONSIDERATIONS, LIMITATIONS, AND FUTURE WORK

Air sampling using multicopters has a number of advantages, including low cost, portability, and the capability to target precise locations aloft that permits vertical profiling. To simplify sampling, we used three quadcopter batteries and a charger that plugs into a vehicle's cigarette lighter, allowing us to charge the batteries between flights or during travel between sampling locations. Adding an additional multicopter drone(s) would greatly increase both the number of samples and the number of locations sampled. While gold traps can be sealed and shipped overnight for analysis, we have shown that using an instrument in the field is feasible

and both increases throughput and informs on sampling plans in near real time. An additional benefit of increased sample throughput is the ability to collect sufficient spatially resolved data to effectively scan an area and create a heat map of airborne Hg.

Other considerations include sampling flight times, which will vary between multicopter types and manufacturers, and will depend on the weight of the sampling equipment. Adding a pump that can be remotely turned on and off would allow sampling from only the desired height and location. Weather is also a factor. High winds can prevent flying, and high humidity and airborne particulates may negatively affect the efficiency of Hg collection. Our quadcopter was able to sample without any difficulty with 26 to 32 km hr^{-1} sustained winds, but operating it above ~40 km hr^{-1} is not advised.

To identify power plant plumes, instruments with fast response and real-time telemetry are required; use of a SO_2 colorimetric tube is insufficient. Employment of electrochemical SO_2 sensors would improve plume detection as demonstrated in volcanic plume studies (McGonigle et al. 2008). While measurements of Hg species in near-field power plant plumes are of interest to study changes in Hg speciation and near-source impacts, how multicopters handle changes in buoyancy within the near-field plume and whether filters clogging will affect pump rates and Hg collection remains to be determined. Similarly, sampling in areas with smoke from biomass burning may prove problematic as the filters will clog with particulates and cause the pump to stall out. Given airspace restrictions around power plants, a collaboration with a CFPP company or the Electric Power Research Institute is needed if multicopters are to be used for sampling near-field plume measurements.

Others have shown that Hg^0 is the dominant form of Hg in downwind plumes of CFPPs (Edgerton et al. 2006); however, there is also significant in-plume (near-field) reduction of Hg

species ($Hg^{II} \rightarrow Hg^{0}$), the degree of which is influenced by the coal's composition and characteristics (Landis et al. 2014). Because of the importance of determining Hg species, future multicopter work should also explore methods to sample Hg species, not just total gaseous Hg. For example, tubes containing Tenax or Carbotrap^{TM} adsorbers can be used to collect volatile organic forms of Hg (e.g., dimethyl-Hg) (Lindberg et al. 2005), although they should be checked to determine to what extent they capture GEM as well. Glass fiber filters can also be incorporated and used for PBM measurements.

CONCLUSION

UAVs are increasingly playing a role in atmospheric and remote sensing studies. This study, for the first time, demonstrated that pilotable multicopter drones can also be adapted to probe Hg concentrations aloft. The technique is robust, has the sensitivity and precision to measure ambient Hg concentrations, and the maneuverability to investigate and characterize specific emission sources. Moreover, because the sampling technique is portable, it may be particularly useful for evaluating Hg emissions from landscapes and transient sources, such as biomass burning, which are poorly characterized and lead to uncertainties in ecosystem budgets. However, airspace and flight restrictions need to be carefully considered before using multicopters for air sampling. The paper includes issues that could benefit from improvements in the future.

ACKNOWLEDGMENTS

We are grateful to Tekran Inc. and Brooks Rand Instruments for helpful advice and technical support, and several anonymous landowners for allowing us to sample from their private property. We thank Ms. Hailey Stewart for help in the field and SKC Inc. for providing us sampling pumps for preliminary work.

CHAPTER THREE

IDENTIFICATION OF POLYMERS AND ORGANIC GUNSHOT RESIDUE IN EVIDENCE FROM 3D-PRINTED FIREARMS USING DART-MASS SPECTROMETRY: A FEASIBILITY STUDY

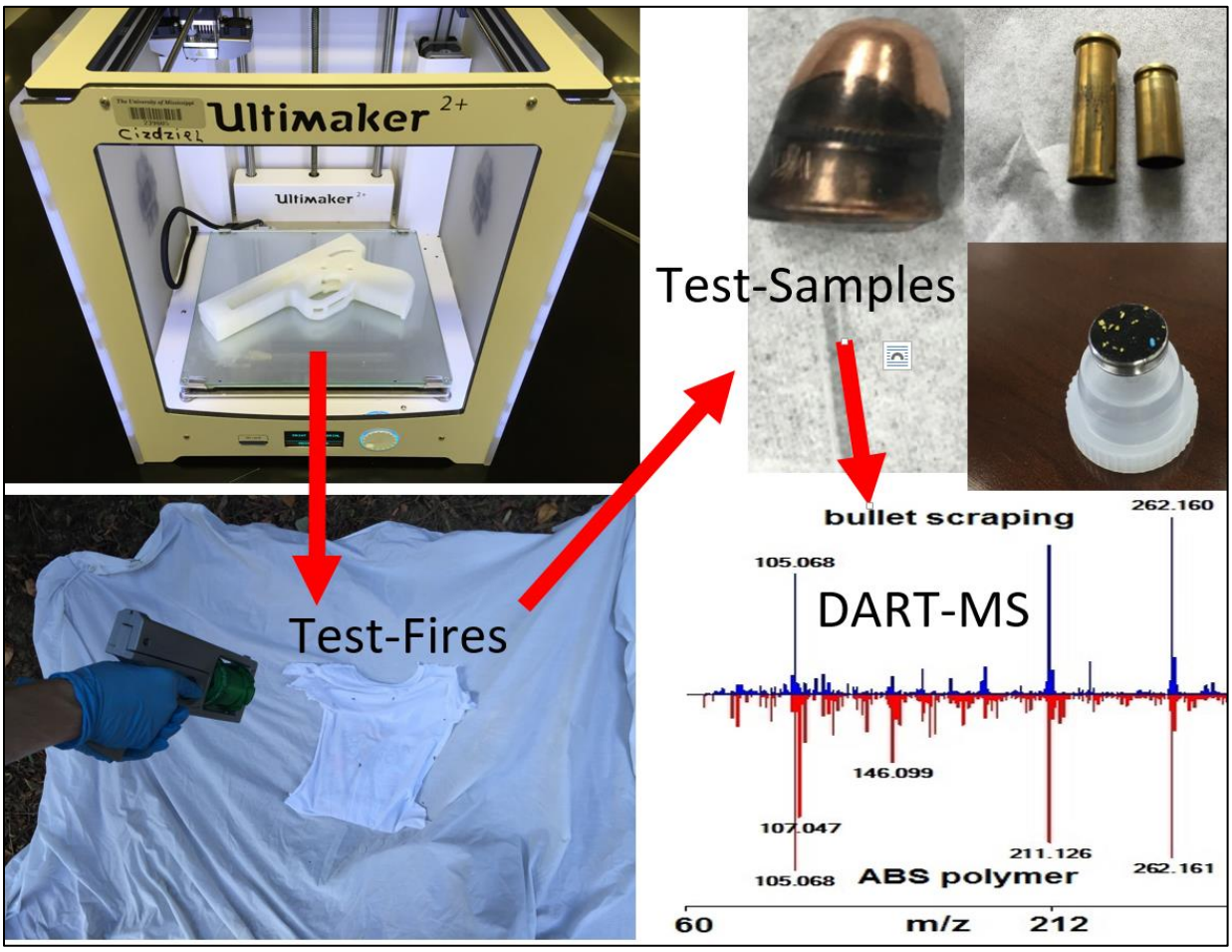

Black O., Cody R., Edwards D., Cizdziel JV (2017) *Forensic Chem*. **5**, 26-32

ABSTRACT

Rapid advances in 3D-printing technology have created an emerging class of firearms. As the movement to self-manufacture firearms with 3D-printing grows, it is reasonable to assume that they will be increasingly used in crimes. Here, we test-fired gun barrels made with acrylonitrile butadiene styrene (ABS), polylactic acid (PLA), polyethylene terephthalate (PETG), chlorinated polyethylene (CPE), and nylon. The resulting cartridge cases, bullets, and gunshot residue (GSR) were examined by direct analysis in real time - mass spectrometry (DART-MS). High-resolution mass spectra detected polymer from the gun barrel on bullets and cartridge casings for a .38 special caliber gun and, to a lesser extent, for the .22 caliber 3D-printed gun. Particles of plastic were identified in some GSR samples collected from clothing used as a backstop for test-fires. DART-MS also readily detected signature organic GSR compounds, including methyl centralite, ethyl centralite, diphenylamine, and nitrocellulose, on recovered bullets, cartridge cases, and in extracts of SEM stubs used to collect GSR from the clothing. Overall, this study demonstrates that analysis of firearm trace evidence using DART-MS deserves more attention, and that the technique may be particularly useful for investigating crimes involving 3D-printed guns.

Keywords: forensic science; 3D-printed guns; DART; mass spectrometry; polymers

INTRODUCTION

Rapid advances in 3D-printing technology have created an emerging class of firearms that we know almost nothing about, forensically speaking. As the movement to self-manufacture firearms with 3D-printing technology grows, and as 3D guns themselves become more functional and reliable, it is reasonable to assume that they will be used increasingly in crimes, especially by individuals who may have less access to traditional guns. Printed plastic guns and bullets are also of concern to public safety because they can potentially go undetected by metal detectors into high security areas, and to criminal justice because they do not bear traceable serial numbers. As the use of 3D-printed guns in crimes grows, criminal justice practitioners will need proven new forensic methods to analyze the particular types of evidence that these guns deposit at crime scenes.

The notion that making a 3D-printed gun is complicated and that the resulting weapon is inefficient is changing. The barrier to the proliferation of do-it-yourself 3D-printed guns has been functionality, but specially-designed bullets and other inventive features have made them one step closer to being widely available to the general public. Already 3D-printed guns have been shown to withstand repeated firing and have been found at crime scenes (Walther 2015, Greenberg 2013, Chiaramonte 2015). Incidents involving 3D-printed guns can be expected to grow as the technology improves, costs decline, and as superior gun blueprints are posted on the Internet. Blueprints for 3D-printed guns first appeared online around 2013 and continue to surface on the internet. The 3D-printable file for the world's first 3D-printed gun, the so-called "Liberator" 3D-printed gun, was downloaded 100,000 times in two days from the high-tech gunsmithing group Defense Distributed Company (Walther 2015). The company removed the files from the website at the request of the U.S. State Department. Whereas such blueprints are

often removed or the web-address blocked, many have been leaked to sites like Pirate Bay where they continue to exist and can potentially be downloaded and stored offline. Effectively, once initially released, such digital files persist indefinitely through download sites and offline storage media (Walther 2015). Moreover, the increased public debate over individual access to firearms can be expected to further increase interest in 3D-printed guns. A report on the security implications of 3D-printed firearms found that law enforcement agencies in many countries are concerned about the ease of access to 3D-printed firearms, which can be created in complete privacy and are difficult to detect with current security measures (Walther 2015). Despite the need for the forensic science community to properly address this emerging class of firearms and the threats it poses, to our knowledge there have been no publications on trace chemical evidence from 3D-printed guns.

DART-MS is a powerful analytical technique that is currently used in many federal, state and private laboratories for forensic applications, including the identification of drugs of abuse, trace evidence analysis, and sexual assault investigations (Lesiak and Shepard 2014, Laramee et al 2007, Musah et al 2012, Cody et al 2005, Chernetsova and Morlock 2011, Laramee et al 2009). DART is a versatile atmospheric pressure ion source allowing the analysis of materials in open air under ambient conditions (Cody et al 2005). Desorbed ions are carried by the gas stream into the sampling orifice of a mass spectrometer. When coupled with a high-resolution mass spectrometer, the system can determine the chemical composition of a sample in its native form, and produce accurate mass spectra with little or no sample preparation. Because so little sample is needed, it can be considered a pseudo-non-destructive technique, allowing the sample to be preserved or used for other analyses.

DART-MS has been used to identify trace particles of explosives in fingerprints (Clemons et al 2013). The technique can measure nitrated propellants and burn stabilizers such as nitroglycerin and dinitrotoluene, in negative-ion mode, and centralites and phthalates in positive-mode (Meyers 2009). In addition, DART-MS can provide "fingerprint" mass spectra for the identification of polymers, their additives, and other materials, and is used at NASA for the identification of spaceflight-related contaminants, including industrial polymers (Loftin 2009, Anderson 2014, Klampfl 2013). However, DART-MS has not been sufficiently applied to GSR and other trace evidence from firearms, in part, because fundamental studies are lacking.

GSR is produced from the combustion of the primer and propellant, and is composed of combustion products, unburned and partially burned propellant, primer particles, as well as lubricants and metal from the cartridge and weapon (Laza et al 2007). Inorganic GSR often includes heavy metals such as lead (Pb), barium (Ba), and antimony (Sb) from the primer, trace metals from metallic parts, and nitrates and nitrites (Laza et al 2007). Organic gunshot residue (OGSR) may contain nitroglycerine, dinitrotoluene, phthalates, ethyl centralite, and diphenylamine, among other compounds (Bell 2013, Goudsmits et al 2015). Some crime laboratories are moving away from traditional (inorganic) GSR testing due to budget constraints, sample backlogs, and concerns regarding interpretation, such as potential environmental sources of particles resembling inorganic primer (Dalby et al 2010, Burleson et al 2009). In addition, "lead-free" contamination has introduced the potential for false negatives with some GSR tests, such as primer GSR analysis by conventional SEM/EDX protocols (Moran and Bell 2014). Recently, several new methods have focused attention on OGSR (Moran and Bell 2014). Advantages of targeting OGSR for analysis include condensates that stick to the skin and are not prone to secondary transfer, multiple target compounds with options for chemical analysis, and

low background which improves limits of detection (Moran and Bell 2014). However, these techniques are often tedious and time-consuming. A relatively new technique that has the capability to detect and identify a wide-range of compounds in GSR is direct analysis in real time (DART) mass spectrometry.

In this study, we fired a gun with barrels made from different polymers and sought to determine whether DART-MS can be used to readily detect and identify traces of polymer and organic GSR compounds on the bullets, cartridge cases, and in GSR collected from clothing.

MATERIAL AND METHODS

FIREARM CONSTRUCTION AND TEST-FIRING EXPERIMENTS

A summary of the experiments and the compounds detected by DART-MS is given in Table 3. The study was conducted in two phases (Figure 15). In phase I, we constructed a crude firearm with a machined polymer barrel (0.359" ID, 2" OD) for proof-of-concept. The .38 special caliber gun consisted of an ABS or Nylon 6/6 polymer for the barrel, a 6061aluminum cap, and a tool steel roll pin. We successfully fired the ABS gun several times and collected GSR, cartridge cases, and the .38 special caliber bullets. However, the Nylon gun broke apart when fired, allowing for only one viable test shot. Because we successfully detected polymer and OGSR compounds on recovered bullets, cartridge cases, and SEM stubs, we proceeded to construct a fully functional 3D-printed firearm for additional testing.

In phase 2, we repeated the study using a 3D-printed .22 caliber firearm generated from "Washbear" blueprint files obtained online (jamesrpatrick.com) and printed using an Ultimaker 2^+ printer with accompanying CURA software. Firearm components were printed in PLA polymer, except the cylinders, which were interchangeable and consisted of four separate

polymers: ABS, PLA, PETG, and CPE. For visual simplicity, the four polymers obtained consisted of different colors, with white, orange, green, and blue corresponding to ABS, PLA, PETG, and CPE respectively. The firing pin was machined from a 1/8" steel drill bit blank using a dremel tool. Polymers were obtained from commercial providers: Ultimaker and MatterHackers.

In both phases of the study GSR was collected from a cotton shirt situated ~0.3 m from the gun using a standard carbon-adhesive GSR stub (Ted Pella Inc.12.7mm SEM pin stub). Spent cartridges, bullets and GSR stubs were wrapped in aluminum foil and shipped to JEOL USA, Inc. for DART-MS analysis.

Figure 15. Phase I test-fire of ABS polymer barrel (top left). Fully 3D-printed gun and interchangeable cylinders composed of blue CPE, white ABS, orange PLA, and green PETG (bottom center). Phase II test-fire of 3D-printed gun (top right)

ACCUTOF-DART ANALYSIS OF CARTRIDGE CASES, BULLETS, AND GSR STUBS

We used an AccuTOF-DART 4G (JEOL USA, Inc., Peabody, MA) time-of-flight mass spectrometer (TOF-MS) for high-resolution mass measurements (resolving power ≈ 10,000, FWHM definition) of cartridge cases, bullets, and GSR stubs (Fig. 2). A melting point (glass capillary) tube was used to scrape the bullet and cartridge cases and then the tube was placed in the DART beam near the sampling inlet orifice of the AccuTOF mass spectrometer. For GSR collected from clothing, we deposited approximately 50 μL of methanol onto the center of the GSR stub using a pipette, and then immediately withdrew the methanol back into the pipette for transfer into a glass sample vial. The 50 μL volume was sufficient to cover the entire surface of the stub without overflow. Approximately 1-3 μL of the methanol were deposited onto the sealed end of a glass melting point tube for analysis in the DART gas stream. A mass spectrum of polyethylene glycol (PEG), with an average molecular weight of 600 g/mol, was used as a reference standard for the mass calibration. The atmospheric pressure interface was operated with the atmospheric pressure interface potentials set to: Orifice 1 = 20 V, Orifice 2 = 5 V, and Ring Lens = 5 V. At these potentials, little to no collision-induced dissociation (CID) occurs and the resulting mass spectra are dominated by protonated molecules ($[M+H]^+$). The RF ion guide voltage was set to 600 V to allow the detection of ions greater than m/z 60. The DART-SVP ion source (IonSense Inc., Saugus, MA) was operated with a helium gas heater temperature of 300°C and exit grid voltage of 250 V. TSS Unity software (Shrader Analytical, Detroit, MI) and Mass Spec Tools software (RBC Software, available from http://www.shop.mass-spec-software.com/) were used for data processing, data interpretation and report generation. Polymers were identified with Mass Mountaineer by matching the DART mass spectra against spectra in a previously compiled custom database that contained DART mass spectra of common polymers,

including the polymers used to construct the 3D-printed firearm components. A summary of the DART experiments carried out is given in Table 3 below.

SCANNING ELECTRON MICROSCOPY AND ENERGY DISPERSIVE SPECTROSCOPY OF GSR STUBS

We used a JSM-IT300LV SEM (JEOL USA, Inc., Peabody, MA) with an Oxford Aztec EDS system with dual X-Max^{N} 80mm^{2} silicon drift detectors to analyze the GSR stubs. The SEM was set to 20kV using the backscatter electron detector for image collection. EDS maps and spectra were then collected.

DIFFERENTIAL SCANNING CALORIMETRY (DSC) OF COMMON 3D-PRINT POLYMERS

DSC analysis was performed on a TA Instruments Q2000. Approximately 5 mg of each polymer was analyzed from 0°C to 250°C followed by 250°C to 0°C with a ramp rate of 30°C min^{-1}. Each sample was run in three replicate cycles.

Table 3. Summary of experiments carried out and compounds detected						
Firearm	Barrel Polymer	DART Mass Spectrometry				SEM
		Cartridge Scraping[1]	Bullet Scraping[1]	GSR on SEM stub[2]		
				Positive Ion Mode	Negative Ion Mode	
Phase I .38 Caliber Machined Barrel	ABS	ABS and OGSR[3]	ABS	OGSR[3]	Not measured	Not measured
	Nylon	Nylon and OGSR[3]	Nylon			
Phase II .22 Caliber 3D-Printed Firearm	ABS	Barrel Polymer and OGSR[3]	ABS	OGSR[3]	Nitro-glycerine	Yes
	PLA		PLA			
	PETG		Polymer not detected			
	CPE					

[1] Measured directly; positive ion mode
[2] Methanol extract; OGSR and nitroglycerine peaks were not detected on a blank SEM stub wash
[3] Organic GSR compounds detected include methyl centralite, ethyl centralite, monomethyl phthalate, and diphenylamine

Table 3 above provides a summary of the major compounds detected by DART-MS. We discuss the results for polymers and OGSR separately below.

RESULTS AND DISCUSSION

DETECTION AND IDENTIFICATION OF POLYMERS

Bullet and cartridge cases from the .38 special caliber gun gave accurate-mass spectra clearly indicating the presence of the polymer used in the gun barrel, as shown by the *m/z* values for major peaks in both the sample and database spectra (Figure 17). Evidence from the gun with the ABS barrel showed all three major spectral peaks (m/z 105.06, 211.12, and 262.16) for the ABS polymer represented in the library spectrum. The nylon 6/6 samples showed both major peaks (*m/z* 227.18 and 452.34), as well as a peak at *m/z* 269.165 corresponding to protonated ethyl centralite. A peak at *m/z* 369.351 is assigned as $C_{27}H_{45}^{+}$ which is commonly associated in DART mass spectra with $[M + H - H_2O]^{+}$ from cholesterol (fingerprints resulting from handling).

Detecting polymer in the trace evidence from the .22 caliber 3D-printed gun was more challenging, perhaps because of the less powerful cartridge used. Another factor that may play a role in how much material is transferred to the bullet and cartridge casing is how tight the cartridge fits in the barrel. Nevertheless, some of the stubs had particles that looked like plastic under a microscope. When those particles were picked out and analyzed by DART-MS, clear spectra were obtained that matched the plastic from the gun.

SEM/EDS analysis of GSR stubs collected in phase II of the study showed small (micron-sized) spherical particles with high levels of Pb and Ba, presumably inorganic GSR condensates, on larger particles (flakes) that had high levels of C and O, presumably partially burnt or unburnt propellant and/or primer (Figure 18). However, using SEM/EDS to distinguish between OGSR and polymer from the 3D-printed gun is problematic given that both are organic and can have a range of particle sizes and morphologies. CPE contains chlorine that may not be present in typical OGSR, and there may be some morphological differences between OGSR and

polymer fragments to key in on, but this requires further investigation and is beyond the scope of this paper. Polymer was not detected in the GSR stub solvent washes; instead, those spectra were dominated by the compounds typical of OGSR discussed earlier. This would likely be the case even if the solvent dissolved small amounts of polymer particles.

DSC was used to characterize common 3D-printer polymers. The DSC melting / crystallizing curves (transition temperatures) were able to distinguish between the types of plastic and were independent of the plastic's color (Supplemental Figure 21, Table 4). A thermal desorption-pyrolysis attachment is commercially available for the DART mass spectrometer, which would make it possible to obtain both thermal desorption profiles and mass spectra on a single sample. This approach may lower the mass spectral background and permit separation of the 3D-printed gun evidence polymer from the GSR stub base polymer. In addition, creating a searchable DART-pyrolysis library spectrum will be useful to identify signature additives such as plasticizers that might aid in identifying specific brands of polymer used.

ORGANIC GSR BY DART-MS

A SEM stub that was not exposed to GSR was extracted with 50 μL of methanol following the same procedure used for the stubs used to sample GSR. Methanol was chosen because it is effective in extracting compounds associated with organic GSR, but it does not dissolve the black adhesive material attached to the SEM stub. In both phases of the study, DART-MS readily detected ethyl centralite, methyl centralite and diphenylamine, commonly found in firearm propellants, on the bullet and cartridge case, as well as in the solvent wash of the GSR stub (Figure 19). In contrast, the blank stub showed trace phthalates and a peak at *m/z* 217.107 corresponding to the elemental composition $C_{10}H_{17}O_5$. The compound responsible for

this peak is not assigned, but the peak was not observed in the stub exposed to GSR. Because positive-ion DART operates by proton transfer, DART is particularly sensitive to compounds with high proton affinities, such as ethyl centralite and diphenylamine that are observed in organic GSR, but it is less sensitive to the background peaks observed in the blank. Both scraping of the material firearm evidence and solvent washes of the GSR stubs were effective in detecting ethyl centralite as shown in Figure 17 and Figure 19A. The presence of both M^+ and MH^+ for diphenylamine and ethyl centralite in the mass spectra is characteristic of compounds that have low ionization energy as well as high proton affinity. The relatively high abundance of ethyl centralite may be associated with the ammunition in these experiments. Because smokeless powder formulations vary with manufacturer and brand, the pattern or organic GSR components is expected to vary for different ammunition (Laramee et al 2009).

A database search of the mass spectrum of the methanol wash of the GSR stub against an in-house DART polymer database returned nitrocellulose as the best match. The peaks observed in the DART database spectrum for nitrocellulose (Figure 20A) are pyrolytic fragments containing only carbon, hydrogen, and oxygen from cellulosic saccharides. Saccharide fragments can be observed for other polysaccharides, such as the cotton from the shirts used as receiving surfaces in these experiments. However, the positive-ion DART mass spectra for nitrocellulose (Figure 20A) shows a clearly different pattern from the positive-ion DART mass spectrum for cotton (Figure 20B). Figure 6C shows a head-to-tail comparison of the measured mass spectrum (top) against the database mass spectrum for nitrocellulose.

Negative-ion DART can provide complementary information about organic GSR by detecting explosives from double-base and triple-base powder. Figure 6A shows the negative-ion DART mass spectrum of the methanol extract from the GSR stub. Nitroglycerine (NG) is

typically detected in DART as an anion adduct, and NG is detected as the nitrate adduct $[M + NO_3]^-$ where the nitrate anion arises from the nitroglycerine itself (Laramee et al 2007). The other peaks in Figure 20B are background peaks that were detected in a methanol wash of a blank SEM stub that had not been used to sample GSR.

Additional studies are needed to optimize DART-MS parameters using experimental design and to explore automated approaches for introducing various firearm evidence samples to create a rapid screening method. Removal or nano-extraction of the selected particles from the GSR stub should minimize organic background and improve selectivity and limits of detection. Adding spectroscopy (e.g. micro-Raman) can give confirmatory information on the same sample.

Figure 16. Categories of trace evidence analyzed in this study. Bullet fired from a gun with a black ABS barrel showing a polymer smear mark and scrape marks from the melting point tube used for DART-MS analysis (left). Cartridge case from the same gun (middle, left shell) showing external black polymer residue, unlike a cartridge case from a traditional gun (middle, right shell). Adhesive stub used to collect GSR and occasionally polymer (colored) fragments from a cotton t-shirt (right)

CONCLUSION

We have shown that DART-MS methods can be used to detect and identify compounds associated with organic GSR as well as polymers from 3D-printed guns in trace evidence. Thus, a spectral library of polymers commonly used in 3D-printing can be used for characterizing samples from crime scenes where a 3D-printed gun is suspected of being involved. Moreover, because DART-MS can rapidly detect OGSR signature compounds on small evidentiary samples, the technique deserves to be further scrutinized as an alternative approach for OGSR analysis.

ACKNOWLEDGEMENTS

We thank the forensic firearm and toolmark professionals at the Mississippi Crime Laboratory for assistance and use of their facility. We are grateful to anonymous reviewers for their insightful comments and helpful suggestions. Scott Watkins at the University of Mississippi Physics department machine shop helped with design and construction of the firearms in phase I. This research was partly funded by an Investment Grant from the Office of Research and Sponsored Programs and the Department of Chemistry and Biochemistry at the University of Mississippi.

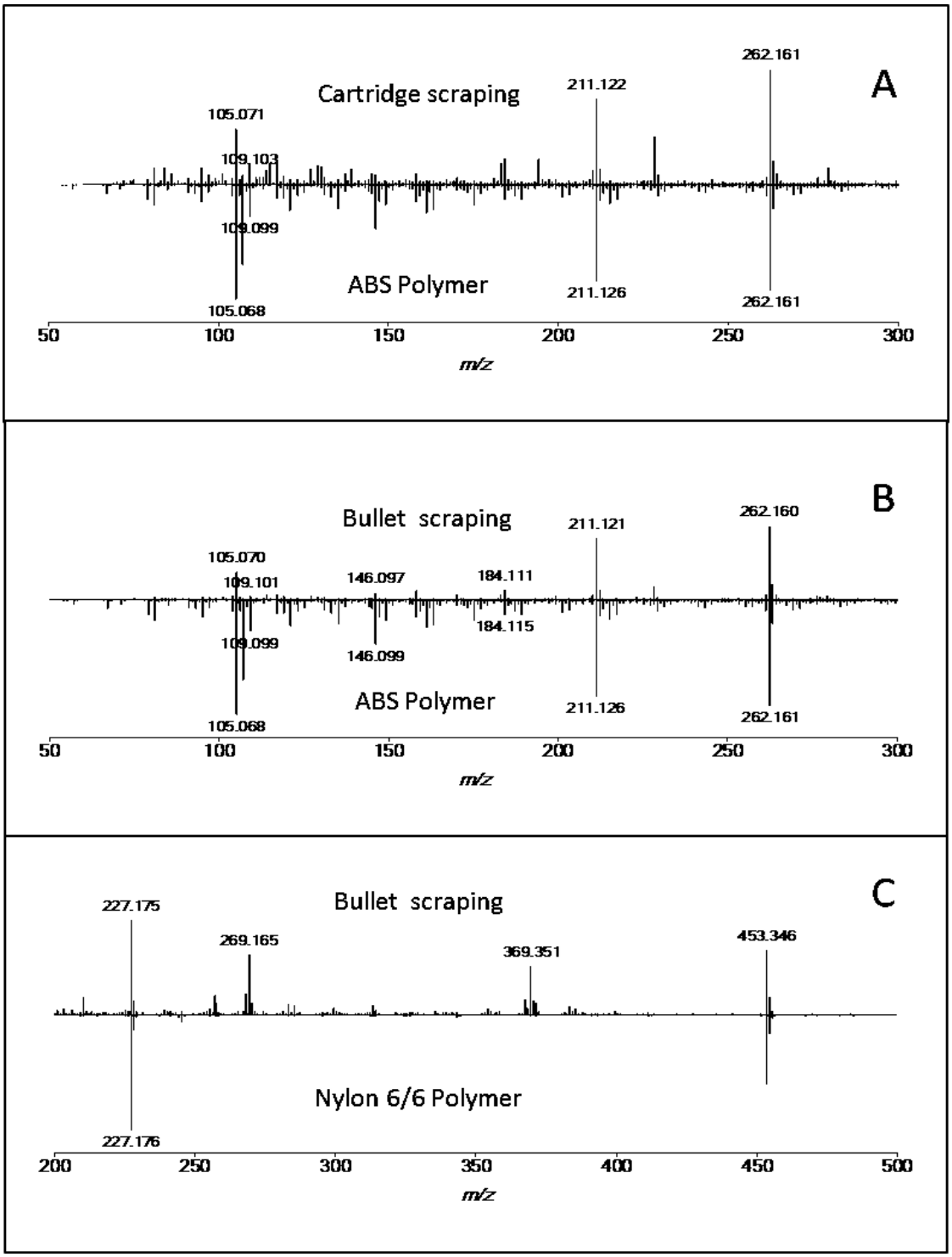

Figure 17. DART-TOF high-resolution mass spectra for cartridge case (A) and bullet (B, C) scrapings. Major peaks were compared to the DART polymer database and correctly identified the polymer used in the barrel. The peaks at *m/z* 269.165 and *m/z* 369.351 in Figure 17C correspond to protonated ethyl centralite and $[M + H - H_2O]^+$ for cholesterol (from handling)

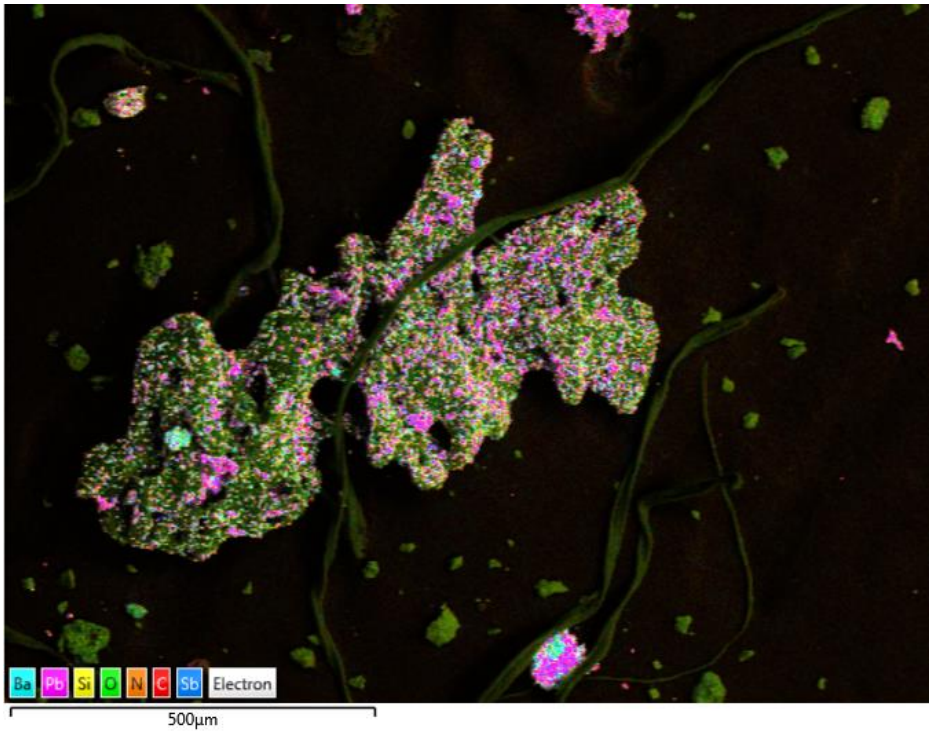

Figure 18. SEM/EDS image showing the distribution of heavy metals (Pb, Ba, and Sb) in GSR from a 3D-printed gun

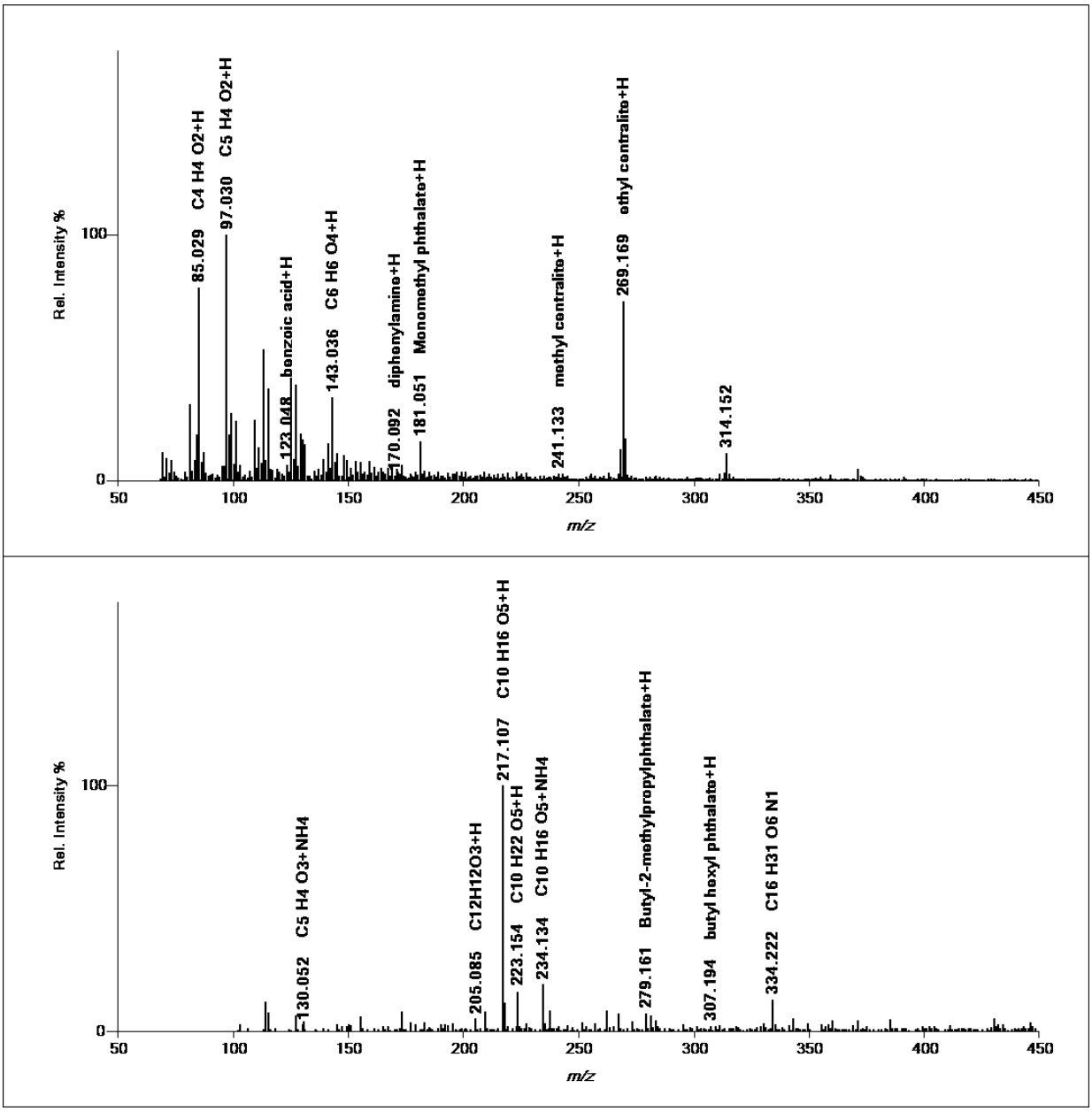

Figure 19.

(A) DART mass spectra of a methanol wash of a GSR stub showing compounds characteristic of OGSR

(B) DART mass spectrum of a methanol wash of a blank GSR stub. The peaks observed in A corresponding to characteristic GSR compounds such as ethyl centralite and diphenylamine are not detected in the blank stub (A). Furthermore, the background peaks in the blank stub (B) are not detected above the chemical noise level in the stub used to sample GSR (A)

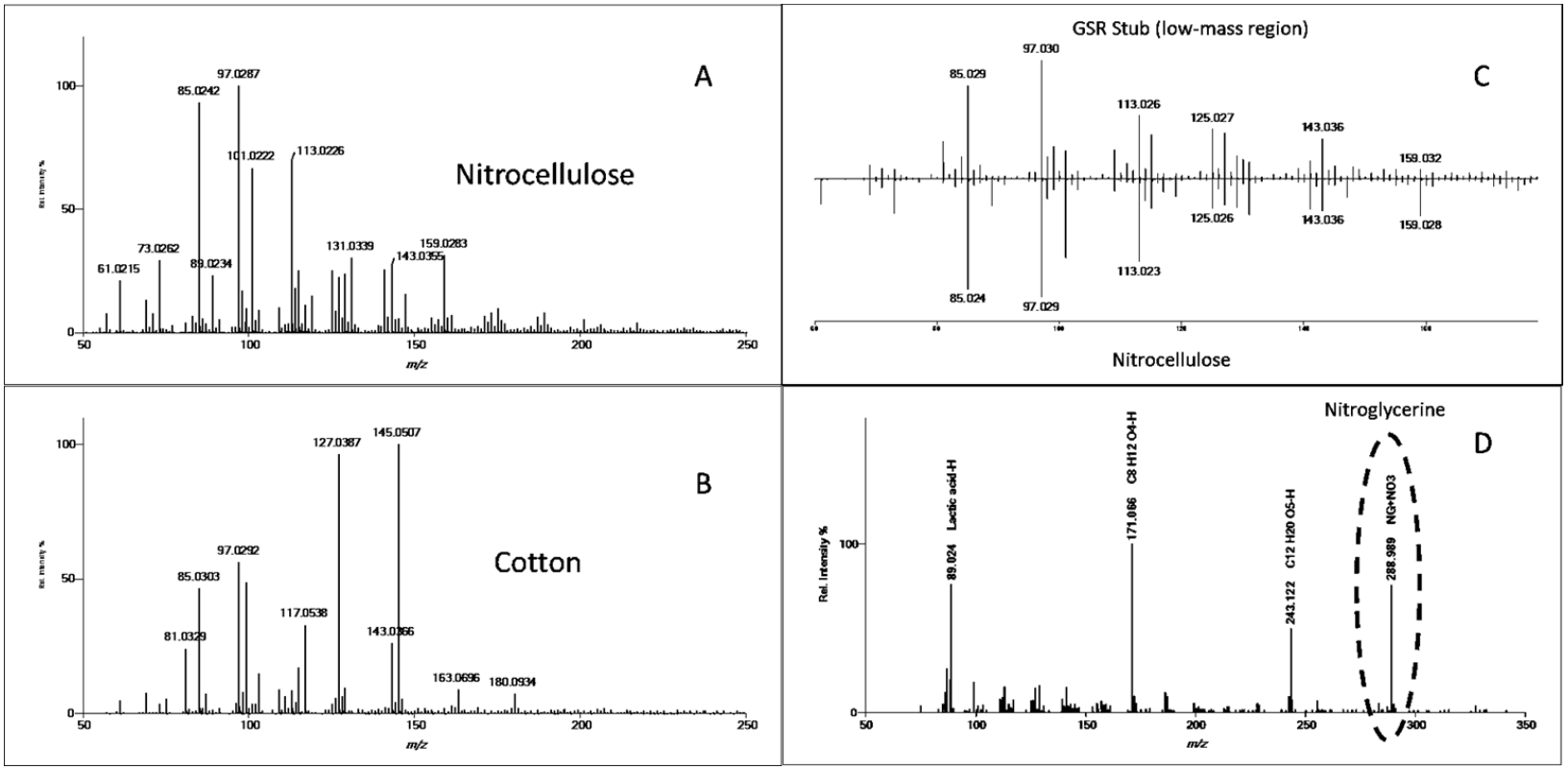

Figure 20.
(A) Positive-ion DART mass spectra of nitrocellulose
(B) Positive-ion DART mass spectrum of cotton
(C) Head-to-tail display showing an expanded view of the low-mass region in the positive-ion DART mass spectrum of the methanol wash from the GSR stub from Figure 5A (top) compared to the positive-ion DART mass spectrum of a nitrocellulose standard.
(D) Negative-ion DART mass spectrum showing nitroglycerine (circled) detected as $[M + NO_3]^-$ at *m/z* 288.989. The other peaks are background peaks present in the methanol wash of a blank SEM stub (not shown)

Table 4. Differential scanning calorimetry transition temperature (mean ± 1 SD; n=3) for common 3D-printer polymers.			
Thermoplastic and Color	**Glass Transition (°C)**	**Crystallization (°C)**	**Melt (°C)**
ABS White	118 ± 5	NP	138 ± 3
ABS Red	115 ± 2	NP	135 ± 2
PLA Blue	66 ± 1	118 ± 1	168 ± 2
PLA Red	67	116	169

***NP = no peak present**

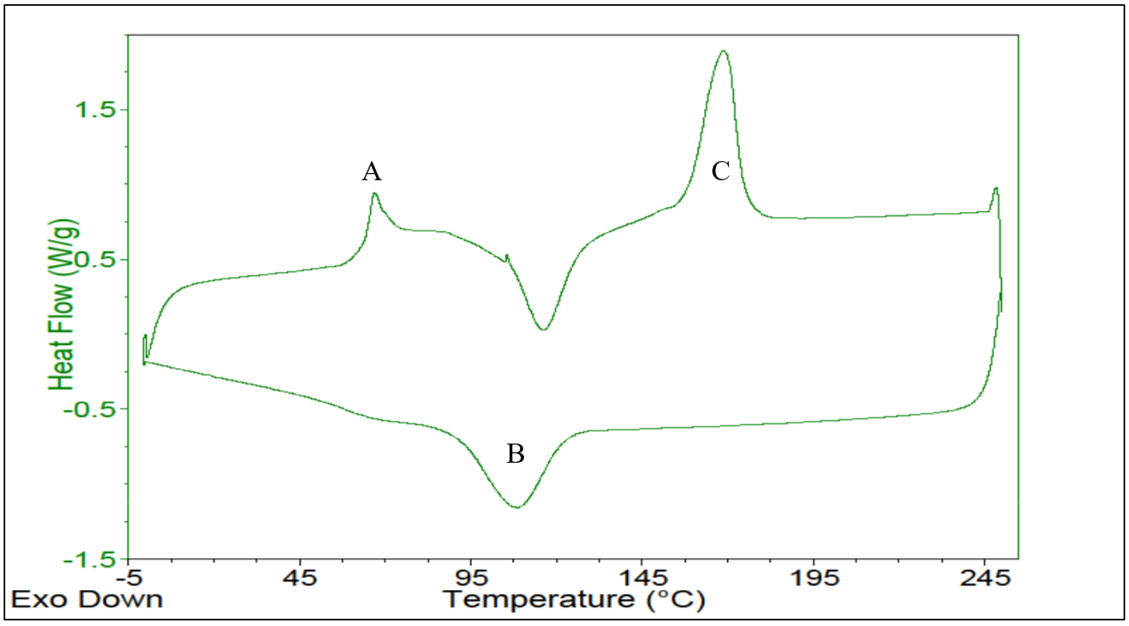

Figure 21. Differential scanning calorimetry plot showing the glass transition peak (A), re-crystallization peak (B), and melting peak (C) for polylactic acid

CHAPTER FOUR

EVALUATION OF TRADITIONAL LATENT PRINT ANALYSIS TECHNIQUES ON 3D-PRINTED FIREARMS

This chapter represents portions of a partnership with Caroline Spencer and Ann-Elodie Robert in Dr. Murrell Godfrey's research group; all contributed equally.

Spencer C., Robert A., **Black O.**, Roy S., Cizdziel J.V., Godfrey M. (2019) Evaluation of fingerprint development techniques on 3D-printed firearms. *Forensic analysis of gunshot residue, 3D-printed firearms, and gunshot injuries: current research and future perspectives.*

INTRODUCTION

3D-printing of firearms has become more common over the last decade with the decrease in cost and increased media attention. As this potential new weapon becomes more prevalent, it is imperative that novel forensic techniques are developed and accepted in the field. Forensic scientists must gain a better understanding of how 3D-printed firearm analysis differs from traditional firearm analysis.

The unique surface morphology of fused deposition modeling (FDM) 3D-printed materials poses challenges to various forensic techniques, particularly fingerprint development. FDM 3D-printers heat the plastic material to a melting point so that it can be ejected from the printer through the extrusion nozzle (Palmero 2013). As the melted plastic is expelled from the printer, it forms the desired 3D object layer by layer until completed. A cross-section of this layered construction is shown in Figure 22. Fingerprint development techniques vary depending on the makeup of the surfaces the fingerprints are deposited on. The inherent ridged nature of 3D-printed objects' surfaces, due to their layered composition, creates potential complications with fingerprint development and visualization that warrant exploration. Here, we explored the applicability of cyanoacrylate ester fuming, or 'super glue fuming', paired with three common fingerprint development techniques including Basic Yellow 40 stain, black fingerprint powder, and black magnetic powder. The use of black magnetic powder in the absence of cyanoacrylate ester fuming was also investigated. We also compared the various strengths and weaknesses of traditional firearm analysis techniques with that of experimental evaluations of 3D-printed firearm analysis methods.

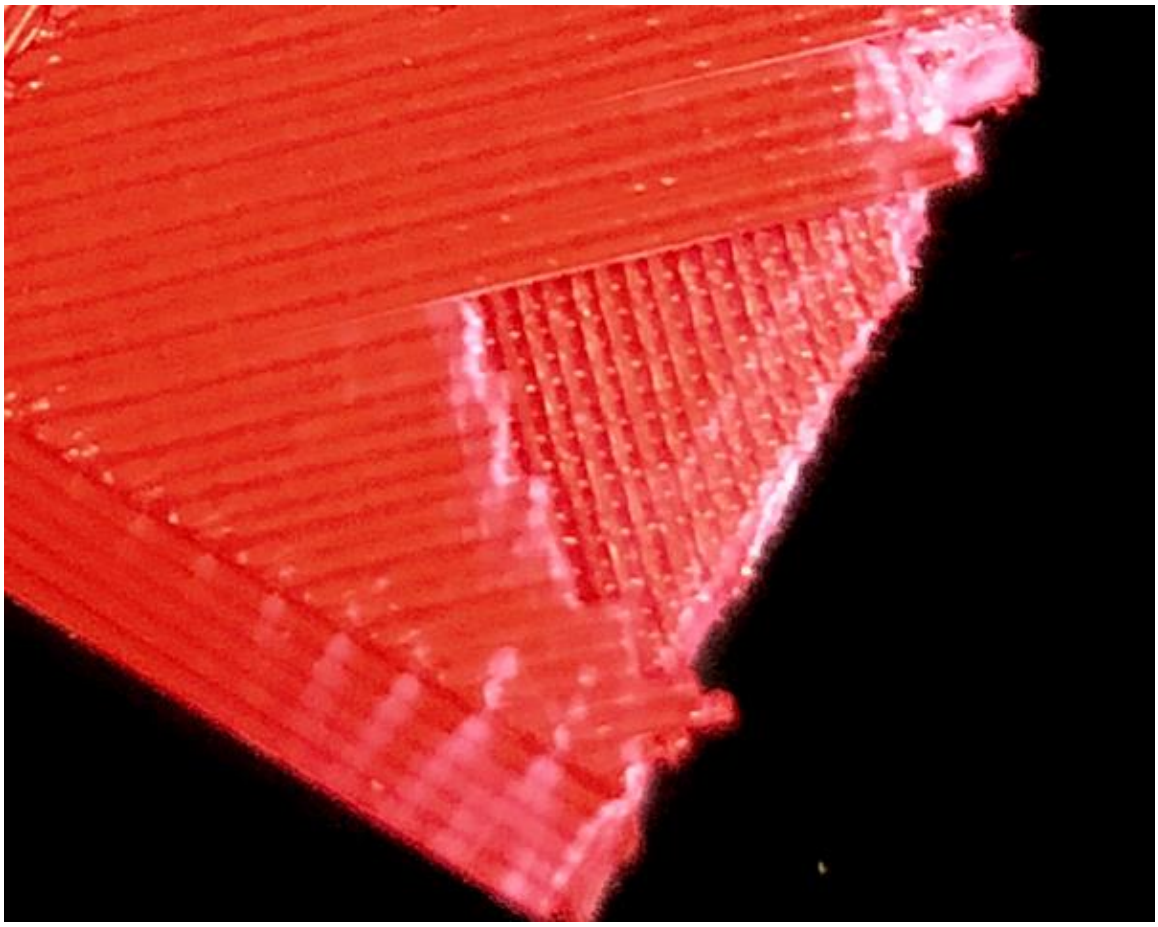

Figure 22. Image showing the layered composition of 3D-printed material

BRIEF BACKGROUND ON FINGERPRINTS AND FINGERPRINT ANALYSIS

Fingerprints are formed from the friction ridge skin that is only found on two areas of the human body, the fingers and palms of the hands and the soles and toes of the feet. The rest of the skin that covers the human body is smooth skin. Friction ridge skin is composed of many layers that contain pores. The ridges and furrows make up the friction ridge skin and consist of both primary and secondary ridges. Primary ridges form under the surface ridges of the skin while the

secondary ridges are found under the furrows on the skin. The raised portions of the friction ridge skin and the deposition of the residue is what leaves behind a latent print (Holder et al 2012). There are three general fingerprint pattern types, which includes arches, loops and whorls, distinguished by the flow of the friction ridges (Field 1959). However, it is the ridge characteristics of the print that make it unique to each individual person. These characteristics called second level detail include, but are not limited to, ridge endings, bifurcations, dots and even scars. The third level detail characteristics like pore location, shape of the outline of the ridges, and creases are all ridge details that can be used for the unique identification of an individual's fingerprint. Fingerprints deposited and found at crime scenes can be divided into three categories; 1) three-dimensional plastic prints, 2) visible prints, and 3) latent, or invisible prints. Plastic prints are formed from the negative ridge impression in a soft material. These fingerprints can be found in items like paint, clay, wax or soap. Visible prints can be seen with the naked eye and occur when a substance like blood, paint or ink is transferred by the finger to a different surface. Latent, or invisible, prints cannot be seen with the naked eye and consist of the residue deposited by the pores that are along the ridges of the print. Latent prints must first be developed before visualization of the fingerprint can take place (Jackson and Jackson 2004).

FINGERPRINT DEVELOPMENT ON TRADITIONAL FIREARMS

Traditional firearms, commonly made of steel and aluminum frames, have well established methods of fingerprint development and visualization. Forensic scientists use methods such as cyanoacrylate ester fuming along with dye stains and powders to develop prints on firearms. These development techniques used to visualize latent prints are sometimes unsuccessful due to the care and maintenance of a traditional firearm that leaves a thin coating of oil on the surface of

the firearm. This oily coating prevents the deposit and usable development of fingerprints (Saferstein 2005). As the popularity of 3D-printed firearms rise, it is necessary to identify and develop new methods that accommodate the textured surface of these firearms.

COMMON FINGERPRINT DEVELOPMENT METHODS

Cyanoacrylate ester fuming is a technique commonly employed for non-porous surfaces including glass, plastic bags, and metals, as seen in traditional firearms. The fuming process uses a cyanoacrylate ester vapor created by heating the cyanoacrylate ester super glue within a fuming chamber (Jackson 1959). Polymerization of the cyanoacrylate ester takes place within the fuming chamber and forms a solid polymer when it makes contact with the moisture in the latent print residue. Fingerprint deposits leave residues of water, amino acids, proteins, fatty acids and lipids, but can also contain food residues, cosmetics or other contaminants (Lee and Gaensslen 2001). The cyanoacrylate ester adheres to the residue of the fingerprints to form the solid polymer along the ridge characteristics of the print (Lee et al 2003).

Following cyanoacrylate ester fuming, one method that can be utilized to visualize fingerprints is the application of laser-sensitive dye stains. Common dye stains include Rhodamine 6G, Ardrox, Basic Yellow 40 and Basic Red. After the cyanoacrylate ester fuming process, the dye stain is applied to the print either by dipping, spraying or immersing the print in the solution. The developed fingerprints can then be visualized with the aid of an alternative light source (ALS). The wavelength of the ALS is adjusted to find the one that is most applicable to the dye stain used to develop the fingerprint [8] When using a dye stain and an ALS, during visualization of the developed print, the proper colored filters and goggles must be used. Filters are used to block out the incident light from the ALS but are also important for the safety of the examiner (Holder et al 2012).

The most common fingerprint development method used in the field and in labs are powders. This method involves the use of inorganic powders that are brushed over the latent print and adhere to the residue left behind (James et al 2009). Fingerprint powder can be used alone to develop fingerprints or following the use of cyanoacrylate ester fuming. The most popular universal powder used on non-porous surfaces of various types of evidence is black latent fingerprint powder. Depending on the color of the surface being examined, other colored powders can be used such as fluorescent, copper or aluminum powders. Traditional firearms typically have a darker colored surface, so colored powders can be used in place of the black fingerprint powder when needed (Fisher and Fisher 2012).

Magnetic fingerprint powders are typically used on textured surfaces, non-magnetic surfaces, and other surfaces where traditional black fingerprint powder would not be useful. These powders consist of the colorants surrounding iron fillings (Safariland 2018). There are many advantages to using magnetic fingerprint powder over nonmagnetic powders. The absence of a traditional fingerprint brush that can often damage a print during the development procedure is a major advantage of using magnetic fingerprint powder. The magnetic powder method uses a magnetic wand that attracts the fine magnetic powder and gently passes the powder over the print. The suspended magnetic powder forms the brush bristles, and this adheres to the residue of the fingerprint, therefore developing it. This method is a less abrasive brushing method when compared to black latent fingerprint powder and is less likely to damage or smear the print (Holder et al 2012, Wertheim 2013). The use of magnetic fingerprint powder results in cleaner prints and this technique does not overdevelop the fingerprint which can be seen with latent fingerprint powder. Most traditional firearms cannot be examined using magnetic fingerprint powder due to the magnetic surface of the firearm. 3D-printed firearms are made from polymer

filament materials. While the material used to create the firearms are considered non-porous, the layering formation of the filaments created by the 3D-printer result in an object that can be considered semi-porous. Because 3D-printed firearms are not magnetic and possess a textured, slightly porous surface, these objects could benefit from the advantages of magnetic fingerprint powder.

The preservation of developed fingerprints is an essential part of fingerprint analysis in the field of forensic science. There are three common preservation methods which include photography, lifting and casting of developed prints. Photographing a developed fingerprint requires the proper camera equipment, lighting, filters and other accessories for visualization. Lifting techniques are commonly used after powdering and consist of some form of lifting tape that is able to remove the powdered print without distorting the developed print. Lifting tapes can vary based on the amount of adhesive, size, color and flexibility. Casting is often used with textured surfaces, curved surfaces, or the human body. Casting has the advantage of being able to mold into the textured details of the surface where the fingerprint is developed (Holder et al 2012).

EXPERIMENTAL METHODS

All firearm frames were printed using the "PM422 Songbird" blueprint, found online. The frames were printed on a Lulzbot Taz 6 3D-printer with a filament extrusion nozzle diameter of 0.5mm, with 70% infill density. Three types of materials were used to print the frames; acrylonitrile butadiene styrene (ABS), nylon 6,6 and polylactic acid (PLA).

Fingerprints were deposited by two volunteers, one male and one female. Each volunteer used their right thumb to deposit the prints after first touching their foreheads to ensure the

opportunity to deposit an oily print. The female volunteer deposited two fingerprints on the left side of each frame, one print on the upper portion of the frame going along the ridges of the firearm, and one print going against the ridges on the grip. The male volunteer repeated the same steps on the right side of each frame. The fingerprint development was done in two phases, as outlined in Figure 23.

PHASE I: FINGERPRINT DEVELOPMENT WITH CYANOACRYLATE ESTER FUMING

Phase I used the most common fingerprinting development method for traditional firearms, super glue fuming using cyanoacrylate ester. All fingerprints on the firearm frames were processed in a Foster+Freeman MVC 3000 fuming chamber. Three different development techniques were then used after the cyanoacrylate ester fuming, which were Basic Yellow 40 stain from Lightning Powder, black latent fingerprint powder from Lightning Powder and black magnetic powder from Lynn Peavey Company. The materials used to print the frames were all white or off-white in color. If another color is used to print the firearm, the color of the stain and powders might have to be adjusted to better develop the print.

Samples were first stained with Basic Yellow 40 and allowed to set. Samples were then visualized, using an alternative light source (ALS), under a 450nm excitation wavelength using a Rofin Polilight PL500, photographed using a Nikon D800 camera and enhanced using Adobe Photoshop CS4. The fingerprints were visualized when using viewing goggles, which act as barrier filters. The goggles are important for proper visualization and for safety purposes when working with an ALS. For light sources of 445-515nm an orange filter is necessary (Polski et al 2011). The Nikon D800 camera also used an orange filter for proper visualization. Following the development with the Basic Yellow 40 stain, the superglued fingerprints were dusted with black

fingerprint powder and black magnetic powder. The prints were then photographed again using a Nikon D800 camera and enhanced using Adobe Photoshop CS4. Before Phase II, each 3D-printed firearm frame was cleaned with methanol to remove the cyanoacrylate ester and as much of the Basic Yellow 40 stain as possible. Results from Phase I displayed the advantage of magnetic powder over the other development methods applied to the frames.

PHASE II: FINGERPRINT DEVELOPMENT WITH MAGNETIC POWDER

In Phase II new prints from the same volunteers were deposited on the surface of the cleaned 3D-printed firearm frames in the same manner as Phase I. Fingerprint development was done using only black magnetic powder. The prints were photographed using a Nikon D800 camera and enhanced using Adobe Photoshop CS4 following the application of the magnetic powder. After Phase II, with the black magnetic powder, two different lifting techniques and a casting method were tried to determine which would be the best method for the textured surface of the 3-D printed firearm frame. The two lifting techniques examined were traditional fingerprint lifting tape and DIFF-Lift lifting tape. The casting material used was AccuTrans Forensic Silicone Casting Material. AccuTrans is made of a vinylpolysiloxane silicone casting material (Accutrans 2018). The lifts and casting were scanned using an Epson Expressions 10000XL scanner.

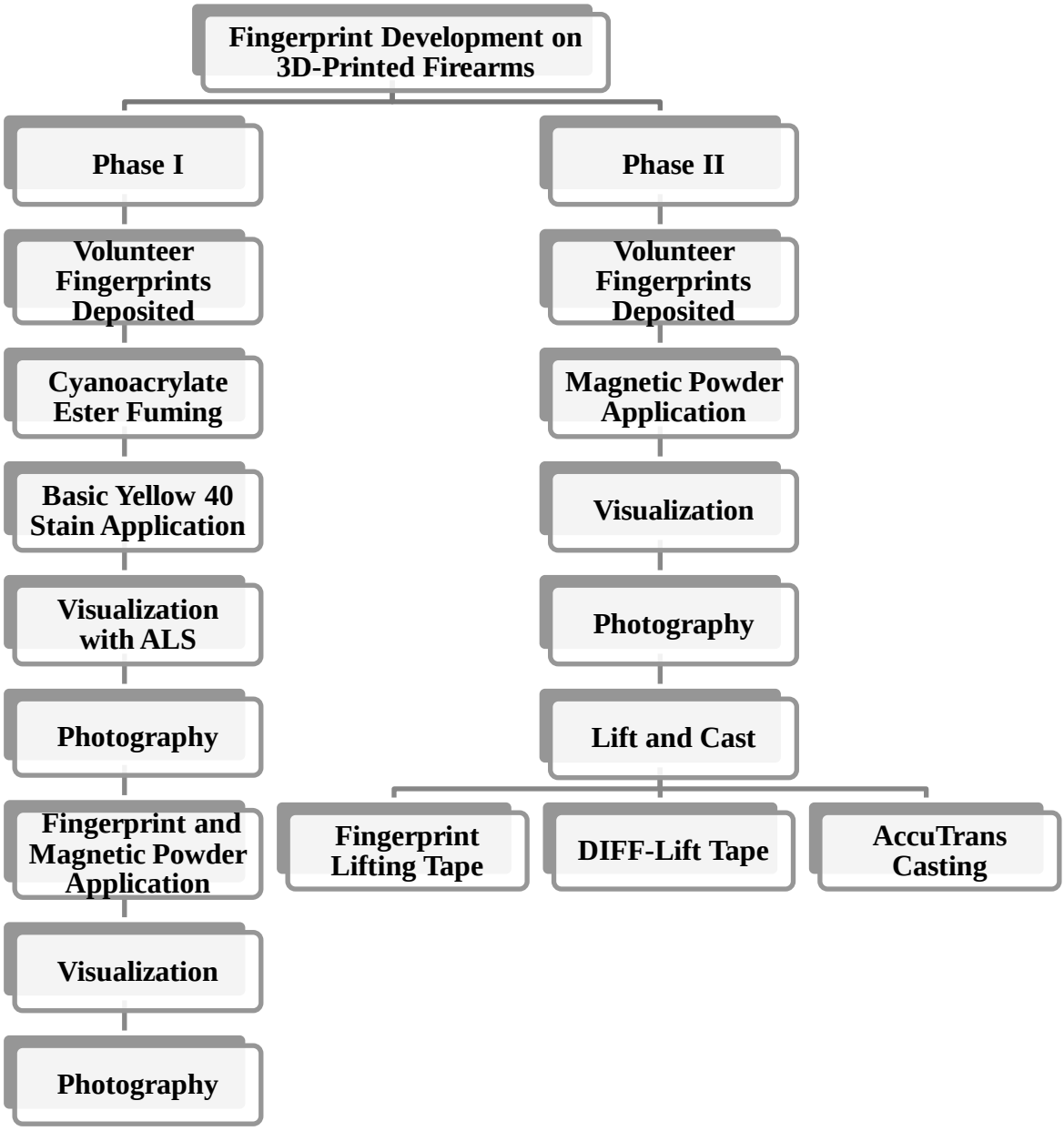

Figure 23. Overview of experimental methods

RESULTS AND DISCUSSION

PHASE I: CYANOACRYLATE ESTER FUMING AND BASIC YELLOW 40 STAINING

The enhanced images in Figure 24 are from the first part of Phase I, development of fingerprints with cyanoacrylate ester fuming followed by Basic Yellow 40 stain on the three 3D-printed firearm frames printed with ABS, nylon and PLA, which were enhanced using Adobe Photoshop CS4. Once the prints were developed it was first determined if the print can be categorized as either first, second or third level detail. First level detail includes pattern type. Based upon how the friction ridges are flowing, fingerprints are classified as arches, loops or whorls. Second level detail includes ridge characteristics like bifurcations, ridge endings, dots, combination of these characteristics, etc. (Polski et al 2011, German 2005). If a print possesses both first level and second level detail and the quality and quantity of second level detail is present, then it is considered an identifiable print. Third level detail cannot be visible in a developed print without first having first and second level detail. Third level detail consist of shapes of the ridge structures of the print and can include the morphology of the print. Morphology refers to the edges, textures, pores and even creases or scars of the fingerprint. Third level detail depends on the clarity of the fingerprint and is not as common as first and second level detail (Holder et al 2012). If only first level detail is present then all that can be said about the developed print is the pattern type, which can be useful for excluding prints during comparison. The prints developed using cyanoacrylate ester fuming along with the Basic Yellow 40 stain, only displayed identifiable prints of second level detail for the frame made of the nylon material. The holes seen in the images of all the prints are characteristics of the design blueprint used to print the firearm frames.

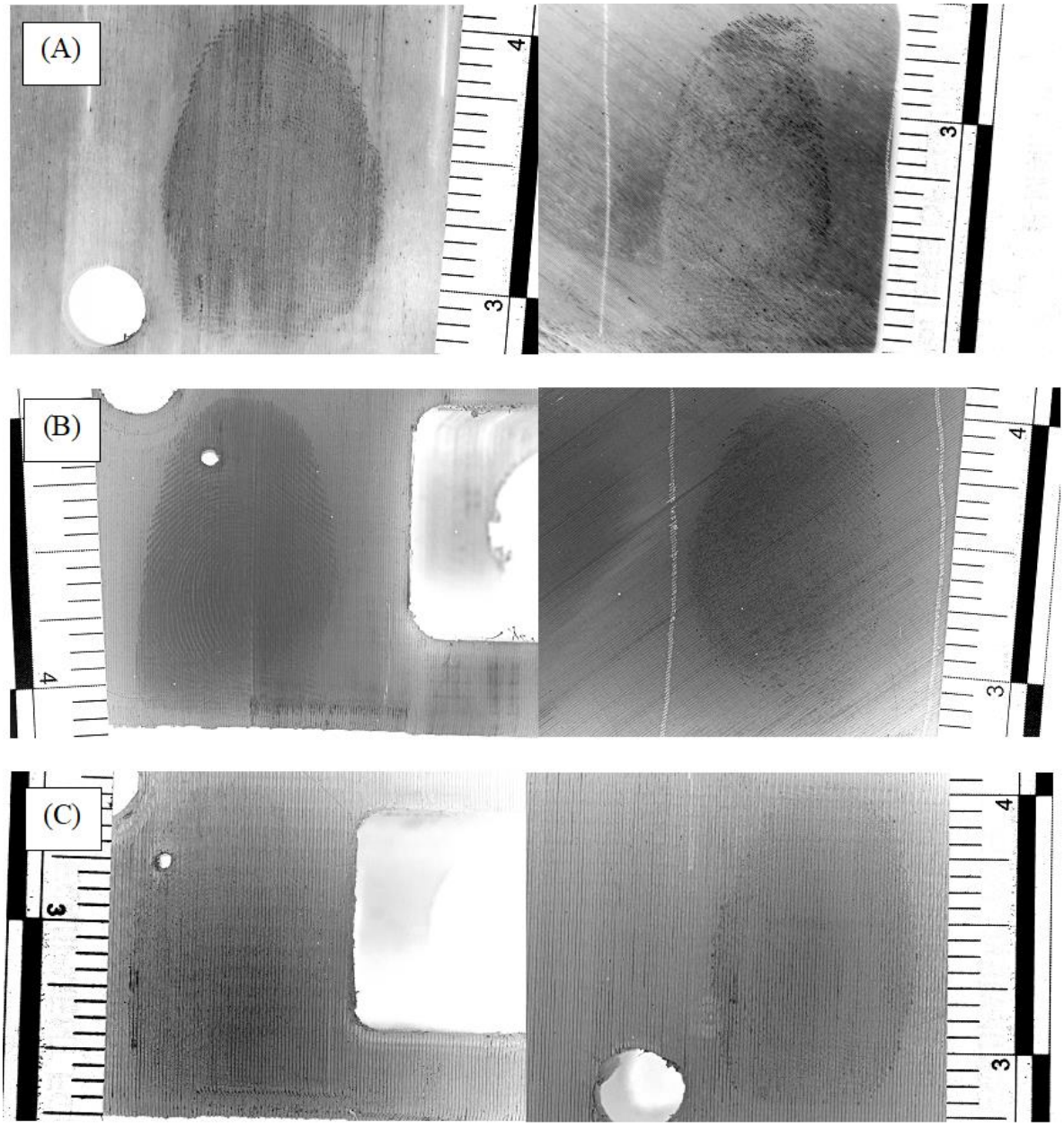

Figure 24. Enhanced images of fingerprints developed with cyanoacrylate ester fuming and Basic Yellow 40 stain on 3D-printed firearm frames made from ABS (A), nylon (B) and PLA (C). Female prints are shown on the left side and male prints are on the right side

PHASE I: CYANOACRYLATE ESTER FUMING WITH BASIC YELLOW 40 STAINING AND POWDERING

Fingerprints developed using the cyanoacrylate ester fuming method and Basic Yellow 40 stain followed by a powder application of either black latent fingerprint powder or black magnetic powder, were also enhanced using Adobe Photoshop CS4, displayed in Figure 25. The powder applications were done after the visualization of the cyanoacrylate ester fumed and Basic Yellow 40 stained prints. The Basic Yellow 40 stain was not removed. When applying the powder to the super glue fumed prints some developed clearer prints with the black magnetic powder over the black latent fingerprint powder. These methods were tried together until a clear print was developed for each sample. With the cyanoacrylate ester fuming development method, the most identifiable prints were developed on the nylon 3D-printed frame, with both Basic Yellow 40 stain and the powder methods. Throughout most of Phase I the 3D-printed frame using the PLA material was unable to produce identifiable prints. However, more ridge detail of the print was able to be seen on the PLA frame when using the magnetic powder compared to the Basic Yellow 40 stain. The PLA material used in the development of the firearm frame resulted in a highly textured surface with deep ridges that made development of the fingerprints more difficult. The ABS firearm frame produced mostly pattern-type prints with the Basic Yellow 40 stain but gave more identifiable prints when using the magnetic powder after cyanoacrylate ester fuming. The nylon frame still has a ridged texture but was considerably smoother than the other frames made of ABS and PLA. When comparing the cyanoacrylate ester fuming development methods, it was determined that cyanoacrylate ester fuming and Basic Yellow 40 staining with black magnetic powders developed more identifiable prints than the cyanoacrylate ester fuming with just the Basic Yellow 40 stain.

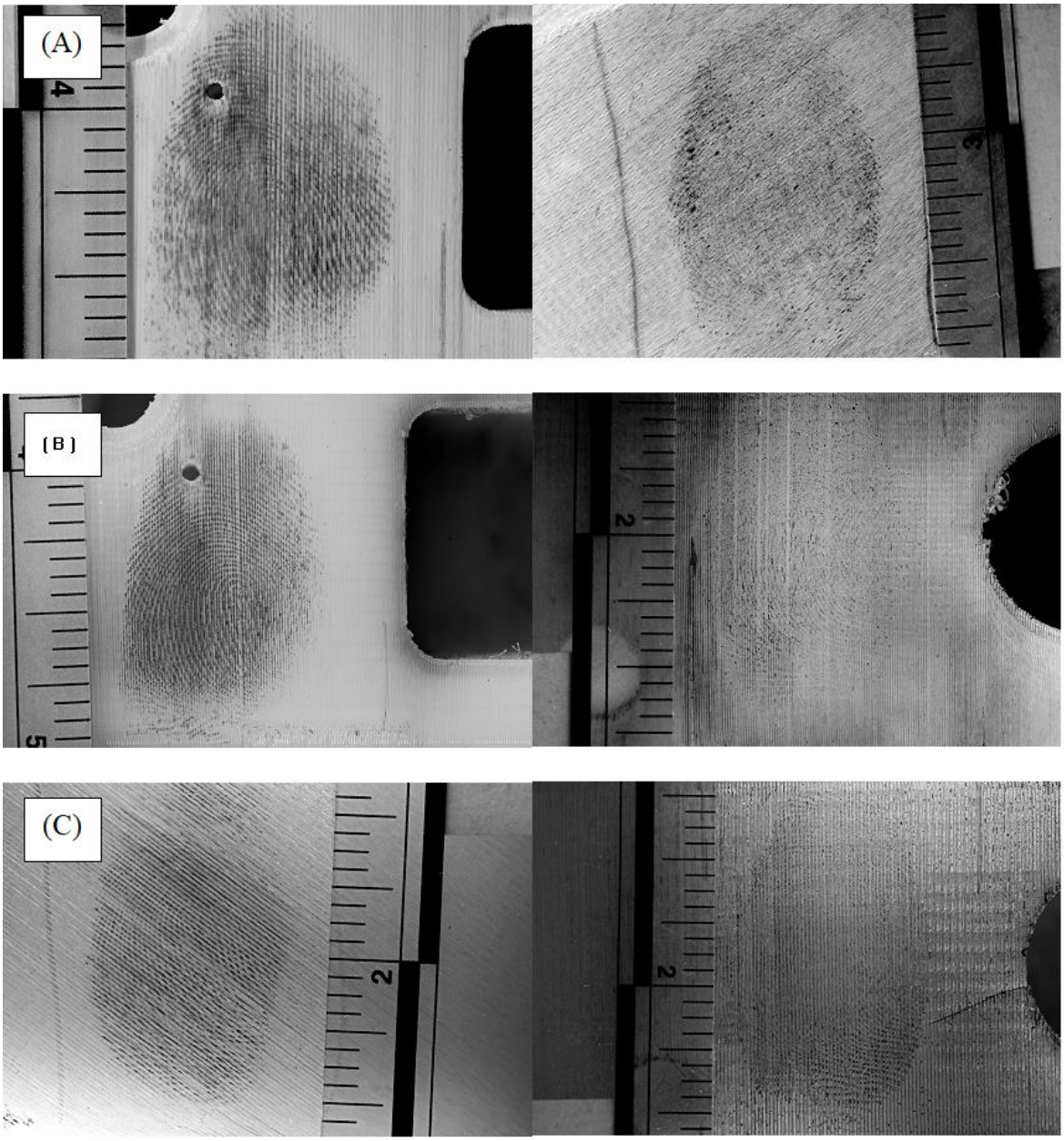

Figure 25. Enhanced images of fingerprints developed with cyanoacrylate ester fuming followed by black fingerprint powder and magnetic powder on the 3D-printed firearm frames made from ABS (A), nylon (B) and PLA (C). Female prints are shown on the left side and male prints are on the right

PHASE II: MAGNETIC POWDER DEVELOPMENT WITHOUT CYANOACRYLATE ESTER FUMING

The results of Phase II, shown in Figure 26 below, demonstrate the advantages of using black magnetic powder on latent prints on 3D-printed firearm frames without the use of cyanoacrylate ester fuming. In Phase I there was difficulty in visualizing an identifiable print from the PLA material using the cyanoacrylate ester fuming. However, without the cyanoacrylate ester fuming, identifiable prints were developed from this frame. The magnetic powder was able to develop fingerprints of high clarity with great ridge characteristics, despite the ridged texture of the frame itself for each 3D-printed firearm frame. Another advantage of the black magnetic powder over the cyanoacrylate ester fuming and development methods used in Phase 1 is the decreased processing time. Cyanoacrylate ester fuming can be time consuming, requiring the setting up of the fuming chamber, reaching the desired temperature and humidity, the fuming process, the ventilation step and finally the use of development methods like Basic Yellow 40 stain and powders, needed to visualize the fingerprints. If the cyanoacrylate ester fuming step is removed and only magnetic powder is used, the development time decreases, only requiring seconds to develop a fingerprint.

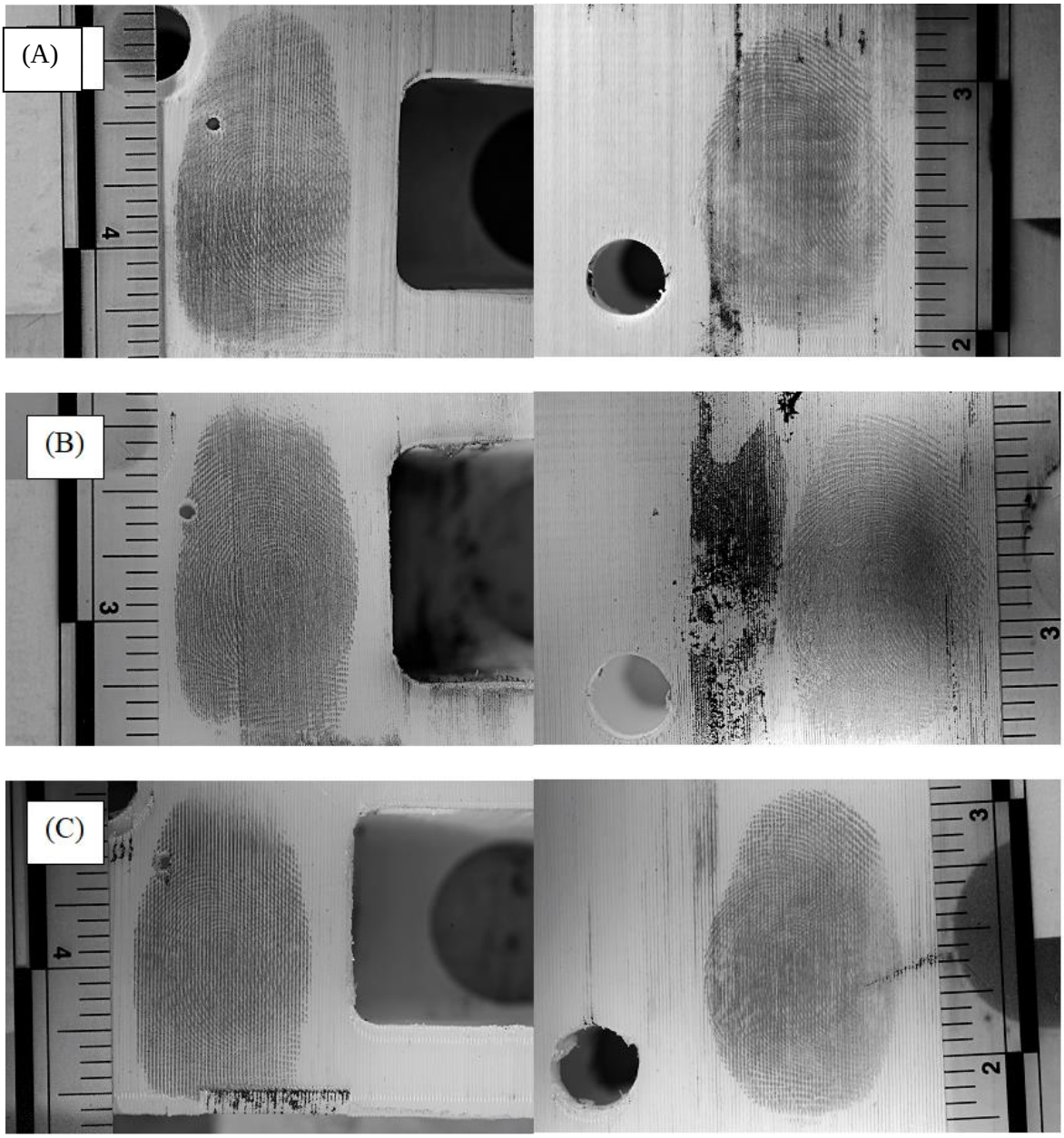

Figure 26. Enhanced images of fingerprints developed with magnetic powder on the 3D-printed frames made from ABS (A), nylon (B) and PLA (C). Female prints are shown on the left side and male prints are on the right

PRESERVATION OF DEVELOPED LATENT FINGERPRINTS

Lifting techniques were examined in Phase II after development with the black magnetic powder, resulting in the images in Figure 27. Two common lifting techniques were utilized; fingerprint lifting tape and DIFF-Lift lifting tape. Of the methods used, the most effective lifting method was determined to be the DIFF-Lift lifting tape. The thicker DIFF-Lift lifting tape is best for the textured surface of the 3D-printed firearm frame as it is able to mold into the ridges of the frame (Diff-Lift citation). Casting material, AccuTrans, was also examined due to the textured surface of the 3D-printed firearm frame. The DIFF-Lift lifting tape still proved to be the better preservation technique for developed fingerprints on 3D-printed firearms. The traditional fingerprint lifting tape and AccuTrans casting lifted too much of the background involving the ridges of the 3D-printed frame that made the ridge characteristics of the fingerprint more difficult to analyze. Development, visualization and photography of the fingerprint on the 3D-printed surface is recommended before any lifting or casting techniques are utilized for preservation of a developed latent print.

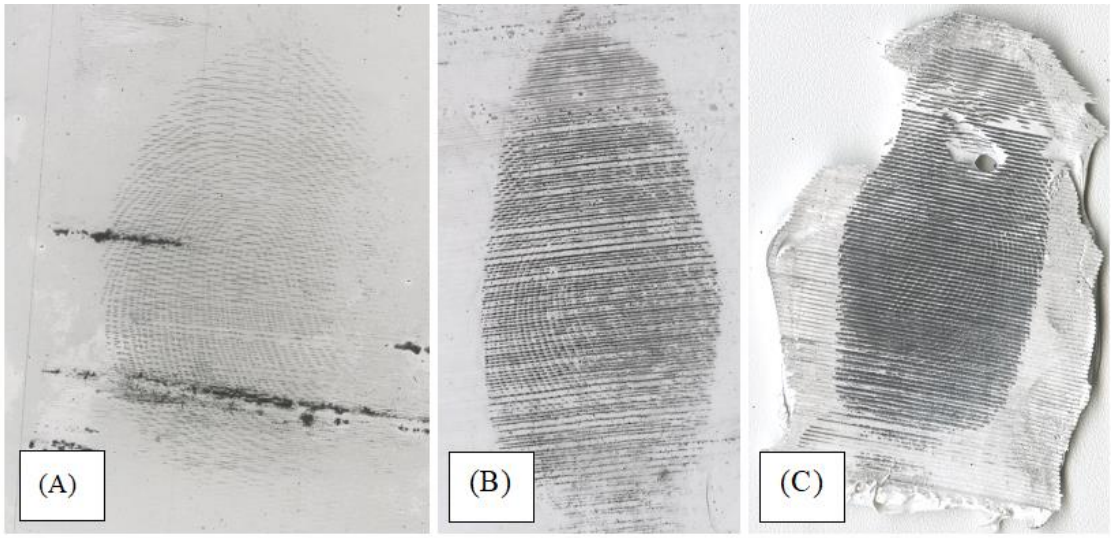

Figure 27. Scanned images from Phase 2 using preservation techniques DIFF-Lift lifting tape (A), fingerprint lifting tape (B) and AccuTrans casting (C)

CONCLUSION

As the popularity of 3D printing has increased over the last decade, so has the concern with 3D-printed weapons. This is particularly applicable to 3D-printed firearms. Forensic science of 3D-printed firearms is a new and undeveloped area and it is necessary for forensic techniques to be examined and adjusted for 3D-printed firearms. We studied three common fingerprint development methods to see how the development methods would be applicable to the textured, semi-porous surfaces of 3D-printed firearm frames. The first two development methods, Phase I, involved first cyanoacrylate ester fuming followed by the application of Basic Yellow 40 stain. Following the fingerprint development and visualization with the Basic Yellow 40 stain, the fingerprints were then further developed with black latent fingerprint powder and magnetic powder. We also examined black magnetic powder without the aid of cyanoacrylate ester

fuming, in Phase II, followed by common preservation techniques. There were two notable conclusions drawn from the results of this study.

- The use of magnetic powder without the aid of cyanoacrylate fuming is the best fingerprint development method for the ridged surface of 3D-printed firearms.
- The best method for preserving a developed fingerprint on a 3D-printed surface is photography, but if the print needs to be preserved off the surface then DIFF-Lift is the favorable preservation method compared to traditional lifting tape and casting.

ACKNOWLEDGEMENTS

This work was supported by Award No. 2017-IJ-CX-001 by the National Institute of Justice, Office of Justice Programs, U.S. Department of Justice. The opinions, findings, and conclusions or recommendations expressed here are those of the authors and do not necessarily reflect those of the U.S. Department of Justice.

CHAPTER FIVE

FORENSIC ANALYSIS OF EVIDENCE FROM .22 AND .38 CALIBER 3D-PRINTED POLYMER FIREARMS

A portion of this work, the application of chemometrics to reference library spectra, was conducted together with Parker Ball, an undergraduate researcher. Publication pending.

ABSTRACT

Despite the recent advancements with 3D-printed firearms, there are few systematic forensic studies on the physical and chemical evidence pertaining to this new class of firearms. This study sought a thorough evaluation of the various forms of trace evidence deposited on and from .22 and .38 caliber 3D-printed firearms using thermal desorption direct analysis in real time mass spectrometry (TD-DART-MS), latent print analysis, gunshot residue (GSR) deposition, and chemometric evaluations. We show that traditional forensic evaluation of firearm and toolmarks (such as barrel striae) can be inconclusive when applied to polymer firearms. Thus, mass spectrometric characterization of the trace polymer evidence is powerful alternative for identifying the use of, and the potentially the sourcing of, a 3D-printed firearm used in the commission of a crime. Using chemometric analysis of spectral data, we conclude that an unknown polymer can be sorted into its base compound classification (ABS, PLA, PETG, Nylon, etc.) This work also produced the first NIST-style reference library of thermal desorption mass spectra for 3D-printer polymers that might be used in the construction of a firearm. We hope that the initial database provided by this study will continue to grow and have further forensic relevance as 3D-printed firearm crime becomes a more mainstream concern.

Keywords: forensic science; 3D-printed guns; DART; mass spectrometry; polymers

INTRODUCTION

With increasing sophistication in 3D-printing technology, there is a new class of firearms that has created unique forensic questions about their polymer-based nature. As 3D-printed firearm designs increase in functionality and reliability, it is reasonable to assume that they will be used increasingly in crimes, especially by individuals who may have less access to traditional firearms. Combined with their lack of serial numbers, 3D-printed firearms present a series of new challenges to traditional forensic practices, demonstrating the need for new forensic methods to analyze and detect the use of this new class of firearms. The objective of this study is to further forensic understanding of 3D-printed firearms by evaluating the applicability of various chemical and physical analysis techniques to the evidence generated by the discharge of a 3D-printed polymer firearm model. The primary hypotheses are that: (1) the use of 3D-printed components will produce inconsistent toolmarks, leading to the need for a different *chemical*-based approach to evidence, instead of the previously established physical microscopy approach; and (2) the individual polymer types that are used in the construction of the firearm will have unique signatures that can be distinguished between lots and/or manufacturer, leading to the creation of a reference library of direct analysis in real time mass spectrometry (DART-MS) spectra that can be used to distinguish the source of a potentially unknown sample of polymer or polymer-containing gunshot residue (GSR) using chemometrics. This work will provide the basis for any future forensic casework involving a 3D-printed firearm, providing forensic practitioners with thoroughly evaluated chemical and physical methods modified to be directly applicable to 3D-printed firearm evidence.

This research further explores our initial findings where the proof-of-concept study found favorable results concluding that DART-MS can positively distinguish between polymer types when GSR resulting from the discharge of differing polymer firearms is collected and analyzed (Black et al 2017). In our 2017 study, bullets, cartridge cases, and SEM stubs collected from the receiving surface of the target were all analyzed and found to contain distinguishable polymeric residues, as well as the expected traditional GSR components stemming from the gunpowder, primer, and manufacturer additives. The following year, Honsberger et al 2018 published part one and two of a study examining the evidence left behind by a "Liberator" .38 caliber printed firearm. The first part of the series confirms that Liberators can be successfully fired and that fragments of polymer are left behind after discharging the weapons. Part two contained similar findings to our own, namely that polymer residue is found on cartridge cases fired through a 3D-printed firearm, and that cartridge cases and barrels are often ruptured during firing. At the time of publishing, Black et al 2017, Honsberger et al 2018, and Honsberger et al 2019 are still the only scientific publications exploring the forensic impact of 3D-printed firearms.

MATERIALS AND METHODS

This study utilized multiple sampling setups and models of polymer firearms, and addresses both physical and chemical evidence. Toolmarks, fingerprints, bullet wipe GSR, and polymer fragments were all analyzed in the course of our study. Where applicable, current forensic methodology was applied to the evidence to better understand the efficacy of current techniques on this new technology, as well as to inform our development of modified methods for future use.

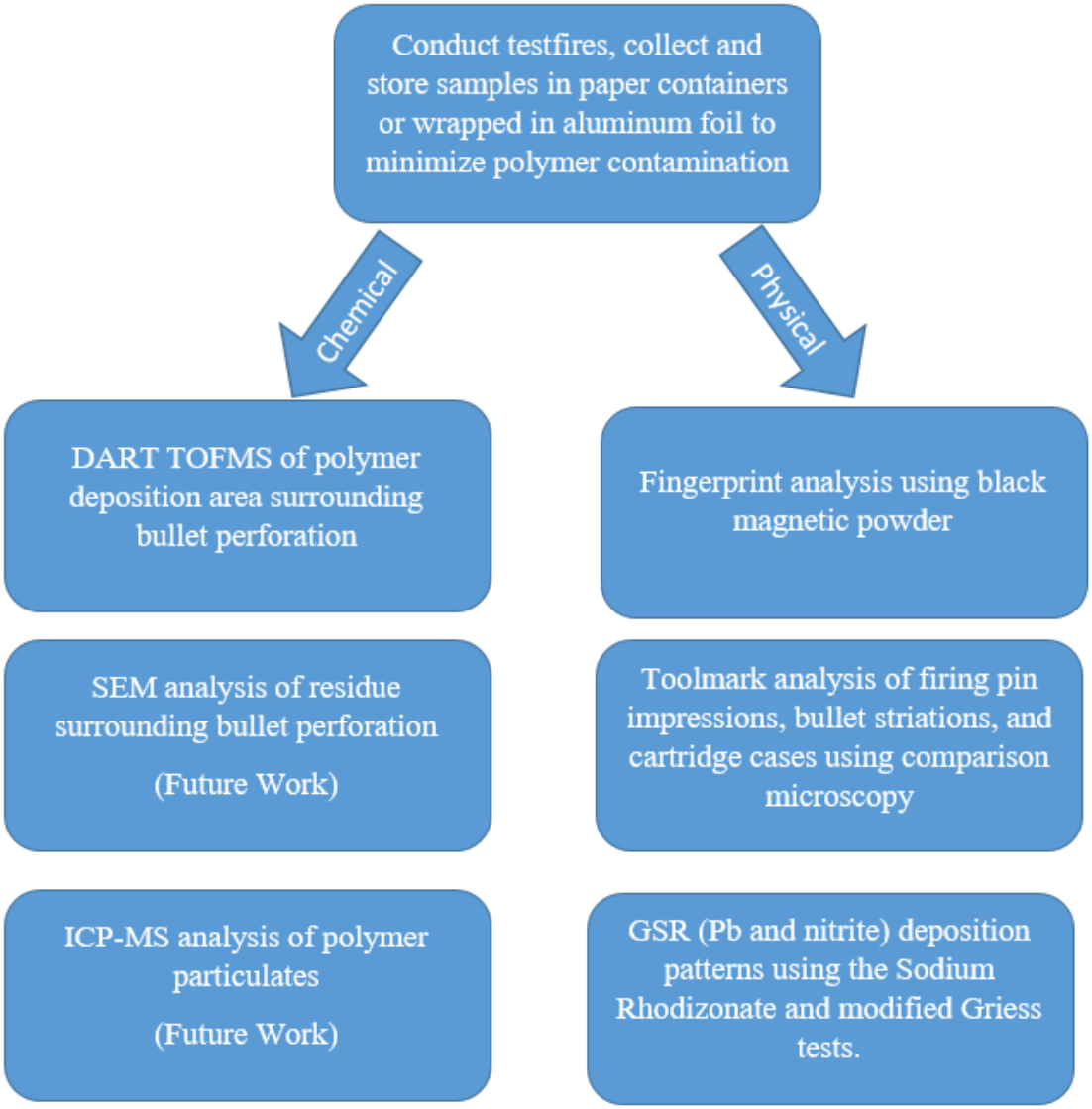

Figure 28. 3D-Printed Firearm Evidence Processing Flowchart (current and future work)

FIREARM CONSTRUCTION

Experiments were conducted in two phases, phase I used .22 caliber 3D-printed firearms, while phase II revisited the .38 caliber machined polymer barrels (0.359” ID, 2” OD) from Black et al 2017. The .22 caliber models consisted of both a revolver style design (“Washbear”) and a semiautomatic style design (“Songbird”); the .stl files for which were found freely available online. Various 3D-print polymers were utilized to produce multiple .22 caliber firearms. Rubber bands were used to power the striker of both firearm designs. The .38 special caliber gun consisted of a barrel composed of acrylonitrile butadiene styrene (ABS), a 6061 aluminum cap, and a tool steel roll pin. The gun was discharged by direct application of force to the steel pin that acted as the firing pin.

Figure 29. Revolver style (left) and pistol style (right) .22 caliber polymer firearms

Figure 30. .38 caliber ABS polymer firearm

.22 CALIBER SAMPLING

All firearm models were discharged in an indoor firearm laboratory by a forensic firearms expert. Thick leather gloves were worn for all testfires. Subsonic CCI brand .22 cartridges were used for all testfires to reduce the pressure load on the barrel and frame. To better distribute the force from the hammer to the firing pin, a thin brass sheet was cut to fit the frame adjacent to the firing pin. The hammer then struck the sheet, allowing for a more efficient transfer of energy. Three rubber bands were used to generate sufficient force from the striker to ignite the primer consistently.

Sampling surfaces consisted of a fresh white t-shirt clamped in place with cardboard backing in front of a bullet catching baffle system. Most of the testfired bullets penetrated the t-shirt, but did not perforate the backside of the material and the cardboard beneath. Lack of perforation was attributed to less efficient pressure channeling down the barrel, due to the expansion of the polymer barrel during discharge. This was consistent for most of the polymer types tested. However, in a few cases, a large amount of pressure was expelled out the side of the barrel during fragmentation events instead of downrange, causing the bullet to lose more velocity and force. Despite these losses of velocity, the firearms were still demonstrated sufficient force to possess wounding potential.

.38 CALIBER SAMPLING

.38 caliber solid, bored-out barrels were again utilized to analyze their discharge for polymer residue (Black et al 2017). Two barrels were used, one of black ABS polymer, and one of white ABS polymer. Sample surfaces consisted of either cardboard cutouts (used as a “blank”) or plain white t-shirts with cardboard backing. The distance from sampling surface to barrel was 1.25m. Sampling was conducted in low-wind outdoor conditions. After conducting the testfires,

all samples were separated by paper to minimize evidence transfer and possible polymer contamination.

CHEMICAL TESTS

DART-MS ANALYSIS OF 3D-PRINT POLYMERS FOR CHEMOMETRICS AND DATABASE CREATION

To facilitate the identification of potential unknown polymer samples collected as evidence, we analyzed a representative sample of 50 polymers that are commercially available as 3D-printer polymers, primarily polylactic acid (PLA), polyethylene terephthalate glycol (PETG), acrylonitrile butadiene styrene (ABS), and nylon (Table 6, Figure 33). Samples were analyzed both directly by DART-AccuTOF, or using a Biochromato IonRocket Thermal Desorption unit paired with the DART-AccuTOF (Figure 31). For the TD-DART analysis, portions of each of the 50 polymers was cut with a scalpel and placed in the TD well of the IonRocket (Table 5). A glass T-junction was used to direct the vaporous decomposition products of the polymers into the heated DART stream (Figure 32). For direct DART analysis, portions of each of the polymers was held with forceps directly in front of the DART source.

Table 5. TD-DART-MS Parameters (JEOL, Peabody MA)

Instrumentation: IonSense DART source, JEOL AccuTOF LC-plus mass spectrometer, Biochromato IonRocket Thermal Desorption unit		
Detector Voltage: 2100V	Acquisition time: 1 second	Ramp: 50°C - 600°C in 5 min. Hold temp at 600°C for 1 min. DART source temp: 250°C
Orifice 1: 20V	Grid Voltage: 350V/150V	
Orifice 2: 20V	RF Ion Guide: 450V	
Ring Lens: 5V	Mass Range: 50-1000 amu	

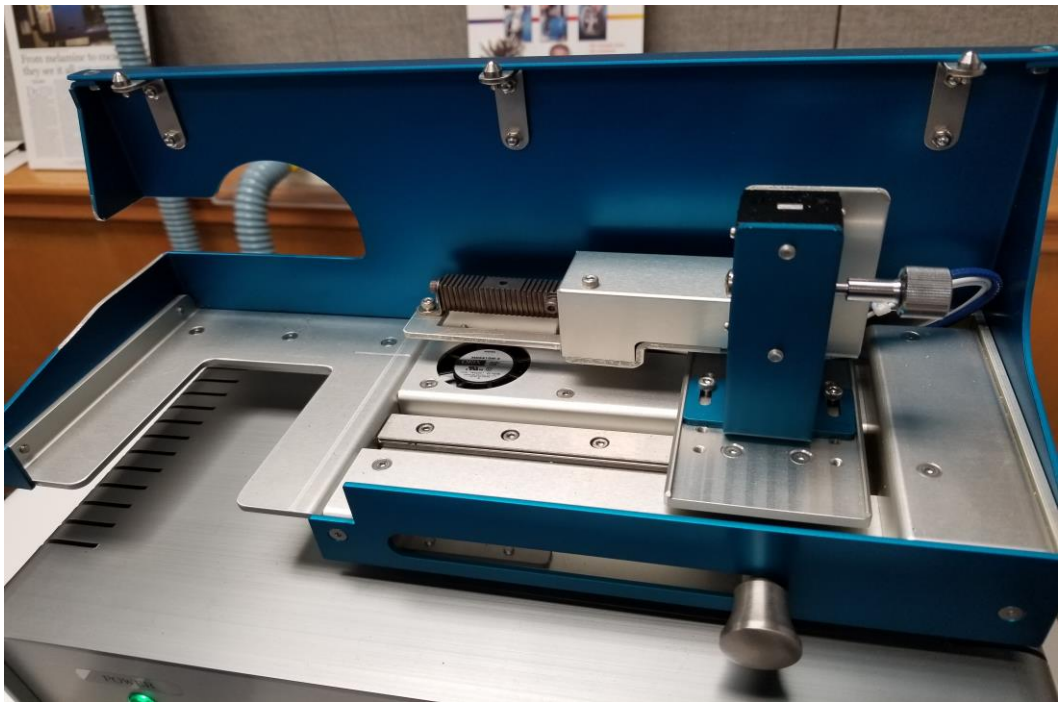

Figure 31. Biochromato IonRocket Thermal Desorption Unit

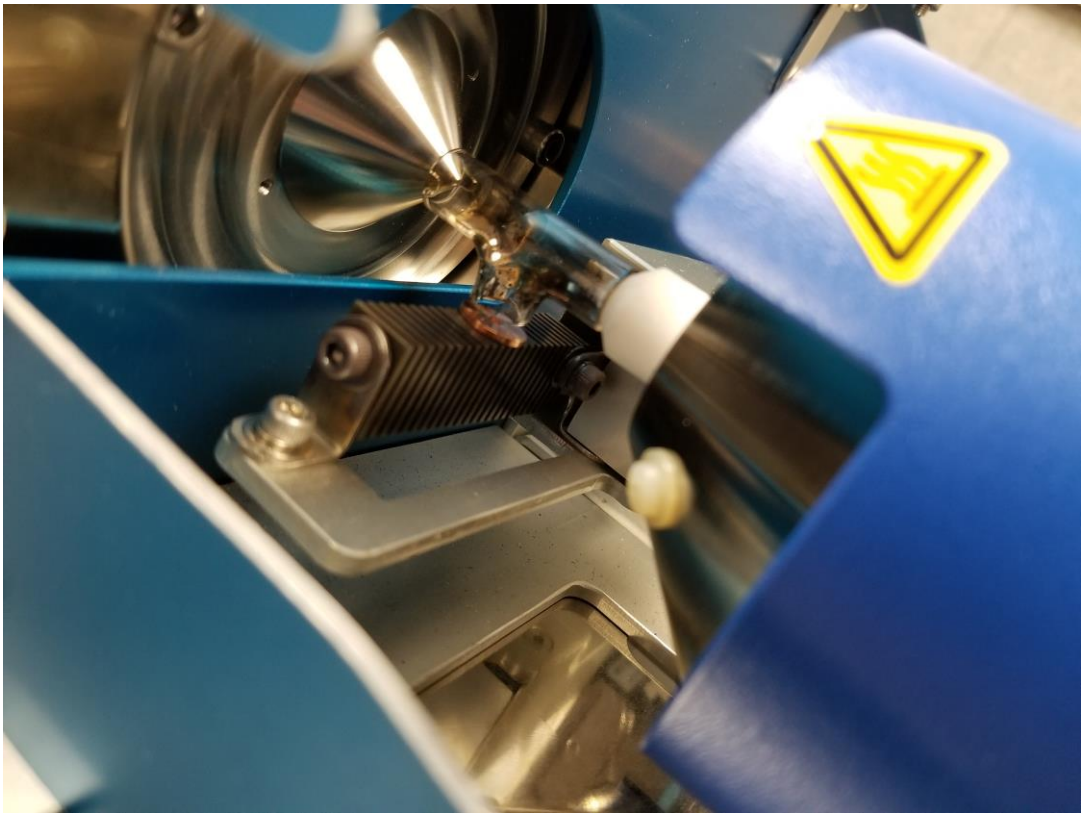

Figure 32. Coupling of IonRocket to DART source at the MS inlet

Treatment of all DART mass spectra was conducted using msAxel Data Processing software (JEOL). All samples were background subtracted against the first 10 seconds of analysis where no samples were introduced to the sample inlet. Background subtracted spectra were exported as "centroided text files" for use in Mass Mountaineer, designed by Dr. Chip Cody (FarHawk). All chemometric evaluations (modified principal component analyses [PCA]) were conducted within Mass Mountaineer, after which 3D-plots were generated. Spectral data was also converted into NIST format .MSP files within Mass Mountaineer and exported to NIST MS Search Program for the generation of two user libraries. Thermal desorption spectral data was exported to Origin data processing software (OriginLab) in order to create 3D-wave plots of m/z vs. intensity, resolved by temperature (z-axis 50°C to 650 °C with 100°C increments).

Table 6. 3D-printer polymers analyzed by mass spectrometry			
PLA		**PETG**	**Miscellaneous**
2. Makergeeks Orange	17. Makeshaper White	6. Hatchbox Red	1. Ninjatek Black TPU
3. Makeshaper Pink	19. ESUN Brown	11. ESUN Black	29. PLAPHAB White PLA/PHA blend
4. Polylite Blue	20. Matterhackers White	16. Hatchbox Blue	35. nGen Black Copolyester
5. Makergeeks Blue	22. Makeshaper Black	18. Makeshaper Grey	38. HT copolyester
7. Makeshaper Purple	24. Matterhackers Blue	23. Makeshaper White	39. Taulman Blue T-glase
8. Makeshaper Blue	25. Makerseries Black	34. ESUN Red	40. Yoyi Black Flexible Filament 7
9. Polylite Red	27. Makeshaper Blue	46. Matterhackers Green	41. GizmoDorks Black Carbon Fiber
10. Makerseries Green	28. Ultimaker Silver	**ABS**	42. DanitiTech Green Silk-like Filament
12. Makeshaper White	30. Makeshaper Blue	21. Hatchbox Red	43. Filament Express Black ASA
13. Makeshaper Orange	36. ColorFabb Woodfill	26. Flashforge Green	44. Taulman Natural Nylon 645
14. ESUN Silver	47. Ultimaker Clear	31. Makeshaper Blue	45. Verbatim White BVOH
15. Matterhackers Gold		32. Matterhackers White	49. Lulzbot Natural Bridge Nylon
		33. Matterhackers Red	50. Taulman Natural Bridge Nylon
		37. IC3D Blue	
		48. 3D-Universe White	

*Numbers correspond to board in Figure 33

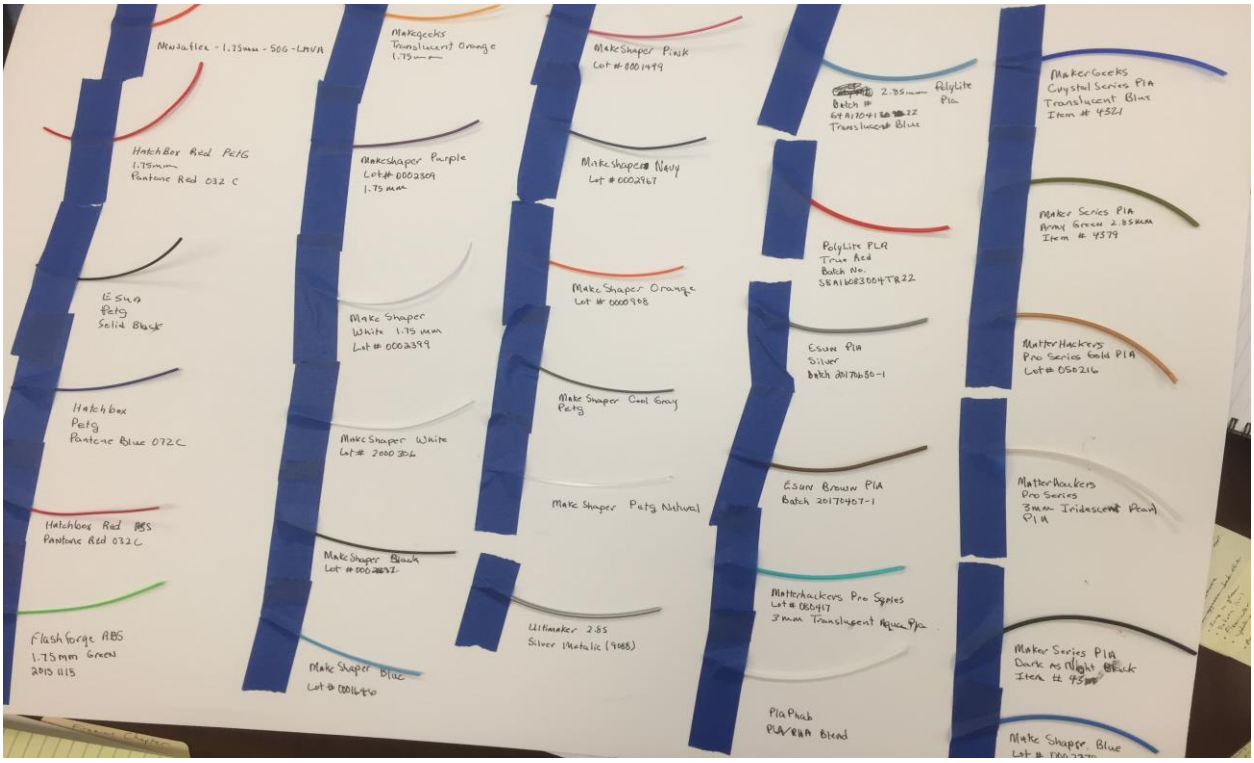

Figure 33. Board containing polymer samples

BULLET WIPE ANALYSIS BY DART-MS

A Bridge Nylon printed .22 caliber firearm was discharged at the Alabama Department of Forensic Sciences firearm and toolmarks shooting range at distances of 3, 3.5, 4.25, 5, and 6 meters onto fresh white t-shirts, respectively. All of the cartridges were subsonic CCI .22s. Samples were discharged one time per shirt. Half of the bullet penetration point was cut vertically with a scalpel, then placed up to the DART source/inlet interface at 250°C (Table 7). Sampling time was set to 2 minutes so that multiple MS peaks could be collected per analysis. Samples from a .38 caliber ABS firearm were also discharged in Oxford, MS and analyzed on a DART-MS at the University of Mississippi. Sampling procedure was the same as stated above for the .22 caliber testfires, with the addition of blank cardboard as an additional testfire surface for background comparison with the t-shirt samples.

Table 7. DART-MS Parameters (University of Mississippi)	
Instrumentation: IonSense DART source, JEOL AccuTOF 4G mass spectrometer	
Detector Voltage: 2100V	Acquisition time: 1 second
Orifice 1: 20V	Grid Voltage: 350V/150V
Orifice 2: 20V	RF Ion Guide: 450V
Ring Lens: 5V	Mass Range: 50-1000 amu
DART source temperature: 250°C	

PHYSICAL TESTS

LATENT PRINT ANALYSIS ON 3D-PRINTED FIREARMS

We analyzed latent print residues on both the "Liberator" and "Songbird" frames. Two different 3D-print designs were chosen to verify that findings were congruent across multiple blueprints, due to the fact that the layering behavior of the individual print might create different surface morphology characteristics, thus affecting the ability of a practitioner to elucidate a viable print. Frames were treated to two different pathways of latent print development: cyanoacrylate fuming, followed by either black powder or magnetic powder; or direct application of black powder or magnetic powder without any prior fuming. Fuming was conducted using the Cyanoacrylate Laboratory Fuming Chamber Kit from Sirchie (Figure 34).

Figure 34. Sirchie Fuming Chamber Kit

(photo credit: https://www.sirchie.com/cyanoacrylate-laboratory-fuming-chamber-kit.html#.XKTts5hKhPY)

GSR DEPOSITION OF LEAD AND NITRITES

Testfire samples were generated the same as listed above for the bullet wipe study, where all GSR samples were collected on fresh white t-shirts with .22 caliber subsonic CCI cartridges. Modified Griess reagent and Sodium Rhodizonate were obtained in powder form (Sigma-Aldrich) and freshly diluted in the laboratory prior to use. The reagents were applied using a liberal spray of each reagent in sequence, using 500mL spray bottles. Samples were allowed to react before images were collected.

RESULTS AND DISCUSSION

IDENTIFICATION OF POLYMERS BY CHEMOMETRIC CLUSTERING

The application of chemometric analysis to the DART spectral interpretation adds another layer of confirmation to the detection and identification of unknown polymer residues. The 50 collected spectra provide a representative grouping of polymer samples, as demonstrated by the ability to parse out the polymers by class using PCA and chemometric software. Modified PCA was chosen to resolve the complex dimensions of the mass spectral parameters into 3-dimensional space for visual pattern recognition. The modified PCA software with Mass Mountaineer utilizes training groups of spectral data, functioning as a pseudo-supervised statistical classification method. The PLA data points exhibited the largest variability between samples in a class (Figure 35 and 36). We primarily attribute this to the wider range of colors and additives present in the PLA samples we analyzed. This could also be partially due to the larger number of PLA samples as compared to PETG, ABS, and the other exotic polymers. All PCA plots shown below were selected for the highest variance percentage covered, and are displayed at the angle that most clearly shows the best separation of points on the first three PC axes. The TD-DART samples produced more distinct clustering by class, when compared to direct DART (Figure 35 vs Figure 36). After evaluating the m/z peaks used as the separation parameters, we found that using most of the individual samples' spectra created plots that accounted for 60-80% of the variability of the data set, although some of the plots with greater variance covered generated less visually distinct clusters than those shown below (Figure 35 and 36).

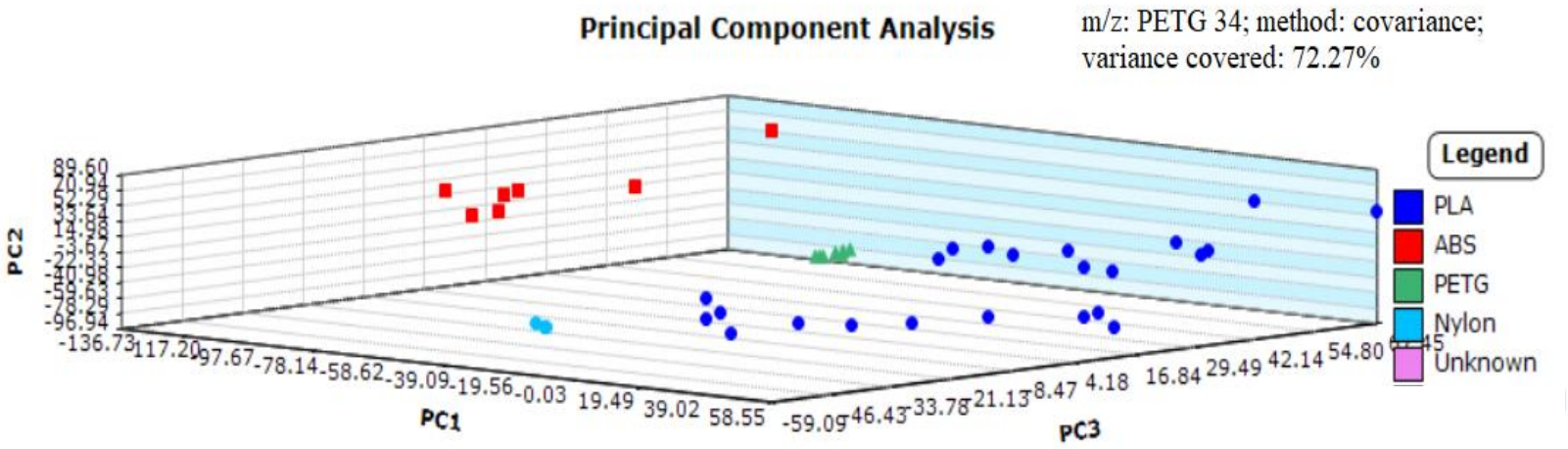

Figure 35. PCA plot for all polymers analyzed by TD-DART-MS (n=40)

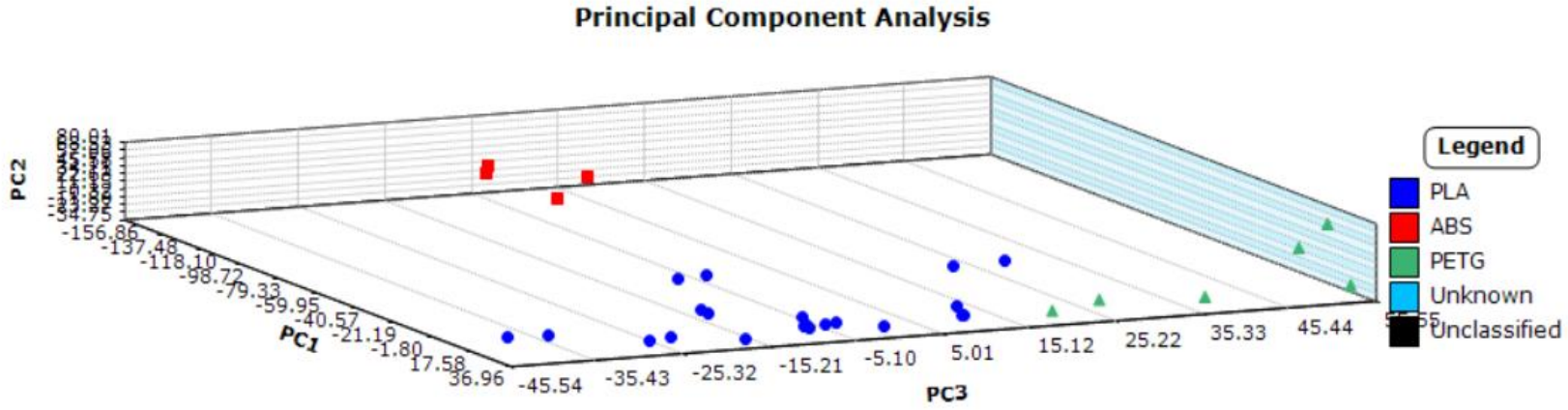

Figure 36. PCA plot for all polymers analyzed by DART-MS (n=34

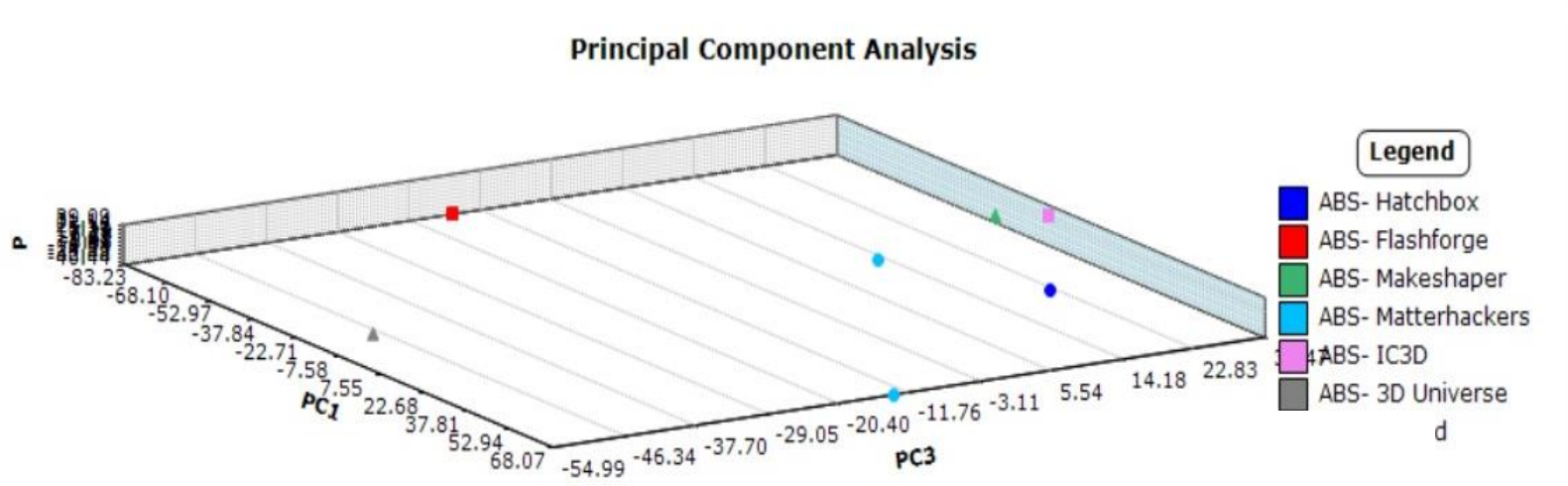

Figure 37. PCA plot of TD-DART-MS for ABS by manufacturer (n=7)

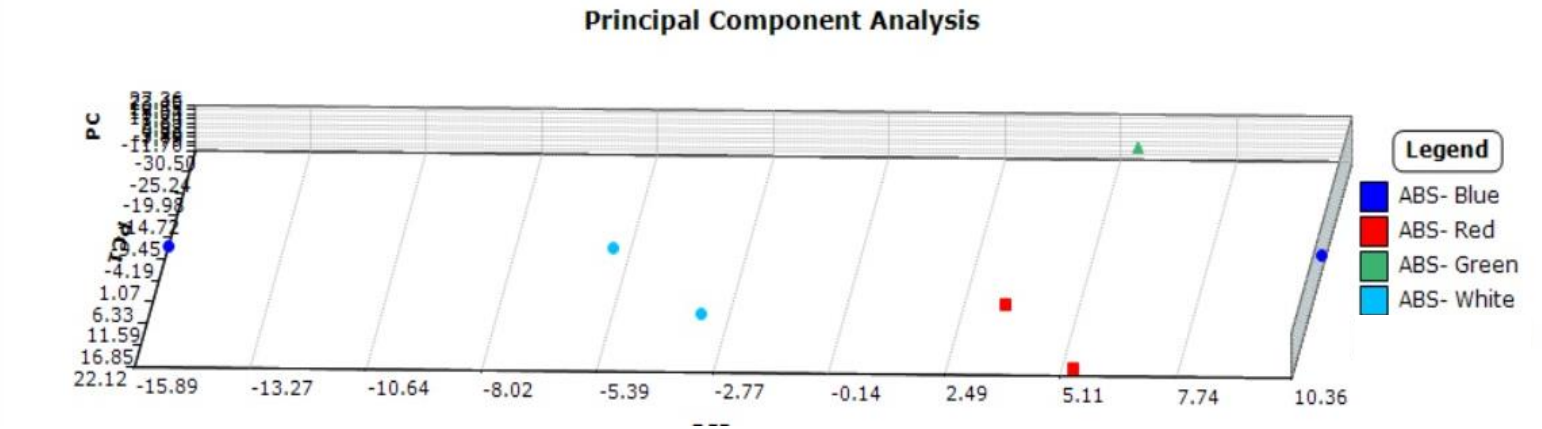

Figure 38. PCA plot of TD-DART-MS data for ABS by color* (n=7)

***ABS "blue" is actually one blue and one navy sample, thus the degree of separation**

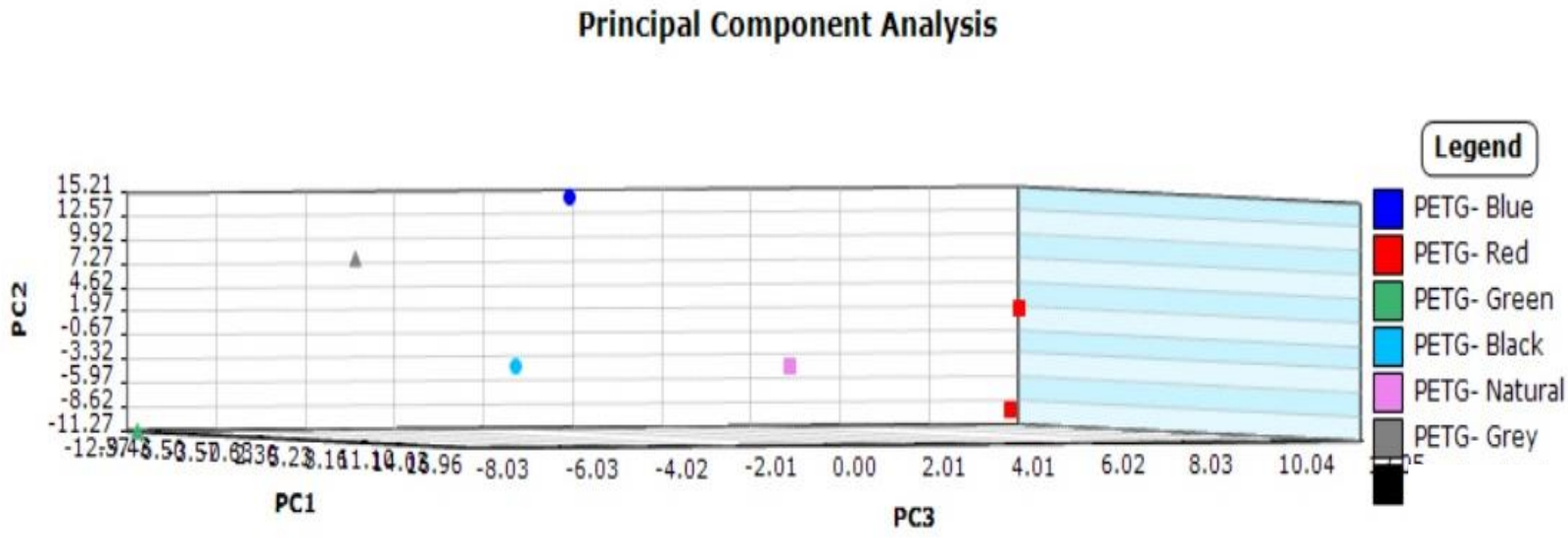

Figure 39. PCA plot of TD-DART-MS for PETG by color (n=7)

The PCA analysis using thermal desorption spectra provided an effective basis for separation of polymers and, using the subsequent clustering of data points, an “unknown” can be positively identified depending on what cluster it falls within (Figures 40 and 41). However, our findings show that the covariance covered by PCA for samples were generated using direct analysis by DART without thermal desorption, were less satisfactory given current parameters, due to the inherent increase in background peaks. The use of the glass T-junction for the TD phase of the analysis created a pseudo-closed environment for the DART to MS inlet region, limiting ambient compound detection.

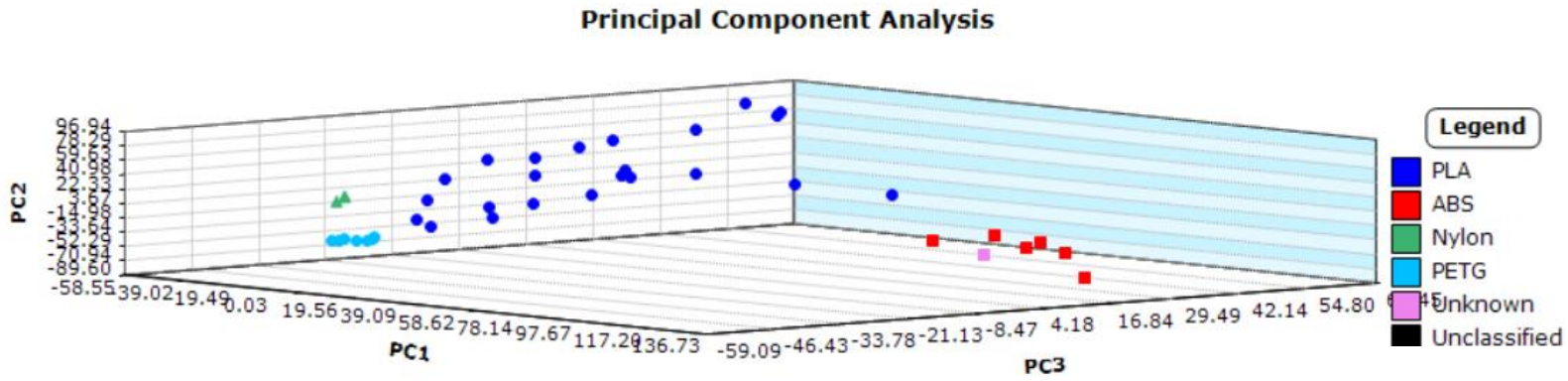

Figure 40. Clustering of Sample #48 ABS (pink square) when treated as an unknown (n=40)

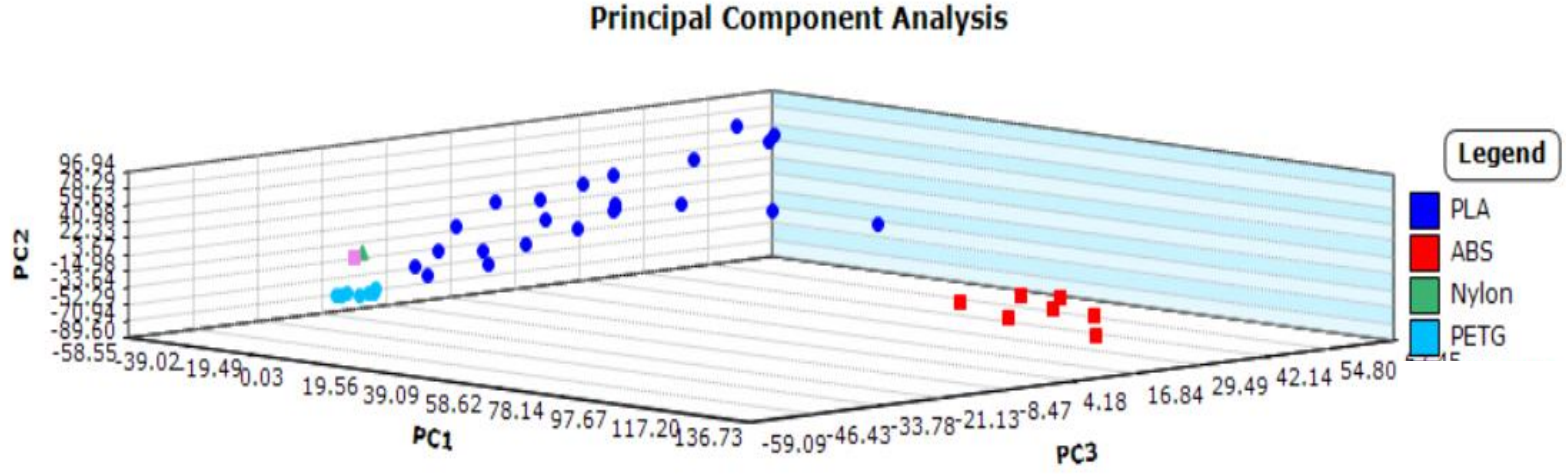

Figure 41. Clustering of Sample #44 Nylon (pink square) when treated as an unknown (n=40)

This finding serves to further reinforce our initial hypothesis that the use of thermal desorption DART can form the basis for more reliable identification of unknown polymer firearm evidence. As the database of polymer spectra grows and the PCA parameters are optimized over time, it is possible that the use of unmodified DART spectra for chemometric identification will become feasible. Also, it is our recommendation that, for effective identification purposes, the "exotic" polymers (polymers other than ABS, PLA, PETG, and nylon) should be excluded to produce distinct PCA clusters.

THERMAL DESORPTION DART-MS OF POLYMERS

There is significant difference when the same sample is analyzed by DART and by TD-DART, with TD-DART giving cleaner spectra (Figure 43). The additional discriminatory power of the analysis of the polymers over various temperatures contributed a much needed layer of complexity to bring forensic scientists one step closer to discerning between individual manufacturers or batches of the same color polymer. Many of the medium to high mass/charge ratio compounds do not begin to decompose and ionize until a minimum of 350 °C, which is lower than the default temperature of the DART source (commonly 250°C) (Figure 42). With more information on the proprietary formulation of the various polymers, it may be possible in the future to further distinguish sources of polymers based on these high mass/charge ratio compounds that may include additives that could serve as a chemical "fingerprint.

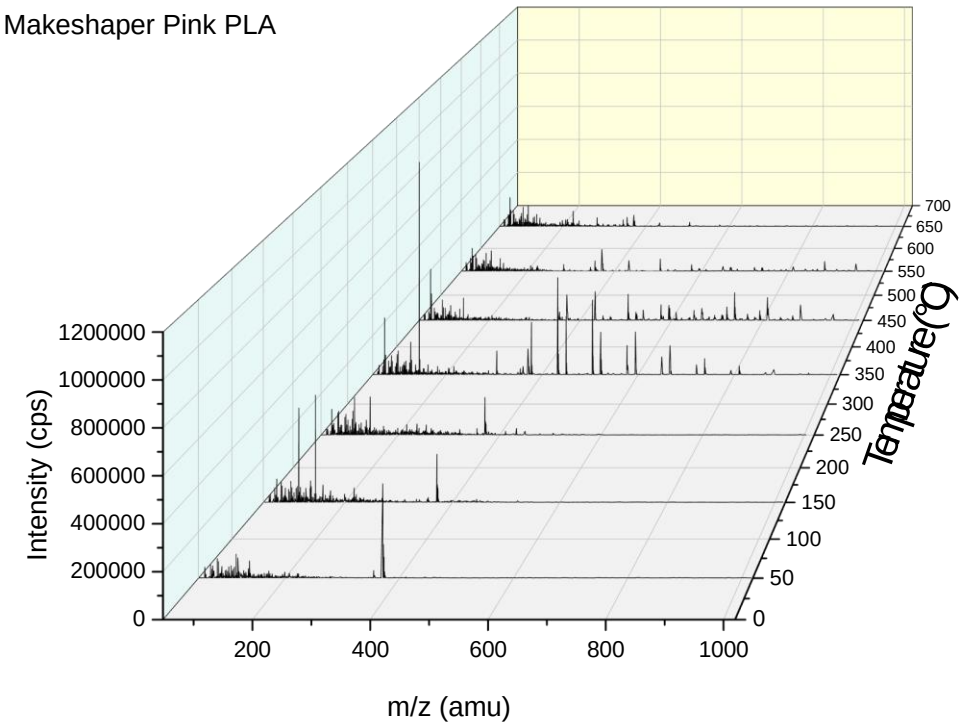

Figure 42. Temperature-resolved mass spectra of pink PLA

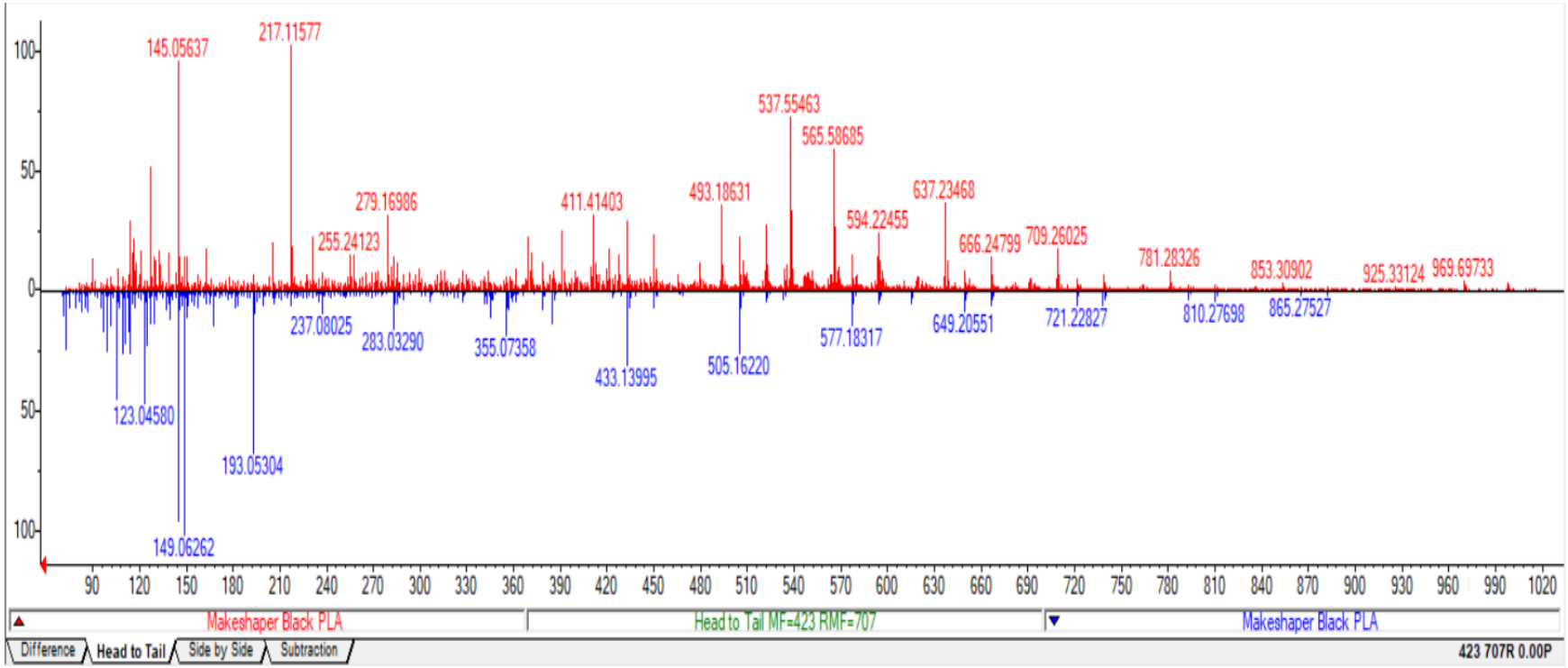

Figure 43. Head to Tail comparison of Makeshaper Black PLA by DART-MS (Red) and TD-DART-MS (Blue)

NIST-STYLE USER DATABASE FORMATION

All polymer samples, both the 50 analyzed by TD-DART-MS and the 34 analyzed by traditional DART-MS were processed using msAxel, Mass Mountaineer, and the NIST MS Search Program to generate two user libraries for future forensic reference. It is our hope that this initial user database will form the foundation of a powerful tool for forensic practitioners to quickly identify unknown polymer fragments that would be collected from surfaces of a firearm-related crime scene. The discriminatory power of the database will grow over time as more samples are added and the treatment of samples and MS spectra are further optimized with experience. It is our recommendation that any unknown polymer fragments recovered as possible evidence be analyzed by TD-DART-MS to provide the cleanest spectra for identification.

**A copy of our NIST user library will be accessible for download as a supplemental file with our future publication. The library can be opened with the free demo copy of NIST MS Search Program found on the NIST chemdata website.*

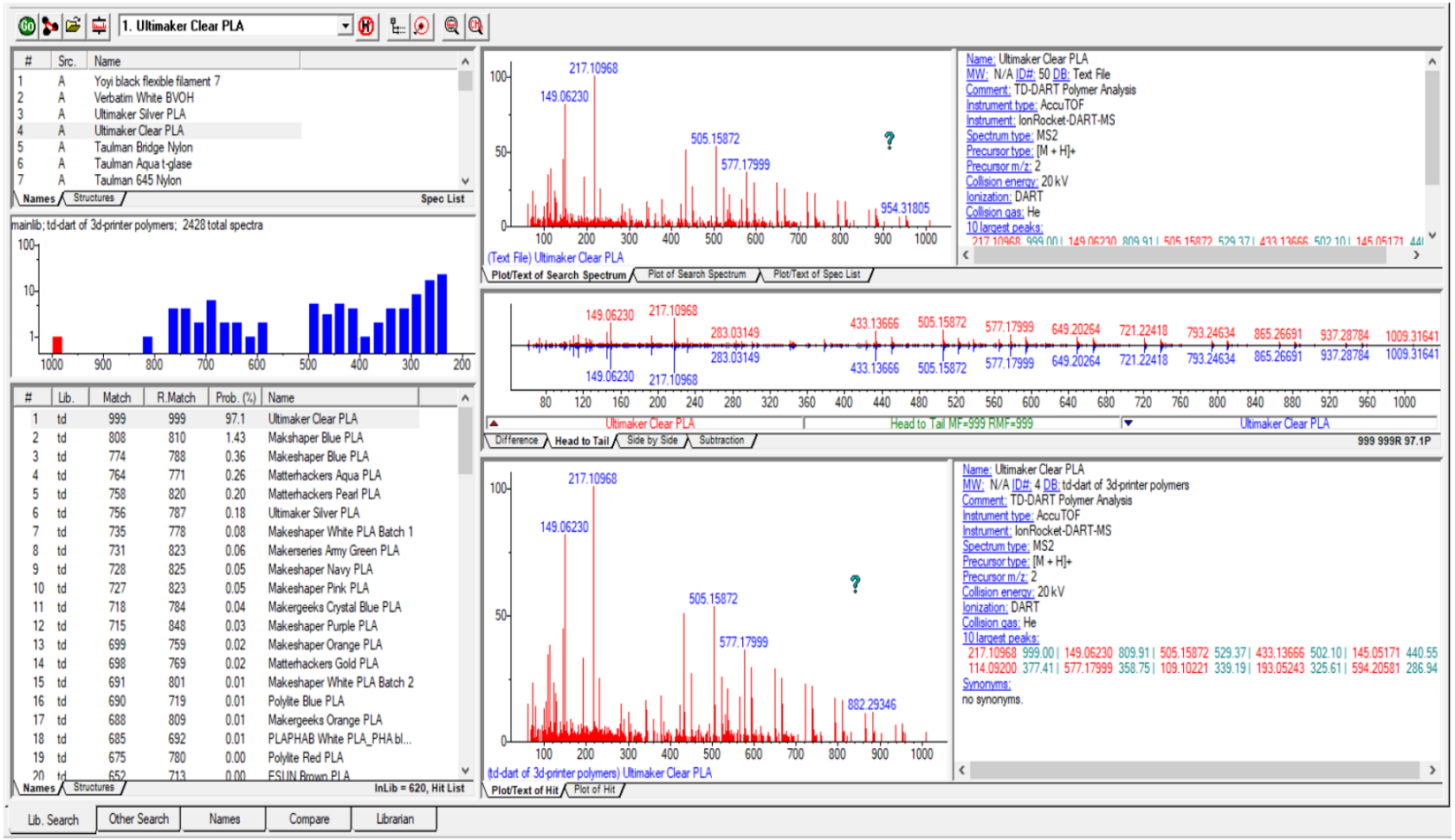

Figure 44. NIST MS Search Program entry for Ultimaker Clear PLA

BULLET WIPE AND DISTANCE ANALYSIS BY DART-MS

Results show that careful consideration must be applied when establishing the presence or absence of polymers stemming from the discharge of the weapon, since several of the common polymer types (i.e. nylon and PLA) are also common in other commercial applications. The presence of the protonated monomer of nylon (m/z 114) is present in all of the DART-MS spectra collected in this study, including 2 different instruments, possibly due to the presence of caprolactam (also m/z 114, a precursor for the synthesis of nylon 6) in the housing of the DART source or MS inlet. Thus it is our recommendation that the monomer, dimer, trimer pattern be established whenever possible to more reliably confirm the presence of a specific polymer from the discharge of a weapon (Figure 45). However, this is not always possible due to the inherently lower signal of the higher tier polymer repeat units due to decomposition to monomeric units once they have been heated through discharge of the weapon and then ionized by DART.

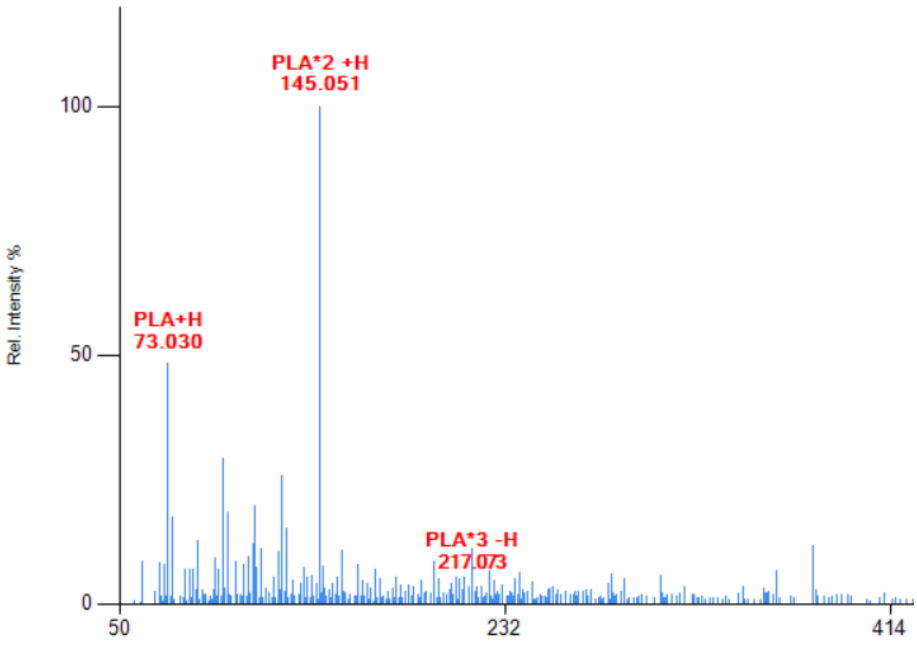

Figure 45. PLA monomer, dimer, trimer peaks for Makeshaper pink PLA

Table 8. Findings from Distance Study	
Sample Name	Relative Peak Height of Nylon
Pure Nylon	Nylon Dimer: 100%
Cotton Blank	Not Detected
Air Blank	Not Detected
3.5 Yards	Not Detected
3.5 Yards	Nylon Dimer: 6.145%
3.5 Yards	Nylon Dimer: 5.177%
4 Yards	Nylon Dimer: 6.332%
4.5 Yards	Nylon Dimer: 4.751%
7.0 Yards	Nylon Dimer: 6.099%

The nylon dimer was detected for all of our tested distances, while also being absent from the blanks (Table 8). The data showed no correlation between distance and peak height of the nylon dimer, so it is our recommendation that DART not be used to quantitate firing distances. Also, the peak height of the dimer is quite low relative to other compounds detected on the testfire t-shirts, so it is unlikely that a practitioner would recognize the presence of such low amounts of polymer residue without prior indication that a polymer firearm was used. Future work should include a study focused on the replication of results in multiple laboratory settings to confirm the monomer/dimer/trimer pattern is detectable and to confirm that different DART setups do not introduce sample carryover.

Black et al 2017 showed that DART-MS can be used to positively identify polymer residue left behind on discharged cartridge cases and bullets. However, this technique is not sufficiently reliable in its current form for the detection of polymers left at the bullet perforation site by bullet wipe, due to low transfer of polymer from barrel-to-bullet and bullet-to-target contact. Consequently, GSR analysis around bullet perforation sites is not effective to identify

polymer firearm use on its own unless larger fragments of polymer are deposited by the firearm, although it is still an effective tool to look at organic GSR evidence. If future efforts can improve the sensitivity of the DART spectra through better sample introduction, (i.e. further work with thermal desorption) this facet of evidence should be revisited. Also of note is the application of 415nm light, as demonstrated in Honsberger et al 2019, that would potentially allow for the visual screening of a shooting victim's clothing to preliminarily determine the presence or absence of polymer fragments.

LATENT PRINT ANALYSIS

Our initial examination of the unique challenges of latent print analysis on 3D-printed firearms is published in our book chapter (Spencer et al 2019). Our previous work focused solely on Songbird frames, with multiple latent print development pathways. We determined that the best technique for latent print development is the use of black magnetic powder without the addition of cyanoacrylate fuming. We conducted the same experimental treatment on Liberator frames, to confirm that the application of latent print development by black magnetic powder is universally the best option for 3D-printed surfaces, independent of the differences of surface morphology produced by different blueprints and 3D-printers (Figures 46 and 47). We determined that the black magnetic powder is still the most effective tool, since the addition of cyanoacrylate fuming produces comparatively poorer friction ridge detail.

To produce a clear image showing friction ridge detail on 3D-printed surfaces, it is necessary to do significant processing post-development using image software (conducted by our collaborator at the Mississippi Crime Laboratory) (Figure 48).

Figure 46. ABS polymer Liberator prior to latent print development

Figure 47. ABS polymer Liberator after latent print development

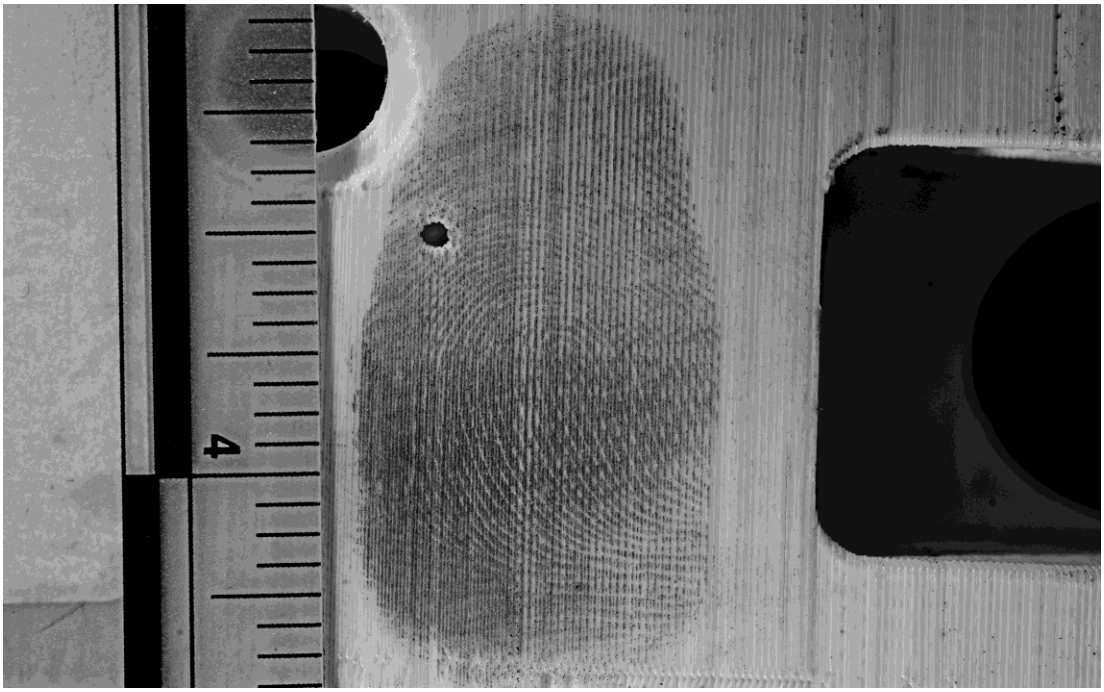

Figure 48. Enhanced latent print after magnetic powder development (Reprint from Spencer et al 2019)

GSR DEPOSITION OF LEAD AND NITRITES

Samples analyzed by the Modified Griess Reagent and Sodium Rhodizonate displayed the expected increase in spread with distance. Samples displayed an increase in spread diameter of 1 cm per 7 cm of shooting distance, when shot between 0.4 - 1.4m (Figure 49). Due to the subsonic .22 cartridges necessary for the safe discharge of the weapons and the nature of the polymers to not properly and reproducibly channel muzzle pressure, the reduced muzzle velocity results in GSR deposition patterns that are unreliable and make muzzle-to-target distance determination difficult.

Figure 49. Lead and Nitrite GSR deposition from a .22 caliber Songbird (increasing distance left to right: 0.46m, 0.91m, 1.37m)

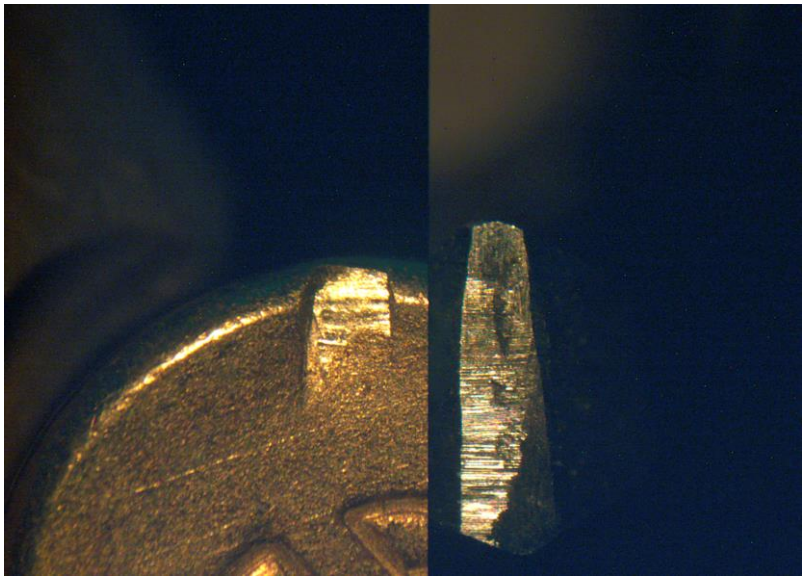

Figure 50. Microscope image of .22 caliber primer impression from hex key firing pin

CONCLUSION

After evaluating both established physical techniques and new chemical techniques for firearm evidence from 3D-printed firearms, it is clear that any pre-existing physical methods like latent print analysis and toolmark analysis will require careful modification to remain applicable to polymer firearms. These disciplines will require significant optimization to address the challenges that only true experts in these fields can address. With regard to latent print analysis our recommendations are to exclusively use magnetic powder for development of latent prints. For toolmark analysis, we recommend that microscopy analysis focus on the unique firing pin impressions left on the primer by do-it-yourself firing pins that are necessary for 3D-printed firearms. For example, we utilized either a hex key or a drill bit blank planed down with a Dremel set, leaving unique impressions behind on the .22 caliber cartridge cases (Figure 50). Any such personal modifications will leave behind characteristic toolmarks which can form the foundation of 3D-printed firearm microscopy identifications in the future. We further highlight the need for additional research into the optimization of chemical techniques to characterize, identify, and source polymer evidence, building on our past work, including our creation of the NIST 3D-print polymer database. The use of chemometrics is currently the most effective tool to classify polymer mass spectra, particularly when coupled with thermal desorption. Chemometric evaluations can be further optimized by the addition of more polymer samples to the database. This work also warrants a full study on optimizing the chemometric parameters used to separate and classify the polymer samples, which the authors hope to pursue further in the future. We hope to assess if discrimination of polymers is further clarified by selecting only high intensity m/z peaks for each sample. The m/z peaks used to generate the first 3 PCs should also be explored fully, possibly building a preset m/z table that highlights the key chemical differences

between the polymers. The use of score and loading plots will also assign numerical separation values to the visual plots generated in this study.

ONGOING WORK

In addition to the work listed above, we are pursuing four additional collaborative projects to be concluded after my dissertation. In addition to the use of modified PCA methods for polymer evidence classification, we are collaborating with Dr. Igor Lednev's research group at SUNY Albany to generate supervised statistical models to classify unknown polymer evidence. After generating appropriate models using our polymer spectra from the database (34 direct DART and 50 TD-DART spectra), we will perform internal cross validation and apply the models to our pre-existing polymer GSR spectra as a method of external validation of the models. Once the models are validated, they can serve as an effective means of classification and identification of possible unknown polymer GSR stemming from a real-world source.

The second collaborative project will be with Dr. Lednev's group as well, as we will be analyzing both traditional firearm GSR (.22 caliber revolver) and 3D-printed polymer firearm GSR by Raman Spectroscopy. This study will lead to parameter optimization of Raman instrumentation to establish a method of distinguishing polymer and non-polymer GSR.

The third collaborative project will be with Dr. Murrell Godfrey's research group at the University of Mississippi. We will be evaluating methods of DNA analysis on 3D-printed firearm surfaces. Once an appropriate method is optimized, a study will be conducted to compare DNA recovery efficacy between traditional firearms and 3D-printed polymer firearms.

The fourth collaborative project is with Dr. John LaRocco. We will develop computational models of various physical stress parameters that are involved in the discharge of

a firearm. Stress models will be developed for several 3D-printed firearm designs, after which functional firearm frames will be printed and discharged to compare real-world stress parameters to the computational projections. Resulting data will be used to optimize the posited computational models for future applications in projecting real-world stress parameters for the discharge of 3D-printed polymer firearms.

ACKNOWLEDGEMENTS

We thank the forensic professionals at the Mississippi Crime Laboratory and the Alabama Department of Forensic Sciences for assistance and collaboration, and for the use of their facilities. Scott Watkins at the University of Mississippi Physics department machine shop helped with design and construction of the .38 caliber firearms in phase II. Parker Ball played a large role in processing all the mass spectral data for the database formation. Dr. Chip Cody graciously provided access to the TD-DART-MS at JEOL in Boston, MA free of charge. We also thank the University of Mississippi USDA lab for allowing access to their DART-MS free of charge.

This work was supported by Award No. 2017-IJ-CX-001 by the National Institute of Justice, Office of Justice Programs, U.S. Department of Justice. The opinions, findings, and conclusions or recommendations expressed here are those of the authors and do not necessarily reflect those of the U.S. Department of Justice.

LIST OF REFERENCES

AFTE Criteria for Identification Committee (1992) “Theory of identification, range of striae comparison reports and modified glossary definitions—an AFTE criteria for identification committee report.” *AFTE J*, 24(2): 336-340.

Anderson MS (2014) “Mass Spectrometry of Spacecraft Contamination Using Direct Analysis in Real-Time Ion Source.” *Journal of Spacecraft and Rockets* 51: 374-378.

Bell S (2013) *Forensic Chemistry, 2nd Edition*, Pearson Education Inc.

Black O, Cody R, Edwards D, Cizdziel JV (2017) “Identification of polymers and organic gunshot residue in evidence from 3D-printed firearms using DART- mass spectrometry: a feasibility study.” *Forensic Chem*. 5: 26-32. DOI: 10.1016/j.forc.2017.05.003

Burleson GL, Gonzalez B, Simons K, Yu JCC (2009) “Forensic analysis of a single particle of partially burnt gunpowder by solid phase micro-extraction–gas chromatography-nitrogen phosphorus detector.” *J. Chromatography A*, 1216: 4679–4683.

Chang CC, Wang JL, Chang CY, et al (2016) Development of a multicopter-carried whole air sampling apparatus and its applications in environmental studies. Chemosphere 144: 484-492.

Chernetsova ES, Morlock GE (2011) "Determination of drugs and drug-like compounds in different samples with direct analysis in real time mass spectrometry." *Mass Spectrometry Reviews* 30(5): 875-883.

Chiaramonte P (1 July 2015) “Proposed regulation could keep 3D-printed gun blueprints offline for good.” *Fox News*

Clemons K, Dake J, Sisco E, Verbeck GFIV (2013) “Trace analysis of energetic materials via direct analyte-probed nanoextraction coupled to direct analysis in real time mass spectrometry.” *Forensic Science International* 231(1):98-101.

Cody RB, Laramée JA, Durst HD (2005) "Versatile New Ion Source for the Analysis of Materials in Open Air under Ambient Conditions." *Anal. Chem*. 77 (8): 2297–2302.

Cordy P, Veiga MM, Salih I, et al (2011) Mercury contamination from artisanal gold mining in Antioquia, Colombia: The world’s highest per capita mercury pollution. Sci Total Environ 410: 154-160.

Corrigan CE, Roberts GC, Ramana MV, et al (2007) Capturing vertical profiles of aerosols and black carbon over the Indian Ocean using autonomous unmanned aerial vehicles. Atmos Chem Phys Discuss 7(4): 11429-11463.

Dalby O, Butler, D, Birkett JW (2010) "Analysis of Gunshot Residue and Associated Materials – A Review." *J. Forensic Sci.,* 55(4): 924-943.

Deeds DA, Banic CM, Lu J, Daggupaty S J (2013) Mercury speciation in a coal-fired power plant plume: An aircraft-based study of emissions from the 3640 MW Nanticoke Generating Station, Ontario, Canada. Geophys Res: Atmos 118: 1–17.

Diaz PV, Yoon S (2018) High-fidelity computational aerodynamics of multi-rotor unmanned aerial vehicles. AIAA SciTech Forum, Areospace Sciences Meeting, Kissimmee, Florida.

DIFF-Lift Lifting Tape. (n.d.) Retrieved from https://www.lynnpeavey.com/product_info.php?products_id=163

Edgerton ES, Hartsell BE, Jansen JJ (2006) Mercury Speciation in Coal-fired Power Plant Plumes Observed at Three Surface Sites in the Southeastern U.S. Environ Sci Technol 40: 4563-4570.

Field A. T., Field A. T. (1959) Fingerprint handbook. Charles C. Thomas Publisher.

Fisher B. A., Fisher D. R. (2012) Techniques of Crime Scene Investigation (8th ed.). Boca Raton, FL: CRC Press.

Friedli HR, Arellano AF, Cinnirella S, Pirrone N (2009) Initial Estimates of Mercury Emissions to the Atmosphere from Global Biomass Burning. Environ Sci Technol 43: 3507-3513.

German E. (2005, January 15) Level 1, 2 and 3 Details... a thumbnail explanation of terms coined by David Ashbaugh. http://onin.com/fp/level123.html

Goudsmits E, Sharples G, Birkett J (2015) "Recent trends in organic gunshot residue analysis." *Trends in Analytical Chemistry* **74**: 46-57.

Greenberg A (14 Nov 2013) "3D-Printed Gun Stands Up To Federal Agents' Testfiring—Except When It Explodes." *Forbes*

Gustin MS (2012) Exchange of mercury between the atmosphere and terrestrial ecosystems. Environmental chemistry and toxicology of mercury; John Wiley and Sons; New York 423-451.

Gustin MS, Evers DC, Bank MS, et al (2016) Importance of Integration and Implementation of Emerging and Future Mercury Research into the Minamata Convention. Environ Sci Technol 50(6): 2767-2770.

Holder E. H., Robinson L. O., & Laub J. H. (2012) The Fingerprint Sourcebook. Washington, DC: U.S. Dept. of Justice, Office of Justice Programs, National Institute of Justice.

Holmes CD, Jacob DJ, Corbitt ES, et al (2010) Global atmospheric model for mercury including oxidation by bromine atoms Atmos Chem Phys 10(24): 12037-12057.

Honsberger H, Rhumorbarbe D, Werner D, Riva F, Glardon M, Gallusser A, Delemont O (2018) How to Recognize the Traces Left on a Crime Scene by a 3D-Printed Liberator?: Part 1. Discharge, Exterior Ballistics and Wounding Potential. *Forensic Sci. Int.* 286. 245-251.

Honsberger H, Werner D, Rhumorbarbe D, Riva F, Glardon M, Gallusser A, Delemont O (2019) How to Recognize the Traces Left on a Crime Scene by a 3D-Printed Liberator?: Part 2. Elements of ammunition, marks on the weapons and polymer fragments. *Forensic Sci. Int.* 295: 137-144.

Huber ML, Laesecke A, Friend DG, (2006) The Vapor Pressure of Mercury. National Institute of Science and Technology NISTIR 6643, p. 17.

Jackson A. R., Jackson J. M. (2004) Forensic science. Harlow: Pearson Education Limited.

James S. H., Nordby J. J., Bell S. (2009) Forensic science: An introduction to scientific and investigative techniques (3rd ed.). Boca Raton, FL: CRC Press/Taylor & Francis Group.

Jiang Y, Cizdziel JV, Lu D (2013) Temporal patterns of atmospheric mercury species in northern Mississippi during 2011–2012: Influence of sudden population swings. Chemosphere 93(9): 1694-1700.

Keeler G, Glinsorn G, Pirrone N (1995) Particulate mercury in the atmosphere: Its significance, transport, transformation and sources. Water Air Soil Pollut 80(1-4): 159-168.

Kim KH, Kim MY (2002) Mercury emissions as landfill gas from a large-scale abandoned landfill site in Seoul. Atmos Environ 36: 4919-4928.

Kim KH, Yoon HO, Brown RJ, Jeon EC, Sohn JR, Jung K (2013) Simultaneious monitoring of total gaseous mercury at four urban monitoring stations in Seoul, Korea .Atmos Res 132–133: 199–208.

Klampfl C (2013) “Mass Spectrometry as a useful tool for the analysis of stabilizers in polymer materials.” *Trends in Analytical Chemistry* 50: 53-64

Krabbenhoft DP, Sunderland E M (2013) Global change and mercury. Science 341: 1457–1458.

Lan X, Talbot R, Laine P, et al (2015) Atmospheric Mercury in the Barnett Shale Area, Texas: Implications for Emissions from Oil and Gas Processing. Environ Sci Technol 49(17): 10692-10700.

Landis MS, Ryan JV, Schure AF , Laudal D (2014) Behavior of Mercury Emissions from a Commercial Coal-Fired Power Plant: The Relationship between Stack Speciation and Near-Field Plume Measurements. Environ Sci Technol (48): 13540-13548.

Laramée JA, Cody RB, Nilles JM, & Durst HD (2007) "Forensic Application of DART (Direct Analysis in Real Time) Mass Spectrometry." *Forensic Analysis on the Cutting Edge: New Methods for Trace Evidence Analysis*, Blackledge RD (ed), Wiley-Interscience Hoboken, NJ

Laramée JA, Durst HD, Connell TR, Nilles, JM (2009) *American Laboratory Online Edition 2*: 1-5.

Laza D, Nys B, De Kinder J, Mesmaeker MK, Moucheron C (2007) "Development of a quantitative LC-MS/MS method for the analysis of common propellant powder stabilizers in gunshot residue." *J. Forensic Sci*. 52(4): 842-850.

Lee H. C., Palmbach T., Miller M. T. (2003) Henry Lees crime scene handbook. London: Elsevier Academic Press.

Lesiak AD, Shepard JRE (2014) "Recent advances in forensic drug analysis by DART-MS." *Bioanalysis* 6(6): 819-842.

Lindberg SE, Southworth G, Prestbo EM, Wallschläger D, Bogle MA, Price J (2005) Gaseous methyl- and inorganic mercury in landfill gas from landfills in Florida, Minnesota, Delaware, and California. Atmos Environ 39(2): 249-258.

Liu B, Keller G J, Dvonch JT, Barres J A, Lynam MM, Marsik FJ, Morgan JT (2010) Temporal variability of mercury speciation in urban air. Atmos Environ 44: 2013-2023.

Loftin KB (2009) "Development of novel DART TOFMS analytical techniques for the identification of organic contamination on spaceflight-related substrates and aqueous media." Ph.D. thesis, University of Central Florida.

Lyman SN, Gustin MS, Prestbo EM, et al (2007) Estimation of Dry Deposition of Atmospheric Mercury in Nevada by Direct and Indirect Methods. Environ Sci Technol 41(6): 1970-1976.

Lyman SN, Jaffe DA, (2011) Formation and fate of oxidized mercury in the upper troposphere and lower stratosphere. Nature Geoscience 5: 114–117.

Mason RP, Reinfelder J R, Morel F M M (1995) Bioaccumulation of Mercury and Methylmercury. Water Air Soil Pollut 80: 915-921.

McGonigle AJS, Aiuppa A, Giudice G, et al (2008) Unmanned aerial vehicle measurements of volcanic carbon dioxide fluxes. Geophys Res Lett 35(6).

McLagan D, Mitchell C, Huang H, Lei Y, Cole A, Steffen A, Hung H, Wania F (2016) A High-Precision Passive Air Sampler for Gaseous Mercury. Environ Sci Technol Lett 3:24-29

Meyers JA (2009) "The Analysis of Smokeless Powders by AccuTOF-DART." (poster presentation) in *Combined Regional Forensic Meeting* (Orlando, FL)

Meyers JA (2009) "The Analysis of Smokeless Powders by AccuTOF-DART." (poster presentation) in *Combined Regional Forensic Meeting* (Orlando, FL).

Moran JW, Bell S (2014) "Skin permeation of organic Gunshot Residue: implications for sampling and analysis." *Anal. Chem.* 86: 6071-6079.

Musah RA, Cody RB, Dane AJ, Vuong AL, & Shepard JRE (2012) "Direct analysis in real time mass spectrometry for analysis of sexual assault evidence." *Rapid Communications in Mass Spectrometry* 26(9): 1039-1046.

National Forensic Science Technology Center (accessed March 2019) Module 12: Gunshot Residue and Distance Determination. *Firearm Examiner Training*
NFST (September 2013) A Simplified Guide to Crime Scene Investigation.Nation Forensic Science Technology Center.

Palermo E. (2013, September 19) Fused Deposition Modeling: Most Common 3D Printing Method. Retrieved from https://www.livescience.com/39810-fused-deposition-modeling.html

Pirrone N, Cinnirella S, Feng X, et al (2010) Global mercury emissions to the atmosphere from anthropogenic and natural sources. Atmos Chem Phys 10(13): 5951-5964.

Polski J., Smith R., Garrett R. (2011) The Report of the International Association for Identification, Standardization II Committee.

Rossi M, Brunelli, D, Adami A, Lorenzelli L, Menna F, Remondino F (2014) Gas-Drone: Portable gas sensing system on UAVs for gas leakage localization. Sensors 1431-1434

Safariland (2018) Dusting for Prints. https://www.safariland.com/fingerprint-powder-guide.html

Saferstein R. (2005) Forensic Science Handbook (Vol. II). Upper Saddle River: Prentice Hall.
Schroeder WH, Munthe J (1998) Atmospheric mercury—An overview. Atmos Environ 32(5): 809-822

Seigneur C, Vijayaraghavan K, Lohman K, et al (2004) Global Source Attribution for Mercury Deposition in the United States. Environ Sci Technol 38(2): 555-569.

Selin NE (2009) Global Biogeochemical Cycling of Mercury: A Review. Annual Review of Environment and Resources 34: 43–63.

Slemr F, Ebinghaus R, Brenninkmeijer CAM, et al (2009) Gaseous mercury distribution in the upper troposphere and lower stratosphere observed onboard the CARIBIC passenger aircraft. Atmos Chem Phys 9(6): 1957-1969.

Snider D. (2003) AR15/M16 FAQs. Biggerhammer. http://www.biggerhammer.net/ar15/cad/

Spencer C, Robert A, Black O, Roy S, Cizdziel JV, Godfrey M (2019) Evaluation of fingerprint development techniques on 3D-printed firearms. *Forensic analysis of gunshot residue, 3D-printed firearms, and gunshot injuries: current research and future perspectives.*

Tao Z, Liu Y, Zhou M, Chai X (2017) Exchange pattern of gaseous elemental mercury in landfill: mercury deposition under vegetation coverage and interactive effects of multiple meteorological conditions. Environmental Science and Pollution Research 24: 26586–26593.

United Nations Environment Programme (2013) Technical Background Report for the Global Mercury Assessment 2013. AMAP, Oslo, Norway.

USEPA United States Environmental Protection Agency (1999) Compendium Method IO-5, Sampling and Analysis for Vapor and Particle Phase Mercury in Ambient Air Utilizing Cold Vapor Atomic Fluorescence Spectrometry (CVAFS). EPA/625/R-96/010a.

USEPA United States Environmental Protection Agency (2010) Toxic Release Inventory. <http://www.epa.gov/tri/>.

Walther G (2015) "Printing Insecurity? The Security Implications of 3D-Printing of Weapons." *Science and Engineering Ethics* 21 (6): 1435-4

Weiss-Penzias P, Jaffe DA, McClintick A, et al (2003) Gaseous Elemental Mercury in the Marine Boundary Layer: Evidence for rapid removal in anthropogenic pollution. Environ Sci Technol 37(17): 3755-3763.

Wertheim P. A. (2013, October 13) Magnetic Powder. http://crimeandclues.com/2013/04/12/magnetic-powder/

What is AccuTrans? (2018) Retrieved from https://www.accutransusa.com/about/https://www.ncjrs.gov/pdffiles1/nij/grants/233980.pdf

Yoon S, Diaz PV, Boyd Jr. DD, Chan WM, Theodore CR (2017) Computational aerodynamic modeling of small quadcopter vehicles. American Helicopter Society (AHS) 73rd Annual Forum, Fort Worth, Texas.

Zhu J, Wang T, Talbot RW, Huang X (2012) Characteristics of atmospheric Total Gaseous

Mercury (TGM) observed in urban Nanjing, China. Atmos Chem & Phys 12(24): 12103-12118.

OSCAR B. BLACK V

Curriculum Vitae, 2019

Department of Biomolecular Sciences, University of Mississippi, University, MS 38677

Email: obblack@olemiss.edu

EDUCATION

Ph.D. in Chemistry with an emphasis in Forensics, University of Mississippi, August 2019

Dissertation: "Physical and Chemical Trace Evidence from 3D-Printed Firearms, and Use of a Quadcopter for Targeted Sampling of Gaseous Mercury in the Atmosphere"

B.S. in Forensic Chemistry, University of Mississippi, 2015

HONORS

Undergraduate

- Dean's Honor Roll (>3.5 GPA) 4 Semesters
- Holmes Scholarship
- Academic Excellence Scholarship (Resident)
- Academic Excellence Scholarship (Non-resident)
- National Society of Collegiate Scholars

Graduate

- NIJ STEM Graduate Research Fellow: Fall 2017-Summer 2019
- Editor of Book (and author of 2 chapters): "Forensic Analysis of Gunshot Residue, 3D-Printed Firearms, and Gunshot Injuries: Current Research and Future Perspectives"
- 4 first author peer-reviewed publications
- 2016-2017 ACS Outstanding Analytical Chemistry Graduate Student Award
- 2018-2019 ACS Graduate Research Award

RESEARCH EXPERIENCE

Undergraduate Research
Dr. James Cizdziel's Lab, University of Mississippi
Topics: Environmental Chemistry, Analytical Method Development, Environmental Monitoring and Fingerprinting
Duties: Paid Research Assistant to Graduate Students performing ICP-OES, ICP-MS, GCMS, Solid Phase Extractions, Derivitizations, Sample Preparation

Graduate Research
Dr. James Cizdziel's Lab, University of Mississippi
Topics: Forensic Chemistry Analytical Method Development, Environmental Chemistry Method Development, Trace Analysis
Instrumentation: ICP-MS, DSC, TGA, FTIR, DART-MS, GC-MS, CVAFS, Comparative Microscopy

Graduate Studies (2015-2019) Research topics focused primarily on developing new analytical methodology. Primarily the evaluation of current protocols and the establishment of new forensic methodology as it pertains to the analysis of 3D-printed firearms and their resulting trace evidence. Secondary work included development of methods for environmental sampling of atmospheric contaminants such as mercury and VOCs using an unmanned aerial vehicle. Extensive teaching assistant experience in analytical chemistry courses, including Quantitative Analysis and Instrumental Analysis. Performed various inter-disciplinary collaborative research projects conducting key instrumental analyses and interpretation of results. Conducted collaborative research efforts with various forensic agencies, including the Mississippi Forensic Laboratory and the Alabama Department of Forensic Sciences. Dissertation work culminated in the publication of a book, several capstone peer-reviewed publications, and a database for law-enforcement agencies to classify 3D-printed polymer materials.

LIST OF PUBLICATIONS

1. **Black O.**, Cody R., Edwards D., Cizdziel J. V. (2017) Identification of polymers and organic gunshot residue in evidence from 3D-printed firearms using DART- mass spectrometry: a feasibility study. *Forensic Chem.* 5, 26-32. DOI: 10.1016/j.forc.2017.05.003

2. **Black O.**, Chen J., Scircle A., Zhou Y., Cizdziel J. V. (2018) Adaptation and use of a quadcopter for targeted sampling of gaseous mercury in the atmosphere. *Environ Sci Pollut Res Int.* 25,13195–13202. DOI: 10.1007/s11356-018-1775-y

3. Chen J., Scircle A., **Black O.**, Cizdziel J.V., Watson N., Wevill D., Zhou Y. (2018) On the use of multicopters sampling and analysis of volatile organic compounds in the air by adsorption/thermal desorption GC-MS. *Air Qual Atmos Health.* 11(7), 835-842.

4. Orr S., Barnes M., George H., Joshee L., Jeon B., Scircle A., **Black O.**, Cizdziel J. V., Smith B., Bridges C. (2018) Exposure to mixtures of mercury, cadmium, lead, and arsenic alters disposition of single metals in tissues of Wistar rats. *J Toxicol Env Heal A.*

5. **Black O.,** Cizdziel J.V. (2019) The advent of 3D-printed firearms and its implications for forensic analysis. *Forensic analysis of gunshot residue, 3D-printed firearms, and gunshot injuries: current research and future perspectives.*

6. Spencer C., Robert A., **Black O.**, Roy S., Cizdziel J.V., Godfrey M. (2019) Evaluation of fingerprint development techniques on 3D-printed firearms. *Forensic analysis of gunshot residue, 3D-printed firearms, and gunshot injuries: current research and future perspectives.*

7. Jeon B., Scircle A., Chen J., **Black O.**, Wallace D., Zhou Y., Lepak R., Hurley J., Cizdziel J.V. (Pending) Historical deposition of trace metals in a marine sapropel in Mangrove Lake, Bermuda with emphasis on mercury, lead, and their isotopic composition

8. **Black O.,** Cody, R., Cizdziel, J.V. (Pending) *Forensic Analysis for .22 and .38 Caliber 3D-Printed Polymer Firearms*

EXTERNAL GRANTS

- $50,000/year (x2 years): National Institute of Justice Graduate Research Fellowship in STEM (2017-2019)

PRESENTATIONS/INTERVIEWS

- 2018. Presented research at the Society of Environmental Toxicology and Chemistry conference (regional meeting, Memphis TN)
- 2019. Guest speaker at Kiwanis International: Oxford, MS chapter meeting
- 2019. Interview with OleMiss News Team
- 2019. Interview with Daily Journal (Tupelo, MS)
- 2019. Interview with Clarion Ledger
- 2019. Interview with The JT Show (SuperTalk MS radio)
- 2019. Interview with Science News Magazine
- 2019. Guest speaker at OleMiss STEM library

REFERENCES

James Cizdziel, PhD
Associate Professor of Chemistry
University of Mississippi
University, MS 38677
cizdziel@olemiss.edu

Kristine Willet, PhD
Chair and Professor of Pharmacology and Environmental Toxicology
University of Mississippi
University, MS 38677
kwillett@olemiss.edu

Eric Warren, PhD
Senior Research Scientist: Structural Biology Dept., St. Jude's Children's Research Hospital
Co-Founder and Forensic Consultant: SEP Forensic Consultants, LLC.
eric@sepforensic.com

Murrell Godfrey, PhD
Director of Forensic Chemistry
Associate Professor
Department of Chemistry and Biochemistry
University of Mississippi
University, MS 38677
mgodfrey@go.olemiss.edu